SPATIAL PATTERN OF BROWN ROT SYMPTOMS AND FINE-SCALE GENETIC STRUCTURE OF *MONILINIA FRUCTICOLA* WITHIN STONE FRUIT TREE CANOPIES

by

SYDNEY ERIN EVERHART

(Under the Direction of Harald Scherm)

ABSTRACT

Spatial patterns of plant disease can provide insights into important epidemiological processes such as sources of inoculum, mechanisms of propagule dissemination, and reproductive strategies of the pathogen population. The goal of this study was to characterize spatial patterns of brown rot (caused by *Monilinia* spp.) and of the associated fungal genotypes in complex stone fruit canopies. An electromagnetic digitizer was used to map and georeference symptoms within individual tree canopies, and three-dimensional methods of spatial statistics were applied to analyze the resultant data points for aggregation and association patterns. The approach was tested and validated in eight sour cherry trees affected by *M. laxa*, and applied subsequently in a 3-year study on peach to characterize spatio-temporal development of pre-harvest brown rot, caused by *M. fructicola*, in 13 trees of different maturity classes. Disease aggregation correlated negatively with disease incidence ($r = -0.653$, $P < 0.0001$), showing that trees with higher brown rot incidence had lower aggregation of affected fruit. Significant disease aggregation was most pronounced for early-maturing cultivars and/or early in the epidemic. This is consistent with a greater importance of localized, within-tree sources of inoculum at the beginning of the epidemic. To complement these results with genotypic information about the associated pathogen isolates, 16 microsatellite markers were developed and applied to examine the fine-scale genetic structure of *M. fructicola* in six of the 13 trees, whereby isolates from

every brown rot symptom in each tree were genotyped. All populations (65 to 173 isolates per tree) showed high genetic and genotypic diversity. The percentage of unique multilocus haplotypes within trees was greater for blossom blight isolates than for fruit rot isolates, indicating a greater contribution of clonal reproduction during the latter phase. Spatial genetic structure was observed among fruit rot isolates, with all six populations showing positive and significant autocorrelation up to 0.37 and/or 0.73 m. Despite high levels of within-tree pathogen diversity, the contribution of locally available inoculum is likely the main factor in generating the observed fine-scale spatial patterns of disease and pathogen genotypes within individual trees.

INDEX WORDS: Blossom blight, Brown rot, Canopy ecology, *Monilinia fructicola*, Peach, Population genetics, *Prunus persica*, Spatial autocorrelation, Spatial pattern

SPATIAL PATTERN OF BROWN ROT SYMPTOMS AND FINE-SCALE GENETIC STRUCTURE OF *MONILINIA FRUCTICOLA* WITHIN STONE FRUIT TREE CANOPIES

by

SYDNEY ERIN EVERHART

BS, University of Iowa, 2005

MS, University of Central Missouri, 2007

A Dissertation Submitted to the Graduate Faculty of The University of Georgia in Partial Fulfillment of the Requirements for the Degree

DOCTOR OF PHILOSOPHY

ATHENS, GEORGIA

2012

SPATIAL PATTERN OF BROWN ROT SYMPTOMS AND FINE-SCALE GENETIC STRUCTURE OF *MONILINIA FRUCTICOLA* WITHIN STONE FRUIT TREE CANOPIES

by

SYDNEY ERIN EVERHART

Major Professor:	Harald Scherm
Committee:	Phillip M. Brannen Anthony E. Glenn Guido Schnabel Dorset W. Trapnell

Electronic Version Approved:

Maureen Grasso
Dean of the Graduate School
The University of Georgia
August 2012

DEDICATION

I dedicate this work to my family. Your support has allowed me to pursue my dreams and your encouragement has kept me going. I owe a lot to you and I love you all very much.

To Tyler, your ability to make me laugh has brought joy to my life. You keep my dreams alive and because of you, they get more exciting every day.

ACKNOWLEDGEMENTS

It is with sincere gratitude that I want to acknowledge the support of my major advisor, Harald Scherm. He has gone beyond the call of duty to provide quality feedback on my work, even at the final hour. At some of the most critical moments, he also provided words of support. These words helped me greatly to arrive at the finish line today. Above all, he has set an example of how to be a thoughtful scientist, from the first idea to completion of the final product. His example is something that I strive for in my own work as a scientist.

I also want to thank Ashley Askew, doctoral candidate in the Department of Statistics. Her programs were the workhorse behind our novel statistical analyses. It should be noted that Ashley was not paid for this work, nor did she receive course credit beyond the first semester of spatial statistics that she took four years ago. Ashley has dedicated countless hours and days to this work and, in the process, has become a very good friend. It is my hope that our partnership will continue as we move on to new projects in the future.

There are also several individuals along the way that have instructed me in techniques and developed my confidence in the lab. In particular, Travis Glenn gave me a foundation in molecular techniques that will serve me throughout my career. His approach to working in a molecular lab instilled a sense of adventure and discovery that I hope to pass on to others in the future. Ken Jones and Anna McKee from the Glenn lab were also extremely helpful in sharing knowledge of techniques and concepts related to the microsatellite development and analysis. Also acknowledged is fellow graduate student, Edwin Palencia, who guided me in the lab and helped me to develop a fungal protoplasting technique. More importantly, Edwin's sense of

humor and encouragement during my early days were something that carried through to all of my lab work and kept me going through difficult times. I also want to thank Rock Christiano, who has become my "rock" while working in the Scherm lab. His feedback and discussions regarding laboratory experiments and techniques have been invaluable. Finally, although Sara Thomas and I have nearly opposite personality profiles according to the Meyers-Briggs test, her advice in living life and being in the lab have balanced me.

There are many other individuals who have helped me in this work that I want to thank, including Imre Holb, Andy Shirley, Marin Brewer, Ashley Turner, Lucky Mehra, Jeremy Haralson, Renee Holland, Katherine Mills, Amy Savelle, Efrat Gamliel-Atinsky, Ryan McNeill, Peter Hartel, David Knauft, and many other graduate students, teachers, faculty, staff, and technicians that have helped and encouraged me along the way. Thank you all.

I also want to thank the people who have helped shape me as a scientist and writer, prior to coming to UGA. Harold Keller was my master's advisor at the University of Central Missouri who taught me much more than the myxomycetes. He taught me about the unspoken formalities and politics of science, writing and academic research. He also taught me how to give an exciting scientific presentation and coached me in strategies for success in my career. The mentorship and guidance he provided in my master's set the stage for success in my doctorate. Most important, he taught me to "never give up!"

Finally, I want to thank my father. He is the person who instilled in me a curiosity for the natural world, even the small. Our scientific discussions and attempts to quantify things around us are moments I have come to treasure and are what I love about being a scientist today.

TABLE OF CONTENTS

Page

CHAPTER 1

INTRODUCTION AND LITERATURE REVIEW

Background

Brown rot of stone and pome fruits is characterized primarily by twig blight, blossom blight, and fruit rot, and is caused by fungal pathogens in the genus *Monilinia* Persoon. In certain conditions, additional symptom types may include latent infections of immature fruit and green fruit rot. Among stone fruits (Rosaceae), brown rot causes economic losses on peach (*Prunus persica* (L.) Batsch), sour cherry (*P. cerasus* L.), and plum (*P. domestica* L.), among others. The disease is common in geographic areas with warm, humid climates, such as the southeastern United States. In Georgia, peach production currently covers over 12,000 acres and represents more than $46 million in value (Wolfe and Luke-Morgan 2011). In rainy years, losses to disease can be high. For example, in 2003 total crop value was reduced by 20%, with some orchards attributing more than 50% of in-field loss to brown rot disease (Williams-Woodward 2004). Economic losses were $8 million in damage and nearly $2 million for control (primarily use of fungicides), which totaled approximately 75% of all peach diseases combined, including scab, bacterial spot, phony peach, gummosis, Armillaria root rot, and Phomopsis constriction canker. In contrast, dry years with effective fungicidal control reduce losses to <1% (Martinez 2005).

Brown rot of fruit was first reported as early as 1729, but the fungus was not described by Persoon until 1796. Species of fungi in the genus *Monilinia* are pathogens of Rosaceous and Ericaceous plants, whereby eight species are considered economically important and three of

these are the primary causal agents of brown rot of stone fruits, *M. fructicola* (G. Wint.) Honey, *M. fructigena* Honey, and *M. laxa* (Alderh. & Ruhland) Honey (Byrde and Willetts 1977). In Europe, the predominant species are *M. laxa* and *M. fructigena*, whereas in North America, the predominant species are *M. fructicola* and *M. laxa*. *Monilinia fructigena* is a quarantine species in the United States, and *M. fructicola* is a quarantine species in Europe that has recently been reported in Switzerland and France (Bosshard et al. 2006); Hungary, Spain, and Italy (Petróczy and Palkovics 2006); the Czech Republic (Duchoslavová et al. 2007), as well as in China (Zhu et al. 2005).

The disease cycle of *Monilinia* is closely linked to seasonal development of its stone fruit hosts. In the spring, apothecia may develop from sclerotinized fruit on the ground and produce the primary inoculum (sexual ascospores) that infects blossoms and shoots. The sexual stage of *M. fructicola* is considered rare in managed peach orchards in the southeastern United Sates (Landgraf and Zehr, 1982). Another source of primary inoculum in the spring, presumably more important in warm climates, is conidia produced on mummified fruit that remain attached to the tree (Byrde and Willetts 1977) or peduncles (Kable 1965). Both ascospores and conidia are capable of infecting flowers, causing blossom blight. Inside flowers, the mycelium penetrates the peduncle and moves into the twig where it may develop into a canker. Asexual sporulation on such cankers constitutes an important source of secondary inoculum for infection of mature fruit later in the season. Another important source of secondary inoculum comes from thinned fruit on the ground (Hong et al. 1998; Holb and Scherm 2007). In peach, fruit are thinned prior to pit-hardening, and the decaying fruit on the ground may become infected by airborne conidia, especially when soil moisture is high. In contrast, developing green fruit are generally resistant to infection (unless injured by insects or hail). Although latent infections of green fruit are known

to occur, most infections and disease development typically occur during the ripening phase in the final few weeks before harvest (Emery et al. 2000). The spread of conidia is primarily via rain splash, fruit-to-fruit contact, and wind (van Leeuwen et al. 2000). Once infected, mature fruit rapidly rot and decay. Thus, *Monilinia* overwinters primarily in fruit mummies in the tree or on the ground, on twig cankers in the tree, and in fruit peduncles in some production areas.

Understanding the temporal and spatial progression of a plant disease is an important prerequisite for comprehending pathogen biology and developing effective disease management practices (Sutton 1996). For *M. fructicola*, the temporal progression of disease has been well documented (Biggs and Northover 1985; Biggs and Northover 1988a, b; Holtz et al. 1998; Hong et al. 1998; Landgraf and Zehr 1982; Luo et al. 2007; Luo and Michailides 2001). In contrast, spatial patterns of disease, which can shed light on the type or source of initial inoculum or the mechanism(s) involved in pathogen dissemination (Real and McElhany 1996), have not been well studied for *Monilinia* spp. Furthermore, most studies on spatial patterns of brown rot have been conducted in pome fruits rather than stone fruits; this distinction is important because mature pome fruit generally require a wound for infection by *Monilinia* spp. (Holb and Scherm 2007) whereas stone fruit do not. For *M. fructigena* on apple, disease was not evenly distributed within orchards, with clusters of diseased fruit aggregated within and between individual trees (van Leeuwen et al. 2000). Similarly, the amount of disease in apple and pear orchards varied according to seasonal differences in weather and with respect to how disease was managed within orchards (Xu et al. 2001). Examining individual trees showed that the distribution of disease among trees was associated with wounds created by insect or bird pests, by growth cracks, and by fruit-to-fruit contact. Fruit-to-fruit contact increased the incidence of brown rot in prune (Michailides and Morgan 1997), but none of these studies examined the level of

aggregation and/or association between distinct symptom types within canopies of individual orchard trees.

Closely related to the spatial pattern of disease is the spatial genetic structure of the pathogen population. Examining the spatial distribution of disease and pathogen population structure and dynamics are particularly challenging when dealing with organisms that have no simple morphological mode of discrimination and lack sufficient genomic data. In the case of *M. fructicola*, vegetative compatibility groups (VCGs) were first used to study population structure. With VCGs, compatibility is more likely between closely related isolates, whereas non-compatible isolates are more likely to be genetically divergent strains, as demonstrated by out-crossing previously compatible isolates to form incompatible isolates (Free et al. 1996). Compatibility between isolates is measured by inoculating a single Petri dish with two separate isolates. Incompatible isolates will form a dark barrage along the line of mycelial contact, whereas compatible isolates will grow into each other seamlessly.

VCG analysis was used to study population structure of *M. fructicola* in peach orchards in Georgia (Scherm and Emery 2002). Isolates were collected in two orchards from blighted blossoms in the spring and diseased fruit at harvest. The isolates were cultured and paired to test for compatibility. Results indicated that isolates from blighted blossoms were very diverse, whereby 96.2% of isolates were incompatible by VCG testing. The majority of these isolates lacked compatibility with subsequent fruit rot isolates (only 2% showed compatibility). This suggested that isolates obtained from the fruit rot phase of disease may have originated from some source other than blighted blossoms within the same tree. Among isolates obtained from symptomatic fruit, an average of 67.5% was compatible, suggesting clonal dispersal within tree canopies. The authors concluded that reproduction in *M. fructicola* is not exclusively clonal and

even a small amount of sexual recombination is occurring, despite the low frequency of apothecia observed in southeastern peach orchards.

The compatibility among *M. fructicola* isolates obtained from three individual nectarine trees in an orchard in California was also compared using VCGs (Sonoda et al. 1991). An average of 18 *M. fructicola* isolates fell into an average of 11 different VCGs within each tree. Thus, approximately 38.8% of isolates were vegetatively compatible within each tree canopy. Additionally, there were 20 isolates collected from trees throughout the rest of the orchard, showing that 11 of the 16 VCGs within this group were shared among the three intensively sampled trees. Overall, these results suggested high diversity among and within individual tree canopies.

Dicarboximide resistance was used as another indirect genetic marker to study the spatial and temporal patterns of brown rot in peach and nectarine orchards (Elmer et al. 1998). Dicarboximide fungicides are used to control *M. fructicola*, but resistance can develop within populations subjected to the fungicide repeatedly. The number of dicarboximide-resistant isolates was determined for each tree within six orchards over 3 years. Data were used to calculate Lloyd's Patchiness Index (LPI) and tested for spatial autocorrelation. This showed that resistance was aggregated in all experimental blocks and in all years, and that high frequencies of resistant isolates were associated with low LPI values. It was concluded that short-distance dispersal by rain was possible within rows, but over farther distances, such as between rows, it was more likely by wind or insect vectoring. No spatio-temporal correlations were found from year to year, indicating independent initial inoculum sources each spring.

In addition to these indirect genetic markers, several molecular marker systems have been developed for *Monilinia.* The first were markers for the small subunit (SSU) ribosomal DNA

(rDNA) group-I intron used to distinguish *M. fructicola* from *M. laxa* and *M. fructigena* (Fulton and Brown 1997). Around the same time, genetic markers based on coding and non-coding rDNA sequences were developed to determine phylogenetic relationships within *Monilinia* (Holst-Jensen et al. 1997). These markers of highly conserved genes are ideal for resolution between species, but are of no value for discriminating among individuals of the same species. Unlike using highly conserved genes for differentiating between species, genetic markers for population studies should have no or neutral selective pressure so random mutations between individuals can be detected (McDonald 1997).

Genetic markers to identify isolates of *Monilinia* were developed using random amplified polymorphic DNA (RAPD) analysis (Förster and Adaskaveg 2000). RAPD analysis is convenient because it does not require sequence data. The primers are designed arbitrarily and long enough (10 base pairs or more) that only a limited number of fragments are amplified. After amplification, polymorphic regions are identified by their presence or absence between isolates. The specificity of RAPD markers is dependent on whether polymorphism is observed between different species or different isolates of the same species. Existing RAPD markers for *Monilinia* resulted in very few polymorphisms within species because primers were selected that distinguished between *M. laxa* and *M. fructicola* (Förster and Adaskaveg 2000). Thus, these particular markers are less useful for population studies.

RAPD markers with greater specificity were developed for *M. laxa* to examine genetic variation within populations in several peach orchards in Spain (Gell et al. 2007). This involved 144 RAPD markers, 59 polymorphic and 85 monomorphic, to show that there was minimal genetic variation throughout the orchards. The authors indicated that this was consistent with clonal populations and regular local extinction events. The majority of the genetic variation

(97%) was shared among all orchards and very little (3%) was isolated within orchards. Consequently, it was proposed that the inoculum was primarily from asexually produced conidia, with a high degree of dispersal among orchards. This is consistent with the life history traits of *M. laxa*, which rarely produces apothecia on fruit mummies; however, RAPD analysis also tends to underestimate genetic variation and may be diminishing any subtle variation present (Tranah et al. 2003). In addition, RAPD markers are dominant markers. This is important because several cytological studies have shown that fungi in the genus *Monilinia* are multinucleate (typically 5 to 10 nuclei per conidium; Hall 1963, Heuberger 1934, Hoffmann 1972, 1974, Willets and Calonge 1969, Margosan and Phillips 1985) and hence may constitute more than one distinct genotype within the vegetative mycelium, representing an additional potential source of genetic variation. Such naturally-occurring heterokaryons have been postulated for *M. laxa* and *M. fructigena* (Hoffman 1972, 1974), with high numbers of nuclei purportedly associated with aggressiveness and greater fitness (Margosan and Phillips 1985). Nevertheless, no studies examining population genetic structure within individual tree canopies using molecular markers have been conducted.

Current Limitations

Characterization of spatial patterns of disease and associated pathogen genotypes in tree canopies is challenged by difficulty in recording spatial location of symptomatic tissues and in selecting the appropriate statistical approach that will account for the naturally occurring non-random pattern of susceptible plant parts. Previous studies examining spatial disease patterns within tree canopies either divided the canopy into layers (Holb and Scherm, 2007) or quadrats (Batzer et al. 2008, Spósito et al. 2008). However, the major limitation of using layers or quadrats is that the associated grouping of data may fail to capture fine-scale patterns within each block. Although

analysis of spatial patterns of plant disease as a means of quantifying spatial structure and inferring processes has come of age during the past two decades (Waggoner and Aylor 2000, Jeger 1999, Moslonka-Lefebvre et al. 2010), there is a paucity of research addressing plant disease aggregation and association patterns in individual plant canopies. This is largely due to the inherent complexity of tree canopies and challenges in measuring and characterizing spatial patterns of disease.

Insight into the corresponding pathogen fine-scale population structure is also challenged by limitations in available methodology. Thus far, fungicide resistance and VCGs have been used to quantify the population structure and dynamics of *Monilinia* spp. within orchards and trees, and suggested a high degree of variation within populations. However, these indirect genetic markers lack the resolution necessary to characterize fine-scale genetic structure within individual canopies. Overall, little is known about pathogen population variation and dynamics, or processes at the population level. Most studies using molecular genetic markers have focused on species delineations, origins, and/or quantifying broad-scale diversity (Fan et al. 2010, Gell et al. 2007, Jänsch et al. 2012, Luo and Schnabel 2008, Ma et al. 2003, Snyder and Jones 1999). In addition, the currently available molecular markers are not co-dominant and therefore may not have the robustness necessary to characterize fine-scale genetic structure of a pathogen population that may include heterokaryotic individuals.

Potential Solutions

Three-dimensional canopy mapping. Spatial measurements within tree canopies have been conducted for horticultural purposes using a number of methods to examine tree architecture and distribution of fruit and associated quality parameters within trees and vines. Categorical

methods include measuring linear distance from the base of the tree to the tips of branches and describing the plant as a collection of functional units (cataphylls, nodes, leaves, buds, number and type of branches; Heuret et al. 2003). Other manual methods have been applied, such as using articulated arms (Lang 1973), measuring height and distance from the base of the tree, and cardinal orientation or angle of the branches (Succi et al. 1997; Lozano-Gonzalez et al. 1992; Trapnell et al. 2004), estimating coordinates using a infrared-adapted theodolite surveying instrument (Smith et al. 1992; 1993), and sound propagation (Sinoquet et al. 1991; Room et al. 1996). More recently, a method based on complete current induction in magnetic fields has been utilized, which is completely electronic and is accomplished with digitizing units such as the FASTRAK 3Space system (Polhemus, Colchester, VT). This instrument consists of a system electronics unit (SEU), an electromagnetic transmitter that is the source of the magnetic field and serves as the origin of coordinates, and a stylus that serves as the receiver and is used to digitize *x*, *y*, and *z*-coordinates on a Cartesian coordinate system within the magnetic field (Anonymous 1993). For the purposes of this study, the FASTRAK system was considered the best choice for ease of use and accuracy of point digitization of diseased elements within stone fruit tree canopies.

The FASTRAK digitizer, commonly used in virtual reality systems, has been used for mapping tree architecture and fruit distribution in a number of studies (Moulia and Sinoquet 1993, Miles et al. 1996; Smith and Curtis 1996; Sinoquet and Rivet 1997, Thanisawanyangkura et al. 1997, Sinoquet et al. 1998, Godin et al. 1999, Turnbull et al. 2007). The SEU is connected to a standard PC via USB connection and, with the use of a graphical user interface (GUI), allows the user to continuously track the movement of the receiver or discretely digitize individual points. The long-range transmitter is positioned in a fixed location near the trunk of

the tree and is the reference for the position and orientation measurement of the receiver up to a 6-m radius.

Digitizing coordinates with the FASTRAK involves two people. One person, the digitizer, identifies symptoms and digitizes coordinates at the tip of the stylus by pressing a button. A second person, the recorder, works at the computer interface to copy the coordinates from the GUI into a Microsoft Excel file (Microsoft, Redmond, WA), whereby a unique identification number and information designating the corresponding symptom type can be recorded. Digitizing points begins at the base of the tree, working upwards, digitizing symptoms on each successive branch, progressing toward the highest point on the tree. Digitizer accuracy is ~1 mm in controlled environments (Moulia and Sinoquet 1993) and ~1 cm in field conditions due to wind movement of objects and operator error (Thanisawanyangkura et al. 1997).

Microsatellite genetic markers. Microsatellites are tandem repeated motifs called simple sequence repeats (SSRs) of 1 to 6 bases found in all prokaryotic and eukaryotic genomes (Zane et al. 2002). They are located in both coding and non-coding regions and occur with a high degree of length variation, likely attributed to slippage events during DNA replication (Schlötterer and Tautz 1992). Although sequence data is the gold standard for fingerprinting individuals, microsatellites are highly useful in genetic forensics and population studies. The major drawback to using microsatellites is that they need to be isolated *de novo* for each species of interest. However, once developed, the procedure for analyzing and scoring individuals is relatively straightforward (Zane et al. 2002). Microsatellite markers offer the advantage over other genetic fingerprinting techniques that they represent co-dominant markers and results are easily reproduced.

For organisms that have greater genetic variation, microsatellite markers should be effective in three-dimensional, fine-scale studies within tree canopies. For example, three-dimensional spatial variation of multilocus genotypes has been examined for the epiphytic orchid, *Laelia rubescens* (although determined with allozyme markers rather than microsatellites in this example; Trapnell et al. 2004). There was measurable genetic variation within individual trees, and spatial autocorrelation analysis indicated relatedness was greatest up to 45 cm. The authors were able to attribute the fine-scale genetic structure of populations to the formation of discrete, vegetatively propagated clusters and to limited dispersal distance of progeny. Examining fine-scale population genetics in *M. fructicola* using microsatellite markers would allow me to infer heretofore unavailable information on inoculum sources, dispersal distance, mechanism of dissemination, and sources of genetic variation in three-dimensional space within and among trees.

Goals and Objectives

This study examined spatial distribution patterns of brown rot symptom types within tree canopies in stone fruit orchards, and investigated the fine-scale genetic structure of *M. fructicola* within peach tree canopies using high-resolution genetic markers. The overall goal is to increase our knowledge of the epidemiological processes related to disease development and spread. This was accomplished with the following specific objectives:

1. develop and validate methodologies to generate three-dimensional maps of brown rot symptoms within trees and analyze spatial aggregation and association patterns of disease in three dimensions within individual canopies (Chapter 2);

2. utilize the prototype generated in Chapter 2 to quantify spatio-temporal development of brown rot within individual peach tree canopies during the pre-harvest fruit rot epidemic (Chapters 3 and 4);
3. develop polymorphic microsatellite markers for *M. fructicola* (Chapter 3); and
4. collect and fingerprint *M. fructicola* isolates within peach trees to determine fine-scale population structure and dynamics with respect to spatial distance in individual tree canopies (Chapter 5).

Literature Cited

Anonymous. 1993. 3SPACE FASTRAK User's Manual, Revision F. Polhemus, Colchester, VT.

Batzer, J.C., Gleason, M.L., Taylor, S.E., Koehler, K.J., and Monteiro J.E.B.A, 2008. Spatial heterogeneity of leaf wetness duration in apple trees and its influence on performance of a warning system for sooty blotch and flyspeck. Plant Disease 92:164-170.

Biggs, A.R., and Northover, J. 1985. Inoculum sources for *Monilinia fructicola* in Ontario peach orchards. Canadian Journal of Plant Pathology 7:302–307.

Biggs, A.R., and Northover, J. 1988a. Early and late-season susceptibility of peach fruits to *Monilinia fructicola*. Plant Disease 72:1070–1074.

Biggs, A.R., and Northover, J. 1988b. Influence of temperature and wetness duration on infection of peach and sweet cherry fruits by *Monilinia fructicola*. Phytopathology 78:1352–1356.

Bosshard, E., Hilber-Bodmer, M., Schärer, H.-J., Bünter, M., and Duffy, B. 2006. First report of the quarantine brown rot pathogen *Monilinia fructicola* on imported stone fruits in Switzerland. Plant Disease 90:1554.

Byrde, R.J.W., and Willetts, H.J. 1977. The Brown Rot Fungi of Fruit. Pergamon, Oxford.

Elmer, P.A.G., Gaunt, R.E., and Frampton, C.M. 1998. Spatial and temporal characteristics of dicarboximide-resistant strains of *Monilinia fructicola* and brown rot incidence in stone fruit. Plant Pathology 47:530–536.

Emery, K.M., Michailides, T.J., and Scherm, H. 2000. Incidence of latent infection of immature peach fruit by *Monilinia fructicola* and relationship to brown rot in Georgia. Plant Disease 84:853–857.

Fan, J.-Y., Guo, L.-Y., Xu, J.-P., Luo, Y., and Michailides, T.J, 2010. Genetic diversity of populations of *Monilinia fructicola* (Fungi, Ascomycota, Helotiales) from China. J. Eukaryot. Microbiol. 57: 206-212.

Förster, H., and Adaskaveg, J.E. 1999. Early brown rot infections in sweet cherry fruit are detected by *Monilinia*-specific DNA primers. Phytopathology 90:171–178.

Free, S.J, Holtz, B.A., and Michailides, T,J.. 1996. Mating behavior in field populations of *Monilinia fructicola.* Mycologia 88:208–211.

Fulton, C.E., van Leeuwen, G.C.M., and Brown, A.E. 1999. Genetic variation among and within *Monilinia* causing brown rot of stone and pome fruits. European Journal of Plant Pathology 105:495–500.

Gell, I., Larena, I., and Melgarejo, P. 2007. Genetic diversity in *Monilinia laxa* populations in peach orchards in Spain. Journal of Phytopathology 155:549–556.

Glenn, T.C. and Schable, N.A. 2005. Isolating microsatellite DNA loci. Methods in Enzymology 395:202–222.

Godin, C., Costes, E., and Sinoquet, H. 1999. A method for describing plant architecture which integrates topology and geometry. Annals of Botany 84:343–357.

Hall, R. 1963. Cytology of the asexual stages of the Australian brown rot fungus *Monilinia fructicola* (Wint.) Honey. Cytologia 28:181–193.

Heuberger, J.W. 1934. Fruit rotting Sclerotinias IV. A cytological study of *Sclerotinia fructicola* (Wint.) Rehm. Univ. Maryland Agric. Exp. Sta. Bull. 371:167–189.

Heuret, P., Guédon, Y., Guérard, N., and Barthélémy, F. 2003. Analysing branching pattern in plantations of young red oak trees (*Quercus rubra* L., Fagaceae). Annals of Botany 91:479–492.

Hoffman, G.M. 1972. Heterokaryose bei Wildstämmen von *Monilinia fructigena.* Phytopathol. Z. 73:326–340.

Hoffman, G.M. 1974. Zum Vorkommen von Heterokaryose bei *Monilinia laxa.* Phytopathol. Z. 79:193–202.

Holb, I.J. and Scherm, H. 2007. Temporal dynamics of brown rot in different apple management systems and importance of dropped fruit for disease development. Phytopathology 97:1104–1111.

Holst-Jensen, A., Kohn, L.M., Jakobsen, K.S., and Schumacher, T. 1997. Molecular phylogeny and evolution of *Monilinia* (Sclerotiniaceae) based on coding and noncoding rDNA sequences. American Journal of Botany 84:685–701.

Holtz, B.A., Michailides, T.J., and Hong, C. 1998. Development of apothecia from stone fruit infected and stromatized by *Monilinia fructicola* in California. Plant Disease 82:1375–1380.

Hong, C., Holtz, B.A., Morgan, D.P., and Michailides, T.J. 1999. Significance of thinned fruit as source of the secondary inoculum of *Monilinia fructicola* in California nectarine orchards. Plant Disease 81:519–524.

Jänsch, M., Frey, J.E., Hilber-Bodmer, M., Broggini, G.A.L., Weger, J., Schnabel, G., and Patocchi, A. 2012. SSR marker analysis of *Monilinia fructicola* from Swiss apricots suggests introduction of the pathogen from neighbouring countries and the United States. Plant Pathology 61:247-254.

Jeger, M.J. 1999. Improved understanding of dispersal in crop pest and disease management: current status and future directions. Agricultural and Forest Meteorology 97:331-349

Landgraf, F.A., and Zehr, E.I.. 1982. Inoculum sources for *Monilinia fructicola* in South Carolina peach orchards. Phytopathology 72:185–190.

Lozano-Gonzalez, R., Storey, J.B., and Harris, M.K. 1992. Three-dimensional characterization of bearing pecan tree. HortScience 27(11):1181–1183.

Luo, C.-X., and Schnabel, G. 2008. The cytochrome P450 lanosterol 14α-demethylase gene is a DMI fungicide resistance determinant in *Monilinia fructicola* field isolates from Georgia. Applied Environmental Microbiology 74:359–366.

Luo, Y. and Michailides, T.J. 2001. Risk analysis for latent infection of prune by *Monilinia fructicola* in California. Phytopathology 91:1197–1208.

Luo, Y., Ma, Z., Reyes, H.C., Morgan, D., and Michailides, T.J. 2007. Quantification of airborne spores of *Monilinia fructicola* in stone fruit orchards of California using real-time PCR. European Journal of Plant Pathology 118:145–154.

Ma, Z, Yoshimura, M.A., and Michailides, T.J. 2003. Identification and characterization of benzimidazole resistance in *Monilinia fructicola* from stone fruit orchards in California. Appl. Environ. Microbiol. 69:7145-7152.

Margosan, D.A. and Phillips, D.J. 1985. Effect of two temperatures on nuclear number of conidia of *Monilinia fructicola.* Mycologia 77(5):835–837.

Martinez, A. (ed.) 2005. 2006 Georgia Plant Disease Loss Estimates. Special Bulletin 41-08, University of Georgia Cooperative Extension Service, College of Agricultural and Environmental Sciences, University of Georgia, Athens, GA.

McDonald, B.A. 1997. The population genetics of fungi: Tools and techniques. Phytopathology 87(4):448–453.

Michailides, T.J., and Morgan, D.P. 1997. Influence of fruit-to-fruit contact on the susceptibility of French prune to infection by *Monilinia fructicola.* Plant Disease 81:1416–1424.

Miles, D.B., Smith, G.S., and Miller, S.A. 1996. Within plant sampling procedures—Fruit variation in kiwifruit vines. Annals of Botany 78:289–294.

Moslonka-Lefebvre, M., Finley, A., Dorigatti, I., Dehnen-Schmutz, K., Harwood, T., Jeger, M.J., Xu, X., Holdenrieder, O., and Pautasso, M. 2010. Networks in plant epidemiology: From genes to landscapes, countries, and continents. Phytopathology 101:392-403.

Moulia, B., and Sinoquet, H. 1993. Three-dimensional digitizing systems for plant canopy geometrical structure: a review. Pages 183-193 in: Crop Structure and Light Microclimate: Characterization and Applications. C. Varlet-Grancher, R. Bonhomme, and H. Sinoquet, eds. INRA, Paris.

Petróczy, M., and Palkovics, L. 2006. First report of brown rot caused by *Monilinia fructicola* on imported peach in Hungary. Plant Disease 90:375.

Real, L.A., and McElhany, P. 1996. Spatial pattern and process in plant-pathogen interactions. Ecology 77:1101–1025.

Room, P.M., Hanan, J.S., and Prusinkiewicz, P. 1996. Virtual plants: new perspectives for ecologists, pathologists and agricultural scientists. Trends in Plant Science 1:33–38.

Scherm, H. and Emery, K.M. 2002. Vegetative compatibility in populations of *Monilinia fructicola* from Georgia peach orchards. Acta Horticulturae 592:725–727.

Schlötterer, C., and Tautz, D. 1992. Slippage synthesis of simple sequence DNA. Nucleic Acids Research 20:211–215.

Sinoquet, H., and Rivet, P. 1997. Measurement and visualization of the architecture of an adult tree based on a three-dimensional digitising device. Trees 11:265–270.

Sinoquet, H., Moulia, B., and Bonhomme, R. 1991. Estimating the three-dimensional geometry of a maize crop as an input of radiation models: comparison between three-dimensional digitising and plant profiles. Agricultural and Forest Meteorology 55:233–249.

Sinoquet, H., Thanisawanyangkura, S., Mabrouk, H., and Kasemsap, P. 1998. Characterization of the light environment in canopies using 3D digitising and image processing. Annals of Botany 82:203–212.

Smith, G.S., Gravett, I.M., Edwards, C.M., Curtis, J.P., and Buwalda, J.G. 1993. Spatial analysis of the canopy of kiwifruit vines as it relates to the physical, chemical and postharvest attributes of the fruit. Annals of Botany 73:99–111.

Smith, G.S., Curtis, J.P., and Edwards, C.M. 1992. A method for analyzing plant architecture as it relates to fruit quality using three-dimensional computer graphics. Annals of Botany 70:265–269.

Snyder, C.L., and Jones, A. 1999. Genetic variation between strains of *Monilinia fructicola* and *Monilinia laxa* isolated from cherries in Michigan. Canadian Journal of Plant Pathology 21:70-77.

Sonoda, R.M., Ogawa, J.M., and Manji, B.T. 1991. Population structure of *Monilinia fructicola* in *Prunus persica* var. *nucipersica* tree canopies. Mycological Research 95:893-895.

Spósito, M.B., Amorim, L., Bassanezi, R.B., Bergamin-Filho, A., and Hau, B. 2008. Spatial pattern of black spot incidence within citrus trees related to disease severity and pathogen dispersal. Plant Pathology 57:103-108.

Succi F., Magnanini, E., Quadretti, R., Miserocchi, O., and Costa, G. 1997. A geometric approach to kiwifruit canopy modelling. Acta Horticulturae 444:181–186.

Sutton, T.B. 1996. Changing options for the control of deciduous fruit tree disease. Annual Review of Phytopathology 34:527–547.

Thanisawanyangkura, S., Sinoquet, H., Rivet, P., Crétenet, M., and Jallas, E. 1997. Leaf orientation and sunlit leaf area distribution in cotton. Agricultural and Forest Meteorology 86:1–15.

Tranah, G.J., Bagley, M., Agresti, J.J., and May, B. 2003. Development of codominant markers for identifying species hybrids. Conservation Genetics 4:537–541.

Trapnell, D.W., Hamrick, J.L., and Nason, J.D. 2004. Three-dimensional fine-scale genetic structure of the neotropical epiphytic orchid, *Laelia rubescens.* Molecular Ecology 13:1111–1118.

Turnbull, T.L., Kelly, N., Adams, M.A., and Warren, C.R. 2007. Within-canopy nitrogen and photosynthetic gradients are unaffected by soil fertility in field-grown *Eucalyptus globulus.* Tree Physiology 27:1607–1617.

van Leeuwen, G.C.M., Stein, A., Holb, I., and Jeger, M.J. 2000. Yield loss in apple caused by *Monilinia fructigena* (Aderh. & Ruhl.) Honey, and spatio-temporal dynamics of disease development. European Journal of Plant Pathology 106:519–528.

Waggoner, P.E., and Aylor, D.E. 2000. Epidemiology: a science of patterns. Annual Review of Phytopathology 38:71-94.

Williams-Woodward, J.L. (ed.) 2004. 2003 Georgia Plant Disease Loss Estimates. Special Bulletin 41-06, University of Georgia Cooperative Extension Service, College of Agricultural and Environmental Sciences, University of Georgia, Athens, GA.

Wolfe K, Luke-Morgan A, 2011. 2010 Georgia Farm Gate Value Report. Area Report 07-01, University of Georgia Cooperative Extension Service, College of Agricultural and Environmental Sciences, University of Georgia, Athens, GA.

Zane, L., Bargelloni, L., and Patarnello, T. 2002. Strategies for microsatellite isolation: a review. Molecular Ecology 11:1–6.

Zhu, X.Q., Chen, X.Y., Luo, Y., and Guo, L.Y. 2005. First report of *Monilinia fructicola* on peach and nectarine in China. Plant Pathology 54:575–575.

.

CHAPTER 2

CHARACTERIZATION OF THREE-DIMENSIONAL SPATIAL AGGREGATION AND ASSOCIATION PATTERNS OF BROWN ROT SYMPTOMS WITHIN INTENSIVELY MAPPED SOUR CHERRY TREES[1]

[1]Everhart, S.E., A. Askew, L. Seymour, I.J. Holb, and H. Scherm. 2011. *Annals of Botany*. 108: 195–1202
Reprinted here with permission of the publisher.

Abstract

● *Background and Aims* Characterization of spatial patterns of plant disease can provide insights into important epidemiological processes such as sources of inoculum, mechanisms of dissemination, and reproductive strategies of the pathogen population. Whilst two-dimensional patterns of disease (among plants within fields) have been studied extensively, there is limited information on three-dimensional patterns within individual plant canopies. Reported here are the detailed mapping of different symptom types of brown rot (caused by *Monilinia laxa*) in individual sour cherry tree (*Prunus cerasus*) canopies, and the application of spatial statistics to the resulting data points to determine patterns of symptom aggregation and association.

● *Methods* A magnetic digitizer was utilized to create detailed three-dimensional maps of three symptom types (blossom blight, shoot blight and twig canker) in eight sour cherry tree canopies during the green fruit stage of development. The resulting point patterns were analysed for aggregation (within a given symptom type) and pairwise association (between symptom types) using a three-dimensional extension of nearest-neighbour analysis.

● *Key Results* Symptoms of *M. laxa* infection were generally aggregated within the canopy volume, but there was no consistent pattern for one symptom type to be more or less aggregated than the other. Analysis of spatial association among symptom types indicated that previous year's twig cankers may play an important role in influencing the spatial pattern of current year's symptoms. This observation provides quantitative support for the epidemiological role of twig cankers as sources of primary inoculum within the tree.

● *Conclusions* Presented here is a new approach to quantify spatial patterns of plant disease in complex fruit tree canopies using point pattern analysis. This work provides a framework for

quantitative analysis of three-dimensional spatial patterns within the finite tree canopy, applicable to many fields of research.

Key words: Spatial statistics, point pattern analysis, canopy architecture, *Monilinia*, brown rot, *Prunus*, magnetic digitizer, 3-D

Introduction

Characterization of spatial patterns and spatial dynamics of plant disease can provide insights into important epidemiological processes, especially those related to sources of inoculum, mechanisms of propagule dissemination, and reproductive strategies of the pathogen population (Wu and Subbarao, 2004). For brown rot disease of pome and stone fruits, caused by fungi within the genus *Monilinia*, temporal epidemiological aspects of disease development have been well characterized (Byrde and Willetts, 1977), but information about spatial aspects of brown rot epidemics is currently limited. The temporal sequence of disease progression includes pathogen survival either on fruit mummies on the ground, on mummies in the tree, or in twig cankers, followed by primary infection of flowers (causing blossom blight) in the spring. These infections can be initiated by sexual ascospores or asexual conidia. Blossom infections can subsequently lead to shoot blight, whereby the distal portion of the shoot is killed back due to girdling at the point of infection (i.e. the development of a twig canker). Conidia produced on blighted blossoms or in twig cankers can be wind or rain-splash dispersed (Corbin *et al.*, 1968; Pauvert *et al.*, 1969) to infect injured green fruit in the tree or thinned fruit on the ground, providing a bridge for subsequent infection of mature fruit near harvest. This then leads to the formation of fruit mummies and/or twig cankers, providing overwintering sites for the pathogen (Landgraf

and Zehr, 1982; Biggs and Northover, 1985, 1988a, b; Hong *et al.*, 1999; Luo and Michailides, 2001; Holb and Scherm, 2007).

Spatial epidemiological aspects of brown rot development in fruit orchards have received considerably less attention than the aforementioned temporal dynamics. Two-dimensional spatial patterns, such as aggregation of symptomatic trees at the orchard scale, have been investigated by van Leeuwen *et al.* (2000) and Xu *et al.* (2001) in pome fruits. In general, these studies showed that infected trees were spatially clustered within orchard rows, with variable intensity of disease among individual trees. Although spatial patterns were more pronounced in pear (*Pyrus communis*) than in apple (*Malus domestica*) orchards, wounding of the fruit by birds, insect damage or growth cracks was considered an influential source of the spatial pattern in both species. In a separate study, Elmer *et al.* (1998) examined the two-dimensional spatial pattern of Monilinia fructicola strains resistant to dicarboximide fungicide in peach and nectarine (*Prunus persica*) orchards, reporting that resistant strains were mostly restricted to individual trees with no spatio-temporal correlations from year to year of trees harbouring resistant strains. This suggested that resistant strains may be re-established annually from external sources rather than overwintering and establishing from within the same tree. Although providing useful epidemiological information, such spatial analyses have not yet been extended to three dimensions to include patterns at the canopy level. Given the complex structure of tree canopies (Costes *et al.*, 2006) adding a third dimension could reveal considerable additional detail about spatial structure, specifically with regard to disease symptom aggregation as well as associations among different symptom types within the canopy.

In general, the number of studies of three-dimensional (3-D) patterns within tree canopies is limited, largely due to the complexity of such canopies and the difficulty in developing

methods to rapidly and accurately map the hundreds or thousands of points that make up the tree canopy. Where plant disease or pest injury within a tree canopy has been examined, studies have generally relied on dividing and monitoring disease or injury within investigator-specified quadrats or sectors of the canopy, such as upper, middle and lower sections (Andrews *et al.*, 1980; Lewis, 1992; Michailides and Morgan, 1998; Spósito *et al.*, 2008). In addition, extending commonly used spatial statistics from two to three dimensions is not trivial mathematically. Scheuerell (2004) and Widder and Johnsen (2000) have published distance-based methods for analysing patterns in the aggregation and association of species in three dimensions and for testing for departure from randomness.

In the present study, a magnetic digitizer was used to map different brown rot symptom types (blossom blight, shoot blight and twig cankers) in individual sour cherry (*Prunus cerasus*) tree canopies, and 3-D methods of spatial statistics applied to the resultant data points. The goal was to determine the level of aggregation of different symptom types in the canopy as well as the degree of association of current year's symptoms with symptoms that resulted from the previous year's infections.

Materials and Methods

Mapping symptomatic elements within tree canopies. The study was conducted in an organically managed sour cherry orchard near Eperjeske, Hungary (47°31′60″N, 21°37′60″E), in June 2008 during the green fruit stage of development. Trees of cultivar Újfehértói fürtös, grafted on *P. mahaleb* rootstock, were approx. 11 years old (planted in 1997), between 2.3 and 3.8 m tall, and spaced 4.0 and 6.0 m within and between rows, respectively. At the time of the

assessment, three main symptom types (blossom blight, shoot blight and twig canker) caused by *Monilinia laxa* were present and readily distinguishable.

Eight trees (Table 2.1) of different sizes and with varying levels of disease incidence were selected for digitizing with a FASTRAK 3Space magnetic digitizer (Polhemus, Colchester, VT, USA) (Smith and Curtis, 1996). The *x*, *y* and *z* co-ordinates of all symptomatic elements were digitized using a stylus attached to the FASTRAK 3Space system, as were all asymptomatic (healthy) fruit for a total of up to 1811 data points per tree (Table 2.1 and Fig. 2.1). In addition, the age of each symptom (i.e. current vs. previous year) was noted, based on whether it occurred on current or previous year's twig growth. Each digitized canopy element was tagged with coloured tape to ensure that points were not measured twice and that no relevant point was omitted. The base of the trunk was designated as the origin of the co-ordinate system for each tree (Fig. 2.1).

Spatial pattern analysis. Spatial patterns of aggregation for a given symptom type within the canopy were characterized based on nearest-neighbour distances, i.e. the shortest Euclidian distance between symptoms derived from the *x*, *y* and *z* co-ordinates of points. The frequency distribution of nearest-neighbour distances within each tree could then be used to determine deviation from randomness (Coomes *et al.*, 1999; Scheuerell, 2004). Aggregation was assessed using two different frames of reference: (1) deviation of all symptomatic elements from complete spatial randomness (CSR) within the canopy; and (2) deviation of a given symptom type from the baseline distribution of all symptomatic elements within each tree. In the former case (deviation from CSR), first a minimum canopy volume for each tree was simulated using the following procedure. A large volume comprised of individual 0.125-m^3 cubes (50 × 50 × 50 cm)

was formulated that contained all points digitized from the tree being modelled. To improve the fit of the volume to the canopy, the algorithm checked each of the cubes on the outermost layer for presence or absence of observations (points). For a given cube, if no observations were found, then it was removed from the volume. This procedure was applied until no cubes without observations were left on the exterior of the canopy volume. This resulted in a complex canopy consisting of 90–360 individual 0.125-m^3 cubes per tree, had no interior gaps, and mimicked the observed tree canopy better than a spherical or ellipsoidal canopy approximation. In the next step, 1000 Monte-Carlo simulations with random placement of all symptomatic elements were conducted within the simulated canopy volume. The cumulative frequency distribution of the actual nearest-neighbour distances between symptoms was compared with that of the Monte-Carlo simulations using a Kolmogorov–Smirnov test. If symptoms were more aggregated than when assigned randomly within the canopy, the cumulative frequency distribution would be above the upper 95% confidence band for the CSR simulations, whereas if data were regular it would fall below the lower confidence band. The test statistic d_w, the maximum departure of the observed cumulative frequency distribution from that obtained for the simulations, was calculated as described in Coomes *et al.* (1999) and was used as an index of aggregation; a positive value of d_w indicates aggregation, whereas a negative value signifies uniformity.

To assess deviation of a given symptom type from the distribution of all symptomatic elements within each tree, the measured co-ordinates of all symptomatic elements served as an empty set of points (baseline) over which the symptom of interest (such as blossom blight or twig canker) was assigned randomly without replacement to generate each of the 1000 Monte-Carlo simulations for each tree. Cumulative frequency distributions of nearest-neighbour

distances and the resultant d_w values were used to assess the magnitude and significance of deviation from randomness.

Nearest-neighbour distances were also used to quantify the degree of pairwise association between different symptom types within the canopy. Here, nearest-neighbour distances were defined as the shortest distance from a given symptom of type A (e.g. blossom blight) to that of type B (e.g. twig canker). Again, the measured co-ordinates of all symptomatic elements served as a set of points over which the two symptom types of interest were randomized 1000 times. In each iteration, no symptoms of the same type were allowed to occupy the same co-ordinates, and co-occurrence of different symptom types at the same co-ordinate was limited to the same number observed in the actual dataset. The cumulative frequency distribution of the actual nearest-neighbour distances between the two symptom types was compared with that of the Monte-Carlo simulations as described for the aggregation analyses above. All computations were carried out in MATLAB v. 7.10 (MathWorks, Natick, MA, USA).

Results

On average, each of the eight digitized trees contained 773 data points, of which 444 and 329 were asymptomatic fruit and symptomatic elements, respectively (Table 2.1). More than half of the symptomatic elements were due to current year's infections (mostly blossom blight), with the remainder being remnants of previous year's infections (primarily twig cankers). Overall, about two-thirds of the specific symptoms were due to blossom blight, with twig cankers and especially shoot blight being less common. Nearest-neighbour distances computed across the eight digitized trees showed that current year's infections were closest to previous year's twig cankers (median 20.6 cm) and blighted blossoms (34.9 cm), whereas greater distances were

found to previous year's shoot blight symptoms (70.4 cm) (Fig. 2.2). These distances were inversely proportional to the number of symptoms in each symptom type class.

Results of the spatial analysis of symptomatic elements are illustrated in Fig. 2.3 for tree no. VIII, the largest tree in the dataset (1811 total points). The most common nearest-neighbour distance among the 807 *M. laxa*-associated symptoms in this tree was 7–9 cm, which was considerably shorter than the most common nearest-neighbour distance (18–24 cm) obtained by Monte-Carlo simulation within the entire tree volume (Fig. 2.3A), suggesting aggregation relative to CSR. This was confirmed by comparative analysis of the cumulative frequency distributions of observed and simulated nearest-neighbour distances, yielding a significant ($P < 0.001$) d_w value of 0.584 (Fig. 2.3B). This value can be interpreted to mean that 58.4% more of the actual symptoms were spaced at a distance equal to or less than approx. 15 cm from each other, as compared with the random simulation. When similar calculations were conducted for the remaining seven trees, symptomatic elements were found to be significantly aggregated compared with CSR in each case, with d_w ranging from 0.522 to 0.657 (Table 2.2). Thus, nearest-neighbour distances for symptomatic elements were significantly shorter than expected if they were distributed randomly within the canopy.

The next step of the analysis evaluated the deviation of each specific symptom type from the baseline distribution of all symptomatic elements within a given tree. In the majority of symptom type-tree combinations (24 out of 40), no significant deviation from the baseline distribution was observed (Table 2.2). In most of the cases where d_w was statistically significant (14 out of 16), symptoms were less aggregated (i.e. more uniform) than the baseline of all symptomatic elements. An illustrative example of this is given in Fig. 2.4 for blossom blight in tree no. VIII. Only two symptom type–tree combinations (previous year's symptoms and shoot

blight in tree no. IV) showed significant aggregation compared with the baseline (Table 2.2). Thus, whereas *M. laxa*-associated symptoms were generally aggregated within the overall canopy volume (based on the above comparison with CSR), there was little evidence that specific symptom types were more or less aggregated than the overall pattern of all symptomatic elements within the tree.

Pairwise association analyses showed that all trees, with the exception of tree no. I (the smallest tree), had significant associations (either positive or negative) between one or more symptom types, with the most common significant d_w values found when testing association of all current year's symptoms with all previous year's symptoms (Table 2.3). In this case, only tree no. IV showed a negative association, whereas all others were positive, indicating that nearest-neighbour distances between these two symptom types were generally shorter than expected by chance alone. This is illustrated in Fig. 2.5, again using tree no. VIII as an example. Five trees each showed significant associations between all current year's symptoms and previous year's twig cankers and between current year's blossom blight and previous year's twig cankers. In contrast, only two associations between blossom blight and twig cankers (regardless of age) were statistically significant. Whether a significant association was positive or negative appeared to depend more on the tree than on the symptom type examined (Table 2.3).

Discussion

Presented here is the first study to quantify spatial patterns of plant disease in complex three-dimensional fruit tree canopies using nearest-neighbour analysis. Although previous workers have collected data on disease and pest injury within individual trees, the spatial resolution used in earlier studies was generally lower (e.g. as a result of using a limited number of strata or

quadrats within the canopy to summarize patterns) and/or the statistical analyses were more limited in scope (e.g. comparisons between the upper vs. lower or exterior vs. interior canopy). For example, dividing the canopy of fig trees (*Ficus carica* 'Calimyrna') into high or low, north or south, and inner or outer layers, the spread of a fungal pathogen via fig-pollinating wasps showed no significant difference in disease incidence based on an analysis of variance (Michailides and Morgan, 1998). Similarly, the canopy of coast live oak trees (*Quercus agrifolia*) was divided into nine sectors, corresponding to upper, middle and lower portions combined with north-east, south and north-west cardinal directions, in order to examine the distribution of weevil-infested acorns (Lewis, 1992). The statistical analysis (analysis of variance and pairwise comparison) of the 36 trees, each assessed for one of the nine canopy quadrats, showed three of the nine quadrats to have significantly more larval infestation than the others. Compared with these quadrat-based studies, the combination of rapid point pattern collection with a high-precision magnetic digitizer (Moulia and Sinoquet 1993; Smith and Curtis, 1996) and data analysis using a 3-D extension of nearest-neighbour statistics (Scheuerell, 2004) has made it possible to quantify aggregation and association patterns for different symptom types within the canopy both efficiently and effectively.

This pilot study showed that symptoms associated with *M. laxa* infection in sour cherry trees are generally aggregated within the canopy volume, but that there is no consistent pattern for one symptom type to be more or less aggregated than the other (Table 2.2). This result could have been related to the high disease pressure in this organically managed orchard, which may have masked differences in disease aggregation patterns among symptom types that may be more apparent in conditions of lower disease incidence. Alternatively, a pronounced effect of environmental heterogeneity within the canopy (e.g. differences in localized moisture

availability) could have resulted in similar patterns of disease aggregation across symptom types. Heterogeneity in surface wetness, a prerequisite for infection by most fungal plant pathogens, can be marked in fruit tree canopies (Sentelhas *et al.*, 2005) and can significantly impact disease development (Batzer *et al.*, 2008).

Interestingly, results of the pairwise association analyses showed that current year's symptoms were generally (in six out of eight trees evaluated) closer to previous year's symptoms than expected by chance alone (Table 2.3), providing statistical support for the long-standing notion (based on disease cycle research with *Monilinia* spp.) that proximity to within-tree inoculum sources is important for disease progression from one year to the next (Landgraf and Zehr, 1982; Biggs and Northover, 1985, 1988a, b; Hong *et al.*, 1999; Luo and Michailides, 2001; Holb and Scherm, 2007). For spores that are primarily airborne, such as those of *Monilinia* spp. (Corbin *et al.*, 1968), the presence of a pronounced dispersal gradient would readily explain the observed association between current and previous year's symptoms. Rain-splashing (Pauvert *et al.*, 1969) and run-off transport of spores in rain water from twig inoculum sources to other susceptible canopy elements would also favour the short-distance association between current and previous year's symptoms, as has been documented for *Venturia carpophila*, another twig-borne pathogen in peach canopies (Lan and Scherm, 2003).

Although associations of current year's symptoms with specific symptom types from the previous year were not consistently significant (possibly because of smaller sample sizes), it is reasonable to assume that twig cankers formed in the previous year would serve as the most important within-tree inoculum source because of their relatively large number and – consequently – their shorter average distance to current year's symptoms (Fig. 2.2). Stensvand *et al.* (2001) previously documented that sporulation of *M. laxa* on twig cankers of sweet cherry

(*Prunus avium*) peaks around the time of bloom, further supporting the role of twig cankers as a key inoculum source for inciting blossom blight (the most frequent current season's symptom in the present study).

Since the organically managed orchard used for this study had very high brown rot levels, it would be important to confirm the aggregation and association patterns observed here in conditions of lower disease pressure, e.g. in orchards managed using conventional or integrated practices. Spatial patterns are likely to be dependent on the overall levels of disease in a tree, as suggested by the variations in aggregation and association patterns across the eight trees included in the present study (Tables 2.2 and 2.3).

Overall, the results of these analyses quantitatively confirm the role of different symptom types in shaping the pattern of brown rot development within the tree canopy. More importantly, the methodologies for data collection and analysis described here have broader applicability, potentially allowing their use in a range of canopy ecology studies. We are currently working to extend the approach to second-order analyses (considering more than just the nearest neighbour of each point in the analysis of aggregation and association), and also to include a temporal element by digitizing symptomatic elements over time as the epidemic develops. We are further collecting pathogen isolates from all infected elements within each tree to determine the fine-scale genetic structure (Trapnell *et al.,* 2004) of the pathogen population at the canopy-level. We hope that these analyses will help to develop a deeper understanding of patterns of pathogen survival, spread and reproductive strategies within tree canopies.

Acknowledgements

This study was supported by the Hungarian Scientific Research Fund (grant no. HSRF 78339), a János Bolyai Research Fellowship and the Southern-Region IPM Program (grant no. 2009-34103-19818).

Literature Cited

Andrews JH, Kenerley CM, Nordheim EV. 1980. Positional variation in phylloplane microbial populations within an apple tree canopy. Microbial Ecology 6:71-84.

Batzer JC, Gleason ML, Taylor SE, Koehler KJ, Monteiro JEBA. 2008. Spatial heterogeneity of leaf wetness duration in apple trees and its influence on performance of a warning system for sooty blotch and flyspeck. Plant Disease 92:164-170.

Biggs AR, Northover J. Inoculum sources for *Monilinia fructicola* in Ontario peach orchards. 1985. Canadian Journal of Plant Pathology 7:302-307.

Biggs AR, Northover J. 1988a. Early and late-season susceptibility of peach fruits to *Monilinia fructicola*. Plant Disease 72:1070-1074.

Biggs AR, Northover J. 1988b. Influence of temperature and wetness duration on infection of peach and sweet cherry fruits by *Monilinia fructicola*. Phytopathology 78:1352-1356.

Byrde RJW, Willetts HJ. 1977. The brown rot fungi of fruit: their biology and control. Oxford: Pergamon.

Coomes DA, Rees M, Turnbull L. 1999. Identifying aggregation and association in fully mapped spatial data. Ecology 80:554-565.

Corbin JB, Ogawa JM, Schultz HB. 1968. Fluctuations in numbers of *Monilinia laxa* conidia in an apricot orchard during the 1966 season. Phytopathology 58:1387-1394.

Costes E, Lauri PÉ, Regnard JL. 2006. Analyzing fruit tree architecture: implications for tree management and fruit production. Horticultural Reviews 32:1-61.

Elmer PAG, Gaunt RE, Frampton CM. 1998. Spatial and temporal characteristics of dicarboximide-resistant strains of *Monilinia fructicola* and brown rot incidence in stone fruit. Plant Pathology 47:530-536.

Holb IJ, Scherm H. 2007. Temporal dynamics of brown rot in different apple management systems and importance of dropped fruit for disease development. Phytopathology 97:1104-1111.

Hong C, Holtz BA, Morgan DP, Michailides TJ. 1999. Significance of thinned fruit as source of the secondary inoculum of *Monilinia fructicola* in California nectarine orchards. Plant Disease 81:519-524.

Lan Z, Scherm H. 2003. Moisture sources in relation to conidial dissemination and infection by *Cladosporium carpophilum* within peach canopies. Phytopathology 93:1581-1586.

Landgraf FA, Zehr EI. 1982. Inoculum sources for *Monilinia fructicola* in South Carolina peach orchards. Phytopathology 72:185-190.

Leeuwen GCM van, Stein A, Holb I, Jeger MJ. 2000. Yield loss in apple caused by *Monilinia fructigena* (Aderh. & Ruhl.) Honey, and spatio-temporal dynamics of disease development. European Journal of Plant Pathology 106:519-528.

Lewis VR. 1992. Within-tree distribution of acorns infested by *Curculio occidentalis* (Coleoptera: Curculionidae) and *Cydia latiferreana* (Lepidoptera: Tortricidae) on coast live oak. Environmental Entomology 25:975-982.

Luo Y, Michailides TJ. 2001. Risk analysis for latent infection of prune by *Monilinia fructicola* in California. Phytopathology 91:1197-1208.

Michailides TJ, Morgan DP. 1998. Spread of endosepsis in calimyrna fig orchards. Phytopathology 88:637-647.

Moulia B, Sinoquet H. 1993. Three-dimensional digitizing systems for plant canopy geometrical structure: a review. In: Varlet-Grancher C, Bonhomme R, Sinoquet H, editors. Crop structure and light microclimate: characterization and applications. Paris: INRA; p. 183-193.

Pauvert P, Fournet J, Rapilly F. 1969. Etudes sur la dispersion d'un inoculum par des gouttes d'eau en fonction du conceptacle sporifère. Annales de Phytopathologie 1:491-493.

Scheuerell MD. 2004. Quantifying aggregation and association in three-dimensional landscapes. Ecology 85:2332-3240.

Sentelhas PC, Gillespie TJ, Batzer JC, et al. 2005. Spatial variability of leaf wetness duration in different crop canopies. International Journal of Biometeorology 49:363-370.

Smith GS, Curtis JP. 1996. A fast and effective method of measuring tree structure in 3 dimensions. Acta Horticulturae 416:15-20.

Spósito MB, Amorim L, Bassanezi RB, Bergamin Filho A, Hau B. 2008. Spatial pattern of black spot incidence within citrus trees related to disease severity and pathogen dispersal. Plant Pathology 57:103-108.

Stensvand A, Talgo V, Borve J. 2001. Seasonal production of conidia of *Monilinia laxa* from mummified fruits, blighted spurs and flowers of sweet cherry. Gartenbauwissenschaft 66:273-281.

Trapnell DW, Hamrick JL, Nason JD. 2004. Three-dimensional fine-scale genetic structure of the neotropical epiphytic orchid, *Laelia rubescens*. Molecular Ecology 13:1111-1118.

Widder E, Johnsen S. 2000. 3D spatial point patterns of bioluminescent plankton: a map of the ‘minefield’. Journal of Plankton Research 22:409-420.

Wu BM, Subbarao KV. 2004. Analysis of spatial patterns in plant pathology. Recent Research Developments in Plant Pathology 3:167-187.

Xu X-M, Robinson JD, Berrie AM, Harris DC. 2001. Spatio-temporal dynamics of brown rot (*Monilinia fructigena*) on apple and pear. Plant Pathology 50:569-578.

Tables

Table 2.1. Summary of point patterns of brown rot symptoms (caused by *Monilinia laxa*) in the canopies of eight sour cherry trees mapped in three dimensions with a magnetic digitizer

			Symptomatic elements			Specific symptom types[a]		
Tree no.	Total points	Asymptomatic fruit	Previous year	Current year	Total	Blossom blight	Shoot blight	Twig canker
I	261	170	35	56	91	64	19	23
II	268	146	59	63	122	71	19	43
III	643	499	54	90	144	105	43	24
IV	358	137	100	121	221	160	31	60
V	397	81	135	181	316	245	32	75
VI	1335	985	128	222	350	245	53	84
VII	1108	526	235	347	582	439	80	134
VIII	1811	1004	319	488	807	543	92	235
Avg.	773	444	133	196	329	234	46	85

[a] Each symptomatic element may display more than one symptom type, hence the sum of the three specific symptom types is usually greater than the total number of symptomatic elements.

Table 2.2. Index of aggregation (d_w) along with corresponding *P*-values (in parentheses) for point patterns of brown rot symptoms (caused by *Monilinia laxa*) in the canopies of eight sour cherry trees mapped in three dimensions with a magnetic digitizer[a]

	Tree number[b]							
	I	II	III	IV	V	VI	VII	VIII
Symptom type	(n = 91)	(n = 122)	(n = 145)	(n = 221)	(n = 313)	(n = 330)	(n = 582)	(n = 807)
Compared with complete spatial randomness within canopy volume								
All symptoms	**0.522 (<0.001)**	**0.607 (<0.001)**	**0.588 (<0.001)**	**0.634 (<0.001)**	**0.523 (<0.001)**	**0.657 (<0.001)**	**0.623 (<0.001)**	**0.584 (<0.001)**
Compared with observed distribution of all symptomatic elements								
Current year's symptoms	**–0.199 (0.007)**	**–0.231 (0.004)**	–0.106 (0.126)	–0.048 (0.051)	**–0.159 (<0.001)**	**–0.112 (<0.001)**	**–0.124 (<0.001)**	**–0.157 (<0.001)**
Previous year's symptoms	0.131 (0.657)	**–0.180 (0.041)**	**–0.229 (0.013)**	**0.473 (0.001)**	0.047 (0.901)	**–0.213 (<0.001)**	–0.034 (0.924)	**–0.156 (<0.001)**
Blossom blight	–0.114 (0.175)	–0.154 (0.056)	0.0600 (0.490)	**–0.094 (0.039)**	–0.054 (0.138)	–0.056 (0.203)	–0.046 (0.078)	**–0.121 (<0.001)**
Twig blight	–0.155 (0.712)	–0.169 (0.227)	0.206 (0.376)	–0.130 (0.371)	–0.150 (0.140)	**–0.295 (<0.001)**	–0.116 (0.093)	**–0.168 (<0.001)**
Shoot blight	–0.179 (0.713)	0.129 (0.934)	0.225 (0.111)	**0.339 (0.016)**	–0.925 (0.0951)	0.145 (0.349)	0.148 (0.189)	0.070 (0.885)

[a]d_w values calculated based on the cumulative frequency distribution of nearest-neighbour distances between symptoms of the same type. Significant positive values ($P \leq 0.05$; boldfaced) indicate aggregation, whereas significant negative values correspond to a more regular distribution compared with the random simulation.

[b]Trees arranged in order of increasing size (number of symptoms).

Table 2.3. Index of association (d_w) along with corresponding *P*-values (in parentheses) for point patterns of brown rot symptoms (caused by *Monilinia laxa*) in the canopies of eight sour cherry trees mapped in three dimensions with a magnetic digitizer[a]

	Tree number[b]							
	I	II	III	IV	V	VI	VII	VIII
Symptom types	(*n* = 91)	(*n* = 122)	(*n* = 145)	(*n* = 221)	(*n* = 313)	(*n* = 330)	(*n* = 582)	(*n* = 807)
Current year's to previous year's symptoms	0.1488 (0.112)	**0.1943 (0.008)**	**0.1922 (0.009)**	**–0.2925 (<0.001)**	**0.1005 (0.025)**	**0.1860 (<0.001)**	**0.0957 (0.003)**	**0.1791 (<0.001)**
Current year's symptoms to previous year's twig cankers	0.0842 (0.664)	**0.1862 (0.018)**	0.1317 (0.156)	**–0.2103 (<0.001)**	**–0.1411 (0.005)**	**0.1024 (0.038)**	0.0736 (0.061)	**0.1615 (<0.001)**
Blossom blight to twig cankers	0.0451 (0.968)	0.1458 (0.079)	–0.0792 (0.484)	–0.0767 (0.220)	**–0.1388 (0.003)**	0.0480 (0.558)	0.0587 (0.110)	**0.1034 (<0.001)**
Current year's blossom blight to previous year's twig cankers	0.1130 (0.366)	**0.2092 (0.004)**	0.1120 (0.214)	**–0.2421 (<0.001)**	**–0.1152 (0.026)**	**0.1223 (0.006)**	0.0660 (0.112)	**0.1624 (<0.001)**

[a]d_w values calculated based on the cumulative frequency distribution of nearest-neighbour distances between symptoms of different types. Significant positive values ($P \leq 0.05$; boldfaced) indicate that the observed symptoms of the two types are closer together than in the random simulation, whereas significant negative values correspond to a more regular distribution of the two symptom types to each other. For the random simulation, the measured coordinates of all symptomatic elements within each tree served as an empty set of coordinates over which the two symptom types of interest were randomized.

[b]Trees arranged in order of increasing size (number of symptoms).

Figures

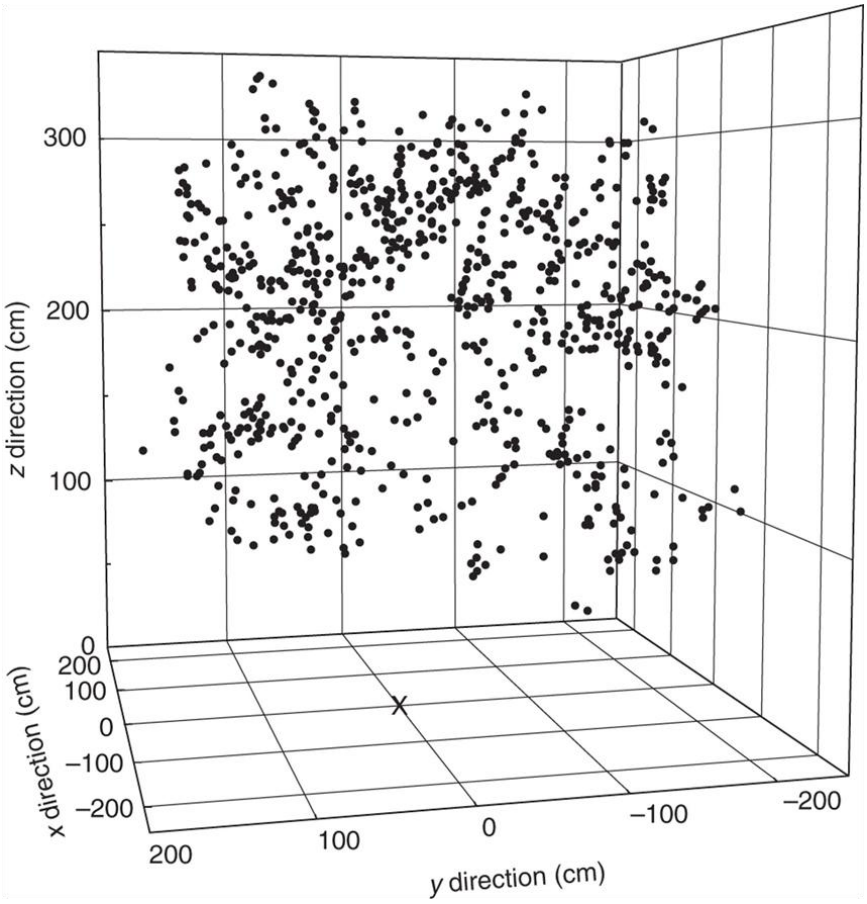

Fig. 2.1. Positions of all 807 brown rot symptoms (blossom blight, blighted shoots, and twig cankers) as mapped in the field in three dimensions with a magnetic digitizer in the canopy of sour cherry tree no. VIII. The data point at the origin (0,0,0) marks the base of the trunk.

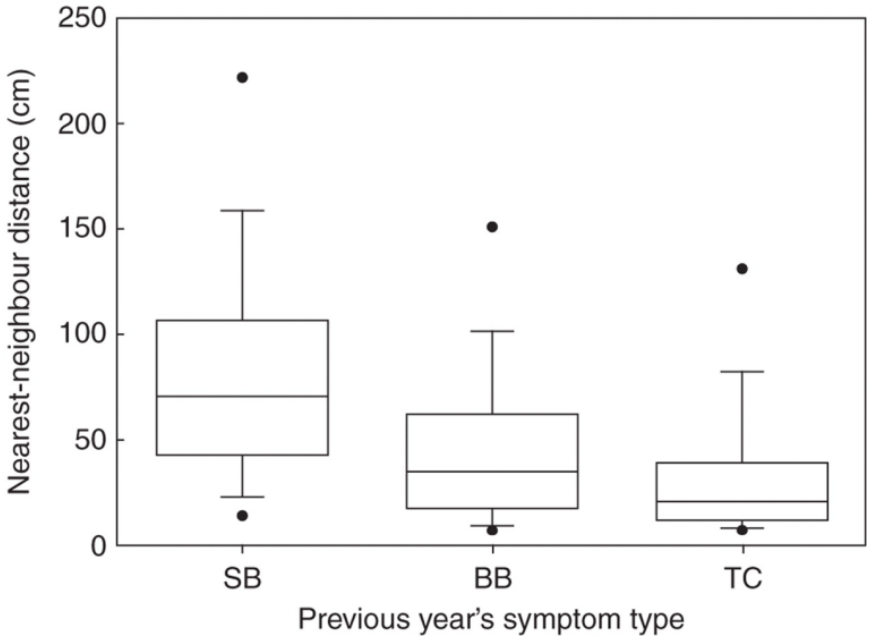

Fig. 2.2. Nearest-neighbour distances between all current year's brown rot symptoms and previous year's shoot blight (SB), blossom blight (BB), and twig cankers (TC) in the canopies of eight sour cherry trees mapped in the field in three dimensions with a magnetic digitizer.

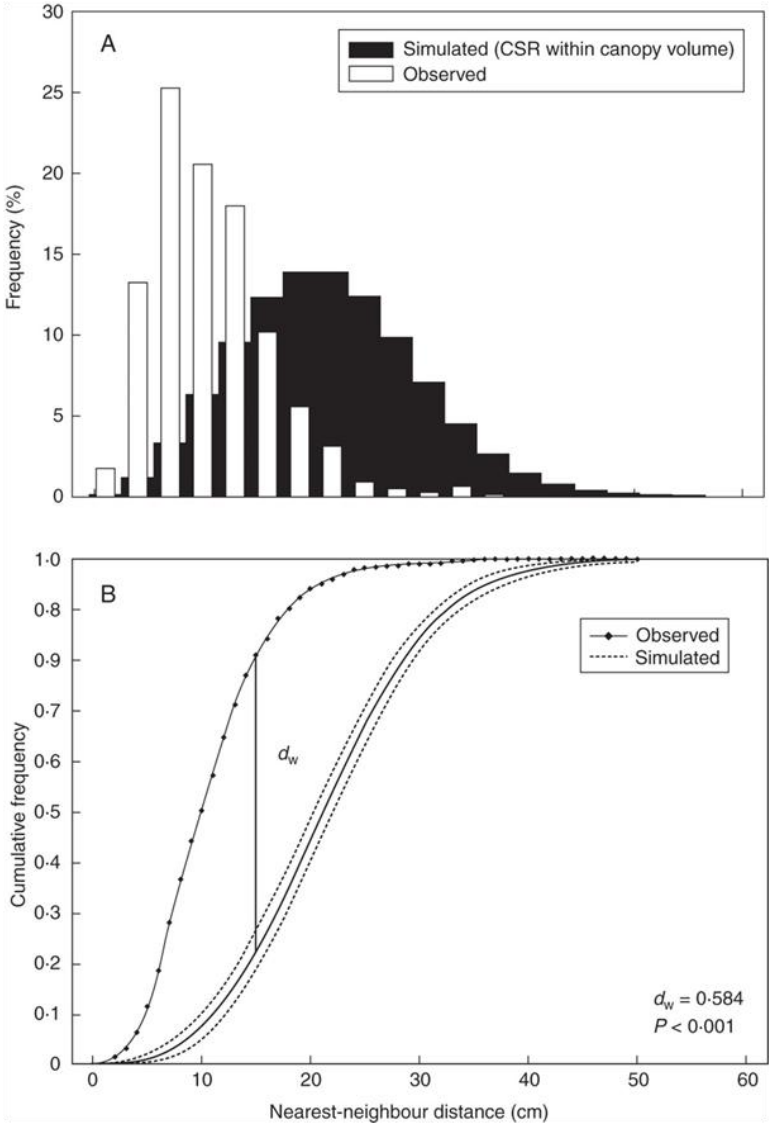

Fig. 2.3. Frequency histogram (A) and cumulative frequency distribution (B) of observed nearest-neighbour distances of all brown rot symptoms in the canopy of sour cherry tree no. VIII, as compared with a simulation assuming complete spatial randomness (CSR) within the canopy volume. The index d_w denotes the maximum deviation between the observed (-●-) and the randomly simulated (---) cumulative frequency distributions; in this case, a significant positive d_w value indicates aggregation of symptoms compared with CSR.

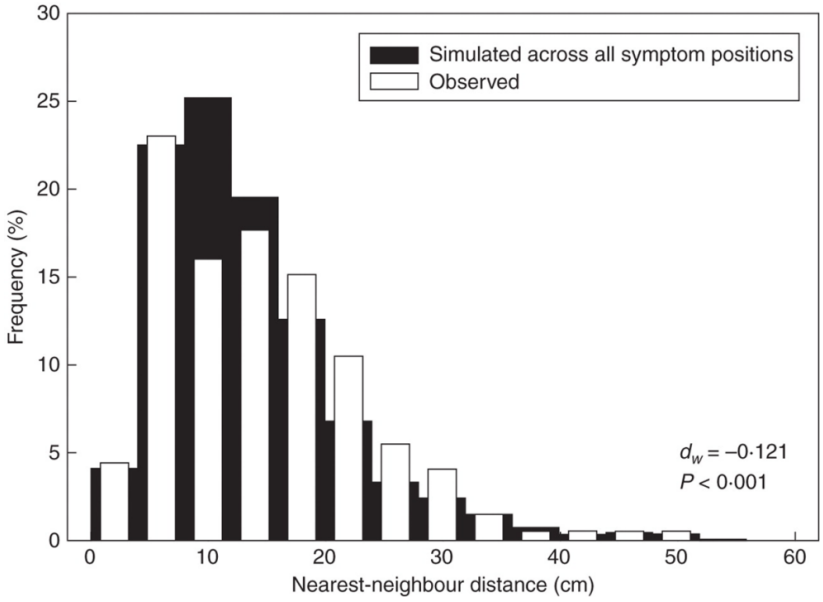

Fig. 2.4. Frequency histogram of nearest-neighbour distances between blighted blossoms in the canopy of sour cherry tree no. VIII, as compared with a simulation assigning the blossom blight symptoms randomly across the coordinates of all symptomatic elements within the tree. The index d_w denotes the maximum deviation between the observed and the randomly simulated cumulative frequency distributions; in this case, a significant negative d_w value indicates a more regular distribution of blossom blight compared with all brown rot symptoms in the tree.

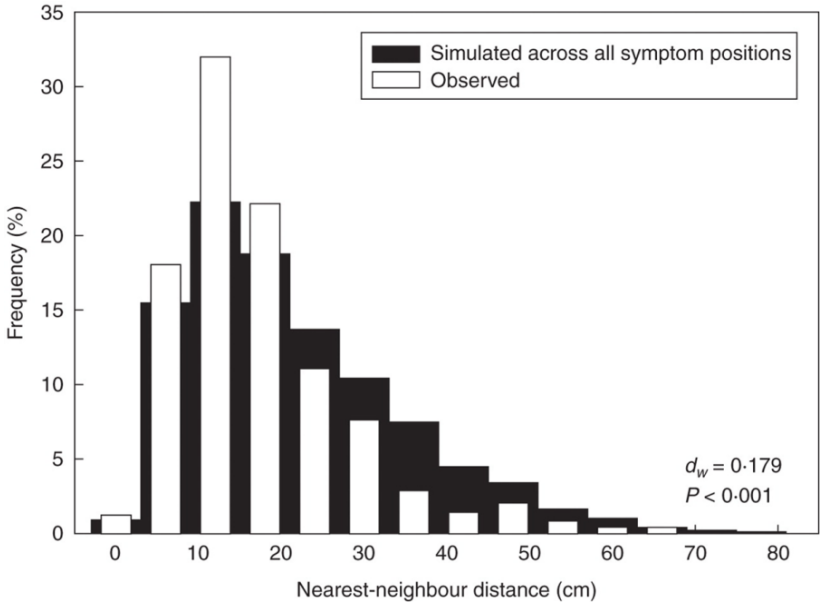

Fig. 2.5. Frequency histogram of nearest-neighbour distances between all current year's brown rot symptoms and previous year's twig cankers in the canopy of sour cherry tree no. VIII, as compared with a simulation assigning the two symptom types randomly across the coordinates of all symptomatic elements within the tree. The index d_w denotes the maximum deviation between the observed and the randomly simulated cumulative frequency distributions; in this case, a significant positive d_w value indicates association, i.e., the observed symptoms of the two types are closer together than in the random simulation.

CHAPTER 3

SPATIAL PATTERNS OF BROWN ROT EPIDEMICS AND DEVELOPMENT OF MICROSATELLITE MARKERS FOR ANALYZING FINE-SCALE GENETIC STRUCTURE OF *MONILINIA FRUCTICOLA* POPULATIONS WITHIN PEACH TREE CANOPIES[1]

[1]Everhart, S.E., A. Askew, L. Seymour, I.J. Holb, and H. Scherm. Accepted in *Plant Health Progress.* Reprinted here with permission of the publisher.

Abstract

To better understand the fine-scale spatial dynamics of brown rot disease and corresponding fungal genotypes, we analyzed three-dimensional spatial patterns of pre-harvest fruit rot caused by *Monilinia fructicola* in individual peach tree canopies and developed microsatellite markers for canopy-level population genetics analyses. Using a magnetic digitizer, high-resolution maps of fruit rot development in five representative trees were generated, and *M. fructicola* was isolated from each affected fruit. To characterize disease aggregation, nearest-neighbor distances among symptomatic fruit were calculated and compared with appropriate random simulations. Within-canopy disease aggregation correlated negatively with the number of diseased fruit per tree ($r = -0.827$, $P = 0.0009$), i.e., aggregation was greatest when the number of diseased fruit was lowest. Sixteen microsatellite primers consistently amplified polymorphic regions in a geographically diverse test population of 47 *M. fructicola* isolates. None of the test isolates produced identical multilocus genotypes, and the number of alleles per locus ranged from 2 to 16. We are applying these markers to determine fine-scale population structure of the pathogen within and among canopies.

Introduction

Analysis of spatial patterns of plant disease in orchard crops can help shed light on the relative importance of different inoculum sources and potential mechanisms of dissemination within and among trees (6,30,33). Most studies have focused on quantifying two-dimensional patterns of disease among trees (i.e., on an *x*-*y* plane), whereas the number of studies explicitly considering three-dimensional disease patterns within canopies (i.e., in an *x*-*y*-*z* cube) has been limited (2,16,28). This is largely due to difficulties associated with accurately mapping and analyzing the hundreds or thousands of points that make up the structurally complex tree canopy. In a previous proof-of-concept study (7),

we utilized a magnetic digitizer to map different brown rot symptom types (blossom blight, shoot blight, and twig cankers) caused by *Monilinia laxa* in individual sour cherry (*Prunus cerasus*) canopies, and applied nearest-neighbor-based, three-dimensional methods of spatial statistics to the resultant data points. This enabled us to determine the level of aggregation of different symptom types in the canopy as well as the degree of association of current year's symptoms with symptoms from previous year's infections. However, since the assessment and mapping in the pilot study were done at a single point in time, prior to the period of fruit maturation, it was not possible to analyze spatio-temporal disease development or to quantify spatial patterns of pre-harvest fruit rot, the most important symptom type, within the canopy. Based on these considerations, we designed a multi-year follow-up study on peach (*Prunus persica*) to monitor the within-canopy development of brown rot (caused by *Monilinia fructicola*) during the course of the season, with special emphasis on the pre-harvest fruit rot phase. Results from five trees monitored in detail during the 2009 growing season are presented herein.

The spatial analysis approach described above considers only phenotypic information, i.e., the location of each symptomatic element (e.g., brown rot-affected fruit) within the canopy. Deeper insight into disease progression may be obtained by including genotypic data about the fungal isolates associated with each symptom. Such information could then be subjected to spatial analysis to describe fine-scale genetic structure within and across canopies (29). This requires isolation of the pathogen from each georeferenced symptomatic element, as well as the availability of suitable markers for quantifying fine-scale genetic structure of *M. fructicola* populations. Most previous studies of the population structure of *Monilinia* spp. in stone fruit orchards (6,10,11,20,26,27) have utilized marker systems with low resolution (e.g., vegetative compatibility groups) or low reproducibility (e.g., RAPDs), hence there is a need to develop a new set of genetic markers for *M. fructicola* that are robust, have high resolution, and are co-dominant to potentially resolve heterokaryotic isolates. Based

on these considerations, a second objective of this study was to develop microsatellite markers for population genetics analysis in *M. fructicola*. Microsatellites are tandem repeated motifs (simple sequence repeats, SSRs) of 1 to 6 bases that are located in both coding and non-coding regions and occur with a high degree of length variation, likely due to slippage during DNA replication (22,23). The major drawback in using microsatellites is that they need to be isolated de novo in each species of interest. However, once developed, the procedure for analyzing and scoring individuals is relatively simple (23).

The purpose of this paper is to report preliminary results of characterizing within-canopy spatial patterns of brown rot epidemics in peach during the pre-harvest fruit rot epidemic, and to describe a set of microsatellite markers developed for *M. fructicola* that can be used for fine-scale genetic analysis of pathogen populations within tree canopies.

Materials and Methods

Spatial data collection. The study was conducted from late March to September 2009 in a research peach orchard at the University of Georgia Horticulture Farm in Watkinsville, GA. The orchard was established in 2000 with six peach cultivars of varying maturity dates, planted in replicated four-tree plots. During the study, no fungicide applications to control brown rot were made, but foliar sprays of wettable sulfur were applied during the cover spray period to suppress peach scab (caused by *Fusicladium carpophilum*); measures for thinning and arthropod and weed management followed standard commercial practice (14). Six trees were pre-selected at the beginning of the season for initial disease monitoring, and 10 additional trees were added in mid-season, prior to fruit rot development. The selection was based on criteria such as having characteristic canopy size (approximately 1.6 to 2.0 m high and 3.4 to 5.8 m wide) and a spherical to oblong canopy without major gaps, representing

different maturity classes, and including trees with and without blossom blight symptoms in the spring. This set of 16 trees was purposefully larger than the number of trees that could be managed later in the season for detailed disease assessment, high-resolution symptom mapping, and pathogen isolation from all symptomatic elements. As the season progressed, trees were eliminated from the monitoring based on factors such as lack of disease development, limb breakage, and bird or insect damage to fruit. This process of elimination resulted in a final set of five trees of different maturity groups and with varying levels of disease incidence at the end of the 2009 harvest season (Table 3.1).

At 3- to 10-day intervals from bloom through final fruit swell and then continuing at 1- to 4-day intervals until the tree-ripe stage of fruit development, trees were monitored visually for symptoms associated with *M. fructicola* infections, including blossom blight, twig blight, twig cankers, green fruit rot, and brown rot of mature fruit. When a new symptom was found, it was swabbed with a sterile cotton-tipped applicator to sample conidia, and a plastic tag was tied to the branch, proximal to the point where the symptomatic element originated. Each symptomatic element was given a unique identifier associated with the tag and the fungal isolate obtained. Thus, the location and approximate date of appearance of each symptom and corresponding isolate was known.

When fruit had reached commercial maturity, high-resolution three-dimensional maps were made for each of the five trees using a FASTRAK 3Space magnetic digitizer (Polhemus, Colchester, VT) (24). This device creates an electromagnetic field within which a stylus is used to obtain coordinates of objects relative to an emitter. The *x*, *y*, and *z*-coordinates of all tags (corresponding to symptomatic elements) were digitized using the stylus, as were all symptomatic and asymptomatic fruit for a total of up to 396 data points per tree. Having a record of the approximate date of appearance of each symptomatic element allowed the production of temporal maps of the symptoms present up to each assessment date (Fig. 3.1).

Spatial pattern analysis. Spatial patterns of aggregation of fruit affected by brown rot within the canopy were characterized based on the frequency distribution of nearest-neighbor distances among symptoms in each tree (4,21), as in Everhart et al. (7). To obtain an appropriate random distribution of the same number of symptoms for comparison, the measured coordinates of all fruit (symptomatic + asymptomatic) served as an empty set of coordinates over which the symptomatic fruit were assigned randomly to generate 1000 Monte-Carlo simulations for each tree. The cumulative frequency distribution of the observed nearest-neighbor distances among affected fruit was compared with that of the simulations using a Kolmogorov-Smirnov test. If symptoms were more aggregated than when assigned randomly, the cumulative frequency distribution would be above the upper 95% confidence band for the simulations, whereas if data were regular it would fall below the lower confidence band. The test statistic d_w, the maximum vertical departure of the observed cumulative frequency distribution from that obtained for the simulations, was used as an index of aggregation (4). A significant positive value of d_w indicates aggregation, whereas a significant negative value signifies uniformity. Cumulative frequency distributions of nearest-neighbor distances and the resultant d_w values were used to assess the magnitude and significance of deviation from randomness. All calculations were carried out in Matlab R2011b (Mathworks, Natick, MA).

Development of microsatellite markers. Microsatellite markers were developed following the general protocol of Glenn and Schable (12). DNA from isolate MfLittle of *M. fructicola* (isolated from the UGA Horticulture Farm in 2008) was digested with Rsa I (New England Biolabs, Ipswich, MA), after which SuperSNX24 linkers (Forward 5'-GTTTAAGGCCTAGCTAGCAGCAGAATC and Reverse 5'-GATTCTGCTAGCTAGGCCTTAAACAAAA) were ligated at the ends, enabling enrichment via PCR. The resulting product was probed for microsatellite repeats (di-, tri-, and tetranucleotide repeats)

using complementary biotinylated oligonucleotides ligated to strepavadin-coated magnetic beads (Dynabeads; Invitrogen, Carlsbad, CA), which enabled hybridization-capture of fragments with microsatellite repeats. The enriched/recovered DNA was subsequently incorporated into a cloning vector (TOPO TA kit; Invitrogen), which resulted in a library of 159 transformed *E. coli* colonies that was sequenced and yielded 58 unique microsatellite repeats.

Amplification primers were designed for 54 microsatellite repeats with suitable flanking sequence (8). To enable indirect fluorescent labeling, primer pairs were synthesized with the addition of a CAG label (CAGTCGGGCGTCATCA added to the 5'-end of the shorter primer), and each PCR reaction included a HEX-labeled primer complementary to the CAG-label (3,9). In total, 40 microsatellite primers and 12 polymorphic microsatellite markers previously developed for *Sclerotinia* spp. (25,32), members of the same family as *Monilinia* spp., were synthesized and screened for amplification with a preliminary subset of seven isolates of *M. fructicola* (7O, 26-N14, D92-2C, W619H, AP16.04, BGA7.04, and SCDL21). All DNA extractions utilized aerial mycelium from 7-day-old cultures and were performed using the DNeasy Plant Mini Kit (Qiagen, Valencia, CA). PCR reactions were mixed using hot-start Taq (JumpStart Taq; Sigma-Aldrich, St. Louis, MO) following the manufacturer's reaction specifications, scaled to 25 µL, and modified to contain a 1:10 ratio of CAG-labeled-primer to CAG label. PCR conditions utilized a touchdown treatment where 20 cycles from 60 to 50.5°C enabled a range of primer melting temperatures to be met, followed by 15 cycles to increase the number of amplicons (5). Specifically, thermocycle conditions consisted of an initial treatment at 95°C for 2.5 min; 20 cycles of 95°C for 20 sec, 60°C for 20 sec (decreased by 0.5°C for every cycle), and 72°C for 30 sec; followed by 15 cycles of 95°C for 20 sec, 50°C for 20 sec, and 72°C for 30 sec. A 1:10 dilution of amplicons was denatured and analyzed using capillary electrophoresis (3730xl DNA Analyzer; Applied Biosystems, Carlsbad, CA). From the 52 primer sets screened, six

yielded amplification in all seven isolates, 11 required re-design of one or both primers to amplify the locus in all isolates, and 35 did not amplify sufficiently (including all those developed previously for Sclerotinia spp.). Ultimately, 17 functional primer sets were developed for preliminary polymorphism screening.

To assess markers for polymorphisms, DNA was purified from a test set of 47 isolates of *M. fructicola* obtained from stone fruit production regions in middle Georgia, north Georgia, North Carolina, South Carolina, and Virginia (Table 3.2). These isolates had been collected either from diseased fruit or blossoms of peach or plum (*Prunus domestica*) between 1982 and 2010. All 17 loci showed amplification, but one locus had more than 10% null alleles and was therefore excluded. Locus Mf-SEA and Mf-SEK yielded two and one null allele(s), but this was not considered sufficient for exclusion. Subsequent data analysis to examine the number of alleles per locus and haploid genetic diversity were performed using GenAlEx 6.4 (18,19). Using Multilocus 1.3b (1), we calculated the multilocus genotype saturation curve as well as the index of association, IA (to test whether two individuals that are the same at one locus are more likely to be the same at another). Finally, the 16 microsatellite primers were screened against four isolates of *M. laxa* (ML15FC and ML11 from Italy, Holb2 from Hungary, and Quince2010 from Delaware) to determine their utility for population genetics analyses in this closely related species. However, none of the primer pairs sufficiently cross-amplified to warrant further development for *M. laxa* (data not shown).

Results and Discussion

Spatio-temporal patterns within the tree canopy. The first brown rot symptoms on ripening fruit were observed 10 to 37 days before commercial maturity, with final fruit rot incidence (at the tree-ripe stage of fruit development) reaching between 30.2 and 58.2% (Table 3.1). Spatial coordinates of

symptomatic and asymptomatic fruit were readily collected with the magnetic digitizer (Fig. 3.1), whereby a single mapping of an individual tree (having 126 to 396 fruit total) required between 2 and 4 hours by a two-person team. Median nearest-neighbor distances, calculated from the spatial coordinates of each fruit, ranged from 5.7 to 14.7 cm among all fruit and 11.8 to 20.6 cm among symptomatic fruit at the time of digitization (Fig. 3.2).

For determining aggregation patterns of symptomatic fruit, epidemics were divided into two or three phases for each tree, corresponding to early, middle, and late assessment periods during the pre-harvest brown rot epidemic; the middle phase was not included for all trees (Table 3.1), especially where the overall duration of the epidemic was short. It is important to note that 'early' in this context does not necessarily correspond to low disease incidence, particularly for the later-maturing trees where disease onset occurred very rapidly and reached high incidence levels within a short period (e.g., Flameprince trees 45 and 120 in Table 3.1). Results showed that the index of aggregation, d_w, was negatively correlated with the number of diseased fruit across all trees and phases (Fig. 3.3), i.e., aggregation was greatest when the number of diseased fruit was lowest. However, only the largest of the d_w values (>0.25) were significantly different from zero. Overall, three of the five trees had random patters of pre-harvest brown rot during all assessment phases, one tree had a significantly aggregated pattern of disease during all phases, and one tree had a pattern of diseased fruit that changed from significantly aggregated during the early phase to random during the mid and late season of the epidemic (Table 3.1).

One tree that deviated somewhat from the pattern of increased aggregation associated with lower disease incidence was Redglobe 7 (Table 3.1). This early-maturing tree suffered some damage from crows (*Corvus brachyrhynchos*) during the ripening phase, requiring bird netting to protect the tree. Despite these efforts, we cannot exclude the possibility that bird damage influenced the spatial

pattern of disease in this tree, possibly leading to lower d_w values at low incidence levels (Fig. 3.3). Indeed, when the data from Redglobe 7 were omitted from the correlation analysis shown in Fig. 3.3, r improved from −0.827 to −0.908 and P from 0.0009 to 0.0007. Overall, these results support the notion that aggregation of disease is more pronounced with fewer inoculum sources (earlier in the pre-harvest season and/or fewer diseased fruit). That is not to say that trees with more inoculum sources lack spatial structure, but that aggregation is likely obscured by multiple, overlapping disease distributions within the same tree.

Preliminary evaluation of microsatellite markers. Sixteen of the 40 primer sets evaluated consistently amplified polymorphic microsatellite regions in the test population of 47 *M. fructicola* isolates, with amplicons ranging from 91 to 270 bp in length (Table 3.2). Although previous cytological studies have shown that fungi in the genus Monilinia are multinucleate (~5 to 10 nuclei per conidium) (13,15,31), only one peak was detected for each locus, which is consistent with the haploid-monokaryotic state of other fungi in the Sclerotinaceae (17,25,32). The number of alleles per locus ranged from 2 to 16, with an average of 9 alleles per locus. With the exception of locus Mf_G6H6 for the isolates from middle Georgia, all primer pairs yielded more than one locus per region. The haploid genetic diversity at each locus was 0.519 to 0.905, with an average of 0.724.

Combining banding profiles across loci for each individual showed that none of the isolates produced an identical multilocus genotype. The index of association was not significant (I_A = 0.086, P = 0.108), indicating no multilocus linkage disequilibrium. As an indication of resolving power of these microsatellite markers, 95% of the multilocus genotypes were resolved with the use of 7 loci, and 99% of genotypes were resolved with 13 loci (Fig. 3.4). Thus, use of all 16 polymorphic microsatellite markers should be suitable for differentiating multilocus genotypes at a fine-scale.

Conclusions

The approach presented here, although preliminary with respect to the one-year data set used for illustration, provides a firm foundation for future research on canopy disease dynamics, particularly with respect to the production and analysis of high-resolution canopy disease maps. Our results showed that the relative degree of aggregation of affected fruit decreased with increasing numbers of diseased fruit. This demonstrates that two-dimensional paradigms in spatial epidemics translate to three-dimensional coordinate systems. Further interpretation of the disease patterns observed in this study will be possible through population genetics analyses of the associated pathogen isolates, for which the set of 16 microsatellites developed and characterized herein provides the necessary foundation. These markers will be used to genotype ~700 isolates collected from diseased fruit or blossoms from canopies monitored between 2009 and 2011, representing all infections within each tree during the entire season. Three-dimensional spatial autocorrelation of multilocus genotypes (29) can then be applied to characterize the fine-scale spatial genetic structure of *M. fructicola* populations within trees, helping to shed light on within-tree inoculums sources and the relative contribution of sexual vs. asexual modes of pathogen reproduction during the growing season.

Acknowledgements

Funded in part by grant no. 2009-34103-19818 from the USDA Southern Region IPM Program. We thank Guido Schnabel, David Ritchie, and Elizabeth Little for providing isolates used in microsatellite development and polymorphism screening, and Amy Savelle, Sara Thomas, and Lucky Mehra for help in digitizing tree canopies.

Literature Cited

1. Agapow, P. -M., and Burt, A. 2001. Indices of multilocus linkage disequilibrium. Molecular Ecology Notes 1:101-102.

2. Andrews, J. H., Kenerley, C.M., and Nordheim, E. V. 1980. Positional variation in phylloplane microbial populations within an apple tree canopy. Microbial Ecology 6:71-84.

3. Boutin-Ganache, I., Raposo M., Raymond M., and Deschepper, C. F. 2001. M13-tailed primers improve the readability and usability of microsatellite analyses performed with two different allele-sizing methods. Biotechniques 31:24-28

4. Coomes, D. A., Rees M., and Turnbull, L. 1999. Identifying aggregation and association in fully mapped spatial data. Ecology 80:554-565.

5. Don, R.H., Cox, P. T., Wainwright, B. J., Baker, K., and Mattick, J. S. 1991. 'Touchdown' PCR to circumvent spurious priming during gene amplification. Nucleic Acids Research 19:4008.

6. Elmer, P. A. G., Gaunt, R. E., and Frampton, C. M. 1998. Spatial and temporal characteristics of dicarboximide-resistant strains of *Monilinia fructicola* and brown rot incidence in stone fruit. Plant Pathology 47:530-536.

7. Everhart, S. E., Askew, A., Seymour, L., Holb, I. J., and Scherm, H. 2011. Characterization of three-dimensional spatial aggregation and association patterns of brown rot symptoms within intensively mapped sour cherry trees. Annals of Botany 108:1195-1202.

8. Faircloth, B. C. 2008. MSATCOMMANDER: detection of microsatellite repeat arrays and automated, locus-specific primer design. Molecular Ecology Resources 8:92-94.

9. Faircloth, B. C., Terhune, T. M., Schable, N. A., Glenn, T. C., Palmer, W. E., and Carroll, J. P. 2008. Ten microsatellite loci from northern bobwhite (*Colinus virginianus*). Conservation Genetics. doi 10.1007/s10592-008-9559-4

10. Förster, H., and Adaskaveg, J. E. 1999. Early brown rot infections in sweet cherry fruit are detected by *Monilinia*-specific DNA primers. Phytopathology 90:171-178.

11. Gell, I., Larena, I., and Melgarejo, P. 2007. Genetic diversity in *Monilinia laxa* populations in peach orchards in Spain. Journal of Phytopathology 155:549-556.

12. Glenn, T. C., and Schable, N. A. 2005. Isolating microsatellite DNA loci. Methods in Enzymology 395:202-222.

13. Hall, R. 1963. Cytology of the asexual stages of the Australian brown rot fungus *Monilinia fructicola* (Wint.) Honey. Cytologia 28:181-193.

14. Horton, D., Brannen, P., Bellinger, B., Lockwood, D., and Ritchie, D. 2011. Southeastern Peach, Nectarine, and Plum Pest Management and Culture Guide. Bulletin 1171, University of Georgia Cooperative Extension Service, Athens.

15. Margosan, D. A., and Phillips, D. J. 1985. Effect of two temperatures on nuclear number of conidia of *Monilinia fructicola.* Mycologia 77:835–837.

16. Michailides, T. J., and Morgan, D. P. 1998. Spread of endosepsis in calimyrna fig orchards. Phytopathology 88:637-647.

17. Njambere, E. N., Vandemark, G., and Chen, W. 2010. Development and characterization of microsatellite markers for the fungal plant pathogen *Sclerotinia trifoliorum*. Genome 53:494-500.

18. Nei, M. 1973. Analysis of gene diversity in subdivided populations. Proceedings of the National Academy of Sciences 70:3321-3323.

19. Peakall, R., and Smouse, P. E. 2006. GENALEX 6: genetic analysis in Excel. Population genetic software for teaching and research. Molecular Ecology Notes 6:288-295.

20. Scherm, H., and Emery, K. M. 2002. Vegetative compatibility in populations of *Monilinia fructicola* from Georgia peach orchards. Acta Horticulturae 592:725-727.

21. Scheuerell, M. D. 2004. Quantifying aggregation and association in three-dimensional landscapes. Ecology 85:2332-3240.

22. Schlötterer, C., and Tautz, D. 1992. Slippage synthesis of simple sequence DNA. Nucleic Acids Research 20:211-215.

23. Selkoe, K. A., and Toonen, R. J. 2006. Microsatellites for ecologists: a practical guide to using and evaluating microsatellite markers. Ecology Letters 9:615-629.

24. Sinoquet, H. Rivet, P., and Godin, C. 1997. Assessment of the three-dimensional architecture of walnut trees using digitising. Silva Fennica 31:265-273.

25. Sirjusingh, C., and Kohn, J. M. 2001. Characterization of microsatellites in the fungal plant pathogen, *Sclerotinia sclerotiorum*. Molecular Ecology Notes 1:267-269.

26. Snyder, C. L., and Jones, A. L. 1999. Genetic variation between strains of *Monilinia fructicola* and *Monilinia laxa* isolated from cherries in Michigan. Canadian Journal of Plant Pathology 21:70-77.

27. Sonoda, R. M., Ogawa, J. M., and Manji, B. T. 1991. Population structure of *Monilinia fructicola* in *Prunus persica* var. *nucipersica* tree canopies. Mycological Research 95:893-895.

28. Spósito, M. B., Amorim, L., Bassanezi, R. B., Bergamin Filho, A., and Hau, B. 2008. Spatial pattern of black spot incidence within citrus trees related to disease severity and pathogen dispersal. Plant Pathology 57:103-108.

29. Trapnell, D. W., Hamrick, J. L., and Nason, J. D. 2004. Three-dimensional fine-scale genetic structure of the neotropical epiphytic orchid, *Laelia rubescens*. Molecular Ecology 13: 1111-1118.

30. van Leeuwen, G. C. M., Stein, A., Holb, I., and Jeger, M. J. 2000. Yield loss in apple caused by *Monilinia fructigena* (Aderh. & Ruhl.) Honey, and spatio-temporal dynamics of disease development. European Journal of Plant Pathology 106:519-528.

31. Willetts, H. J., and Calonge, F. D. 1969. Spore development in the brown rot fungi (*Sclerotinia* spp.). New Phytologist 68:123-131.

32. Winton, L. M., Krohn, A. L., and Leiner, R. H. 2007. Microsatellite markers for *Sclerotinia subarctica* nom. prov., a new vegetable pathogen of the High North. Molecular Ecology Notes 7:1077-1079.

33. Xu X. -M., Robinson, J. D., Berrie, A. M., and Harris, D.C. 2001. Spatio-temporal dynamics of brown rot (*Monilinia fructigena*) on apple and pear. Plant Pathology 50:569-578.

Tables

Table 3.1. Spatial point patterns of pre-harvest brown rot, caused by *Monilinia fructicola*, in five intensively mapped peach tree canopies.

Tree[a]	Total fruit	Assessment period[b]	Symptomatic fruit	Disease incid. (%)	d_w [c]	*P* value	Pattern
Redglobe 7	248	Early	26	10.5	0.135	0.812	Random
		Mid	63	25.4	0.116	0.454	Random
		Late	87	35.1	0.099	0.405	Random
O'Henry 26	244	Early	35	14.3	0.360	0.003	Aggregated
		Mid	128	52.5	0.079	0.342	Random
		Late	142	58.2	0.047	0.806	Random
O'Henry 127	126	Early	25	19.8	0.359	0.024	Aggregated
		Late	38	30.2	0.264	0.026	Aggregated
Flameprince 45	385	Early	122	31.7	–0.116	0.097	Random
		Late	169	43.9	–0.064	0.450	Random
Flameprince 120	396	Early	76	19.2	0.128	0.256	Random
		Late	128	32.3	0.054	0.821	Random

[a] Arranged in order from earliest to latest-maturing cultivar.
[b] Trees were monitored for disease at 1- to 4-day intervals during the pre-harvest period, and data are summarized for two or three assessment periods for each tree to facilitate data presentation and analysis.
[c] d_w represents the index of disease aggregation and is calculated based on the cumulative frequency distribution of nearest-neighbor distances among brown rot-affected fruit. Significant positive values ($P \leq 0.05$; underlined) indicate aggregation, whereas significant negative values correspond to a more regular distribution compared with the random simulation.

Table 3.2. Primer details, core sequences, allelic properties, and gene diversity (*h*) of 16 polymorphic PCR-based microsatellite markers developed for *Monilinia fructicola* and evaluated in a test population of 47 isolates.

						No. of alleles for sub-populations[a]			
Locus	Primer sequence (5'-3')	Repeat motif	Cloned allele (bp)	Size range (bp)	No. of alleles	Middle GA	North GA	Carolinas	*h*
Mf-SEA	GAGTTTTCGGGATGGGGAG (CAG)-AACTGATATACGAACTTCTAGGAC	$(CTTT)^{9}$	139	124-156	8	6	5	4	0.519
Mf-SEB	(CAG)-AGGATTCGTCAAGAAGTCAATC TCTGCGTATTTATTACTTTGGGTAG	$(GGAT)^{10}$	129	119-231	16	7	9	8	0.905
Mf-SEC	CTCTCAACACCTGGGCATTC (CAG)-GAAGAGAGGGAAAGAGAGCG	$(AATC)^{5}$ $(CATT)^{5}$	139	144-199	15	8	9	9	0.907
Mf-SED	(CAG)-TTGGCATGGCATTTGGAGC CCATTTTATTCATATCCAACGCCC	$(GGAT)^{6}$	106	111-149	12	9	7	7	0.875
Mf-SEE	(CAG)-TGGACCAACACAGCTACGG GGGTCCTCGCGTTTGATTTG	$(GT)^{12}$	128	144-152	2	1	2	2	0.083
Mf-SEF	TGTCTCTCAACTTTTAAATCAGCC (CAG)-GACTATAGAGTTTTCTACGGATGG	$(AATC)^{8}$	113	111-156	11	6	8	5	0.850
Mf-SEG	(CAG)-CCTACCCAATCTACCTAGTAACC CCAAAGCAAAGTAGAGCAAAGC	$(AGGATG)^{4}$	124	99-139	4	2	4	2	0.549
Mf-SEI	(CAG)-CTCAAGCGGTGGCTCAAAG TAACCACCACGACCACGAC	$(ATC)^{7}$	87	91-139	10	6	7	4	0.746
Mf-SEJ	(CAG)-TCCTTTCCGTTCCTCTTCCTG CCGACGACAGACCAACAAAC	$(CCTTT)^{4}$	89	97-132	6	6	8	3	0.735
Mf-SEK	(CAG)-GCTACTAAGAGCCTAGCG TGCTTTACTGGAGCTGTGTTTG	$(CATT)^{6}$	227	228-268	13	7	6	9	0.872
Mf-SEL	(CAG)-GAGTATAACCAACCCAACGGC AGAGATGGAGTCAGGAGTGTTG	$(CATT)^{7}$	127	135-147	4	3	4	3	0.726
Mf-SEM	(CAG)-GGGAGAGTGGGAGATTGGG GGGACCCTTGGACAGCAG	$(ACTC)^{7}$	108	121-187	12	9	7	6	0.892
Mf-SEN	(CAG)-TGCGTGTCATGTCGTCC CGAGGCTTAACTTCCGTGC	$(CT)^{12}$	138	219-252	5	3	5	4	0.742
Mf-SEP	(CAG)-TCCCATACTAGGCCACAGC ATCAATTGGTTTGGGTCCTTG	$(ACCT)^{6}$	233	242-270	8	5	6	2	0.629
Mf-SEQ	(CAG)-GGAGGTGGATGGTGGGTAG TGGCTGTGGGTTGAGTGAG	$(AG)^{10}$	131	129-143	8	4	6	6	0.837
Mf-SER	(CAG)-GCGTGCGGCCTATCAAAC TGCTTGGATTTTCTGTGAAGGG	$(ACCT)^{6}$	117	130-182	10	6	7	4	0.722

[a] Test populations were obtained from stone fruit production regions in middle Georgia (*n* = 14 isolates); north Georgia (*n* = 21); and North Carolina, South Carolina, and Virginia (*n* = 12).

Figures

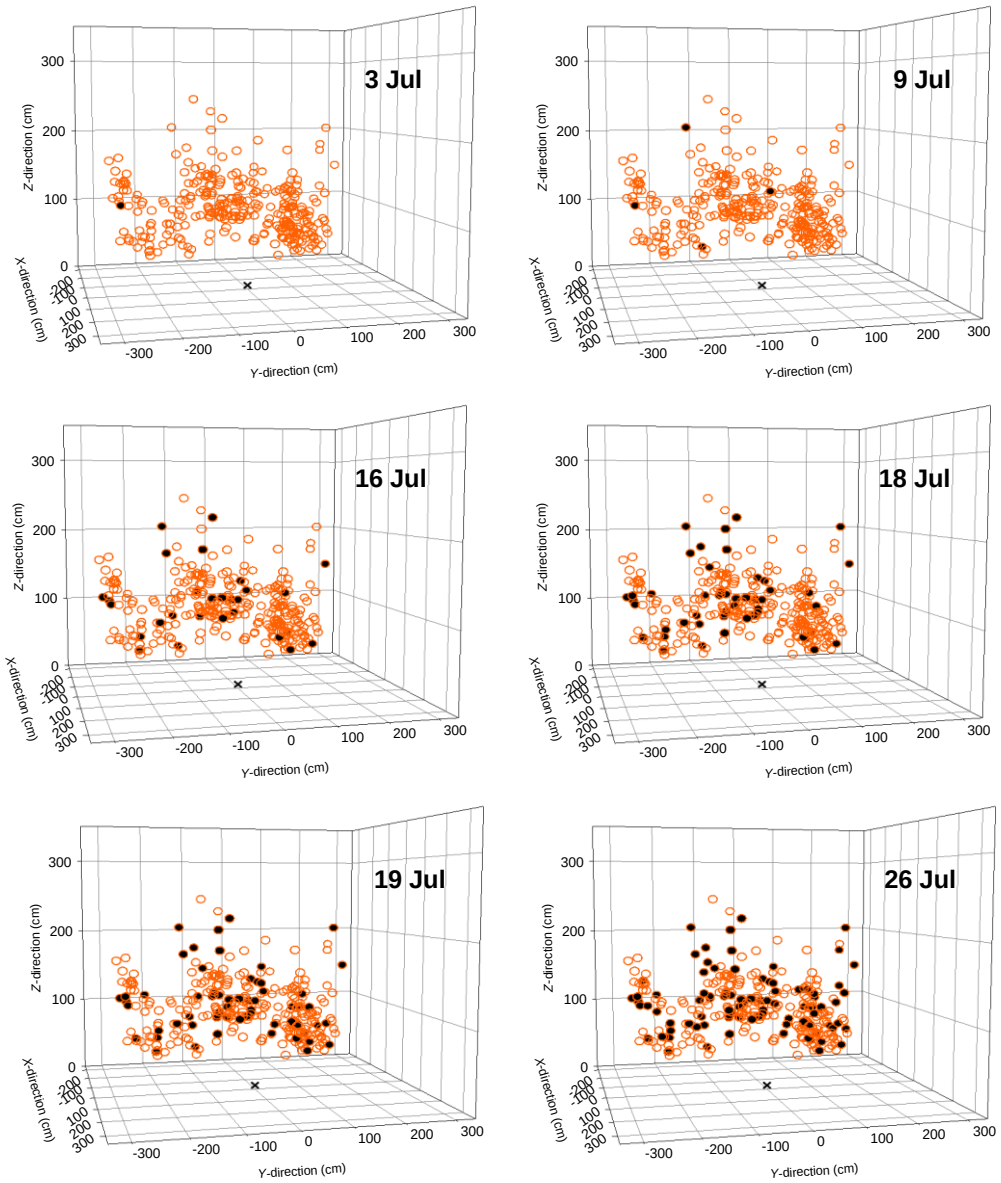

Fig. 3.1. Three-dimensional canopy map of peach tree Redglobe 7 showing the spatial location of each peach fruit and the development of brown rot on selected assessment dates from 3 through 26 July 2009. Open and closed symbols represent asymptomatic and symptomatic fruit, respectively. The x symbol marks the base of the trunk.

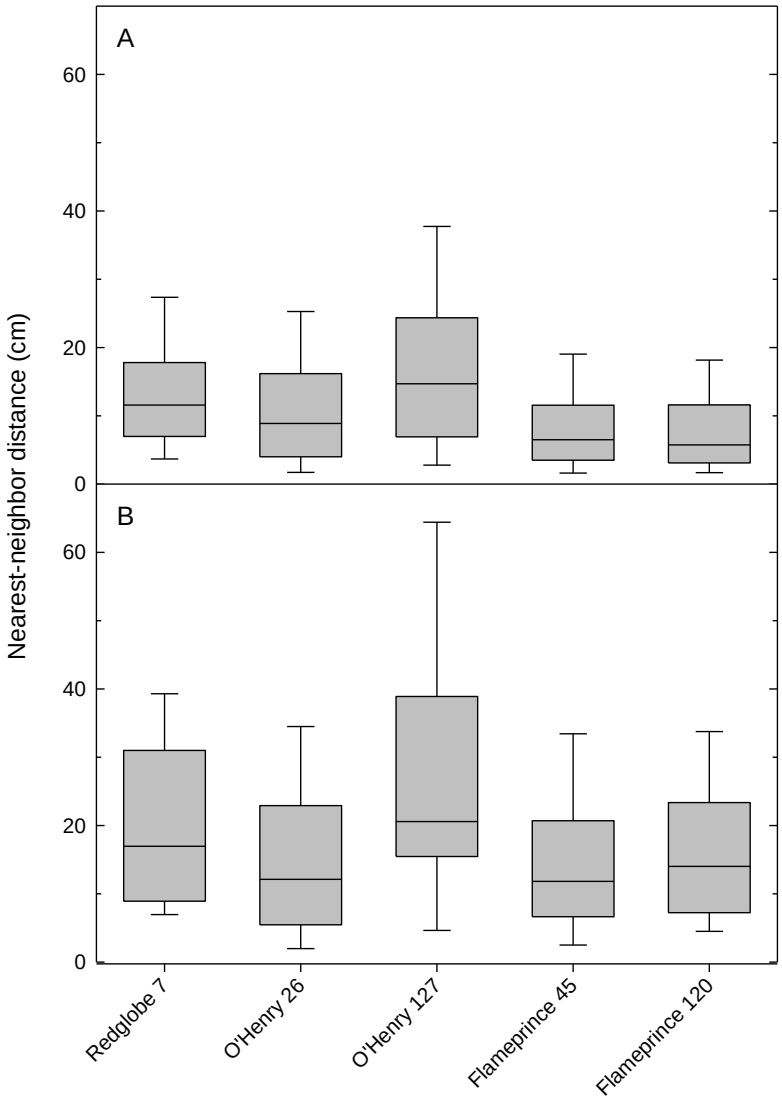

Fig. 3.2. Distributions of nearest-neighbor distances among all fruit (A) and among brown rot-affected fruit at the end of the epidemic (B) in five intensively mapped peach tree canopies.

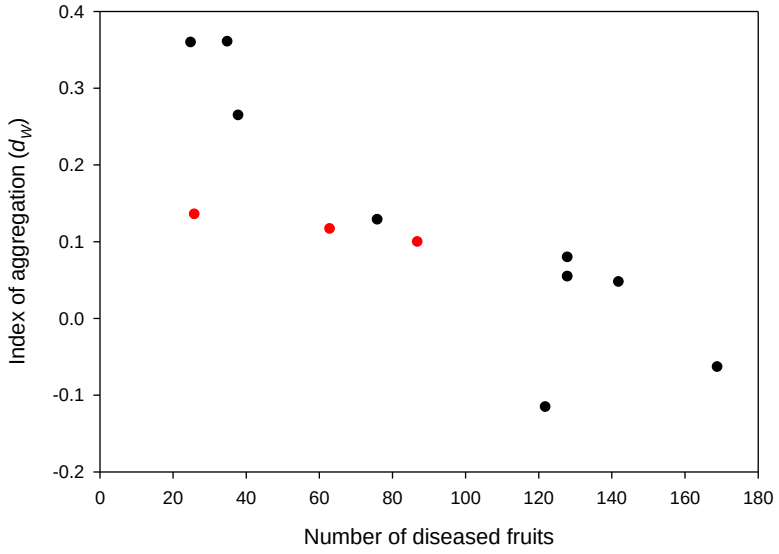

Fig. 3.3. Plot of d_w, an index of disease aggregation, vs. the number of brown rot infected fruit in five intensively mapped peach tree canopies. d_w is calculated based on the cumulative frequency distribution of nearest-neighbor distances among brown rot-affected fruit. Positive values indicate aggregation, whereas negative values correspond to a more regular distribution compared with the random simulation. Data are from early, mid, and late assessment periods during the epidemic as shown in Table 3.1. Data points in red correspond to the early-maturing cultivar Redglobe 7, which suffered some bird damage to fruit.

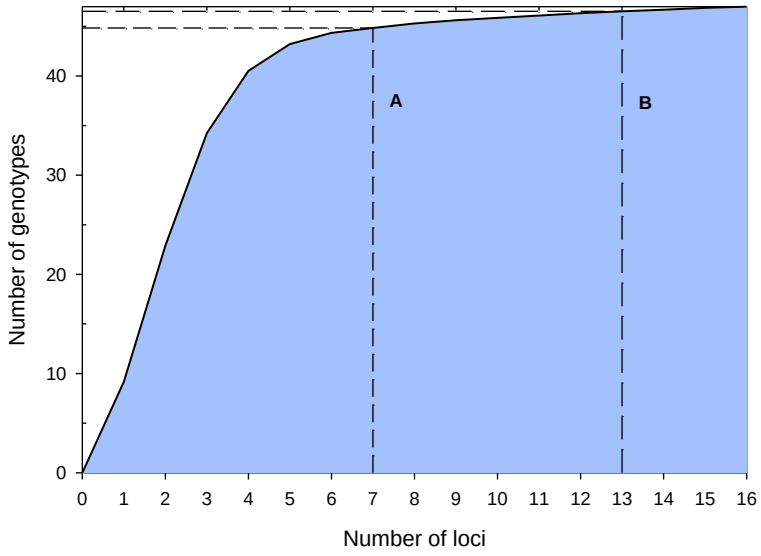

Fig. 3.4. Performance of 16 microsatellite markers developed *de novo* for *Monilinia fructicola* when evaluated with a test populations of the fungus from stone fruit production regions in middle Georgia (*n* = 14 isolates); north Georgia (*n* = 21); and North Carolina, South Carolina, and Virginia (*n* = 12). Seven markers resolved 45 of 47 genotypes (A) whereas 13 markers resolved 46 of 47 genotypes (B).

CHAPTER 4

SPATIO-TEMPORAL PATTERNS OF PRE-HARVEST BROWN ROT EPIDEMICS WITHIN INDIVIDUAL PEACH TREE CANOPIES[1]

[1]Everhart, S.E., A. Askew, L. Seymour, and H. Scherm. Submitted to *European Journal of Plant Pathology*, 6/25/2012.

Abstract

Tree canopies are inherently complex and pose several challenges for quantifying and characterizing spatial patterns of disease. Recently developed methods for fine-scale canopy mapping and three-dimensional spatial pattern analysis were applied in a 3-year study to characterize spatio-temporal development of pre-harvest brown rot of peach, caused by *Monilinia fructicola*, in 13 trees of different maturity classes. We observed a negative correlation between an index of disease aggregation and disease incidence in the same tree ($r = -0.653$, $P < 0.0001$), showing that trees with higher brown rot incidence had lower aggregation of affected fruit in their canopies. Significant ($P \leq 0.05$) within-canopy aggregation among symptomatic fruit was most pronounced for early-maturing cultivars and/or early in the epidemic. This is consistent with the notion of a greater importance of localized, within-tree sources of inoculum at the beginning of the epidemic. Four of five trees having >10 blossom blight symptoms showed a significant positive spatial association of pre-harvest fruit rot to blossom blight within the same canopy. Spatial association analyses further revealed one of two outcomes for the association of new fruit rot symptoms with previous fruit rot symptoms in the same tree, whereby the relationship was either insignificant or exhibited a significant negative association. In the latter scenario, the newly diseased fruit were farther apart from previously symptomatic fruit than expected by random chance. This unexpected result could have been due to uneven fruit ripening in different sectors of the canopy, which could have affected the timing of symptom development and thus led to negative spatial associations among symptoms developing over time in a tree.

Key words: Canopy, *Monilinia fructicola*, peach, *Prunus persica*, spatial analysis, spatial pattern

Introduction

Analysis of spatial patterns of plant disease as a means of quantifying spatial structure and inferring processes has come of age during the past two decades (Jeger 1999; Waggoner and Aylor 2000). In recent years, emphasis has begun to broaden from the traditional focus of characterizing disease patterns at the field scale toward analyzing spatial patterns at larger (landscape) or smaller (within-plant) scales, or across hierarchies from plants to landscapes (Moslonka-Lefebvre et al. 2010; Plantegenest et al. 2007; Vereijssen et al. 2007). Nevertheless, there is a paucity of research addressing plant disease aggregation and association patterns in individual plant canopies, especially in trees which possess complex canopies. Such within-canopy patterns may arise due to the non-random arrangement of susceptible plant parts (such as leaves, blossoms, or fruit) in the tree canopy, and/or the proximity of within-tree inoculum sources (such as cankers). Disease patterns in tree canopies may also be influenced by abiotic factors such as within-tree variability in microclimate (e.g., wetness duration) or fungicide coverage (Batzer et al. 2008; Smith and MacHardy 1984). Thus, pathogen, host, and abiotic factors may interact to produce complex spatial patterns of disease within these canopies.

Characterization of spatial patterns of disease in tree canopies is challenged by difficulty in recording spatial location of symptomatic tissues and in selecting the appropriate statistical approach that will account for the naturally non-random pattern of susceptible plant parts. Previous studies examining spatial disease patterns within tree canopies either divided the canopy into layers (Holb and Scherm 2007) or quadrats (Batzer et al. 2008; Spósito et al. 2008). However, an important limitation of using layers or quadrats is that the associated grouping of data may fail to capture fine-scale patterns within each block. In a recent pilot study (Everhart et al. 2011) we used an electromagnetic digitizer to map different brown rot symptom types

(blossom blight, shoot blight, and twig cankers) caused by the fungal plant pathogen *Monilinia laxa* in individual sour cherry canopies and applied nearest neighbor-based spatial analysis methods to the resultant three-dimensional map of data points. This enabled us to determine the level of aggregation of different symptom types in the canopy as well as the degree of association of current year's symptoms with symptoms from previous year's infections. However, since disease assessment and mapping in the aforementioned study were done at a single point in time, prior to the period of fruit maturation, it was not possible to analyze spatio-temporal disease development or to quantify spatial patterns of pre-harvest fruit rot, the economicallymost important symptom type, within the canopy. Hence, we designed a 3-year follow-up study on peach (*Prunus persica*) to monitor the spatio-temporal development of brown rot (caused by *Monilinia fructicola*) during the course of the season and to quantify spatial aggregation and association patterns within each canopy. Preliminary results based on the first year of data have been reported in a conference paper (Everhart et al. 2012).

Materials and methods

Disease Monitoring and Canopy Mapping. The study was conducted in an experimental peach orchard at the University of Georgia Horticulture Farm (Watkinsville, GA, USA) from late March to September in 2009, 2010, and 2011. The orchard had been planted in 2000 and consisted of six cultivars of varying maturity classes, arranged in replicate four-tree plots having within and across-row spacing of 4.6 and 6.1 m, respectively. Early-season cultivars reached commercial ripeness in mid-June, mid-season cultivars in early July, and late-season cultivars in early August. No fungicide applications to control brown rot were made to the test trees, but foliar sprays of wettable sulfur were applied during the cover spray period across the orchard to

suppress peach scab (caused by *Fusicladium carpophilum*). All other horticultural and pest management followed standard commercial practice (Horton et al. 2011). Trees were thinned relatively lightly to ensure a sufficient number of fruit per tree for within-tree mapping and spatial analysis.

Factors considered in selection of the individual trees used in this study were as follows: canopy shape and structure (spherical to oblong, without major gaps); size of the tree (characteristic size of 1.3 to 2.0 m high and 2.9 to 5.8 m wide); and inclusion of trees from early-, mid-, and late-season maturity classes. Some trees were monitored for disease from blossom blight to fruit drop, whereas others were monitored only during the pre-harvest fruit rot phase. Candidate trees were selected in the spring based on the aforementioned criteria. As the season progressed, some trees were eliminated from the monitoring based on factors such as lack of disease development, limb breakage, and bird or insect damage to fruit. Collectively across the 3 years, this process resulted in a final set of 13 trees of different maturity classes and varying levels of disease incidence at the end of the season (Table 4.1).

Trees were monitored for disease at 3- to 5-day intervals through final fruit swell and then every 1 to 4 days until fruit were tree-ripe. Symptoms and signs associated with *M. fructicola* infections, including blossom blight, twig blight, twig cankers, green fruit rot, and brown rot of mature fruit were noted, and the position of each was preserved by tying a plastic label on the twig proximal to the node associated with the symptom. Each label was marked with the date of symptom appearance and a unique identifying number. Thus, the spatial location and approximate date of appearance of each symptom were preserved.

High-resolution three-dimensional maps of the positions of symptom tags and of all fruit (symptomatic and asymptomatic) were created for each tree using an electromagnetic digitizer

(FASTRAK 3Space, Polhemus, Colchester, VT, USA; Sinoquet et al. 1997). This device creates a low-level electromagnetic field from an emitter positioned at the base of the tree and allows the user to position a sensor at the location of each point and record the corresponding *x*-, *y*-, and *z*-coordinates (Everhart et al. 2011). The instrument's range and accuracy are 4.6 m and 0.76 mm, respectively. Trees were digitized once in 2009 (when fruit were tree-ripe) and twice in 2010 and 2011 (at the beginning of the pre-harvest interval for all fruit and again at the end of the epidemic for all tagged symptoms). The resultant data set consisted of the *x*-, *y*-, and *z*-coordinates of all fruit (126 to 861) and all symptoms (38 to 169) for each tree, along with the date when each symptom was first recorded.

Analysis of Spatial Aggregation and Association. Spatial patterns of aggregation of fruit affected by brown rot within the canopy were characterized based on the frequency distribution of nearest-neighbor distances among symptomatic fruit in each tree (Everhart et al. 2011). To obtain a corresponding random distribution of the same number of symptoms for comparison, the measured coordinates of all fruit (symptomatic + asymptomatic) were used as a set of coordinates over which the symptomatic fruit were randomized to generate 1000 Monte-Carlo simulations for each tree. The cumulative frequency distribution of the observed nearest-neighbor distances among affected fruit was compared with that of the simulations using a Kolmogorov-Smirnov test ($P \leq 0.05$). The test statistic d_w, the maximum departure of the observed cumulative frequency distribution from that of the simulations, was used as an index of spatial aggregation (Coomes et al. 1999). A significant positive value of d_w indicates aggregation, whereas a significant negative value signifies uniformity or regularity. Cumulative frequency distributions of nearest-neighbor distances and the resultant d_w values were used to

assess the magnitude and significance of deviation from randomness. All calculations were carried out in Matlab R2011b (Mathworks, Natick, MA, USA).

Aggregation indexes were calculated separately for different phases (early, mid-period, and late) of the pre-harvest brown rot epidemic (Table 4.1). Each of these phases was defined individually for each tree using roughly equally sized groups of fruit that had become symptomatic over time, or by using natural breakpoints in disease progression. For example, epidemics in which the disease developed over regular intervals were divided into two to three roughly equal-sized groups, with no group containing less than ten affected fruit. Other epidemics yielded a large number of newly symptomatic fruit in a single assessment, and in those cases symptoms that appeared on the same assessment date were not partitioned into separate groups for analysis.

Nearest-neighbor distances were also used to quantify spatial associations among all pre-harvest fruit rot symptoms to the position of blighted blossoms earlier in the season for trees having ten or more blossom blight symptoms present (this was the case for five of the 13 trees). Similarly, associations among symptomatic fruit within the pre-harvest fruit rot epidemic were compared for all trees between phases of the epidemic recorded at different periods during the pre-harvest interval. A spatial association index was calculated among the fruit that became newly symptomatic during the mid-period (or late period) and those that had been symptomatic in the previous period. As with aggregation, the index of association was based on a comparison of the cumulative frequency distribution of the actual nearest-neighbor distances among fruit in the two classes with that of the corresponding random simulation. In the case of blossom blight association analyses, the randomization consisted of 1000 Monte-Carlo simulations of pre-harvest fruit rot assigned across the coordinates of all fruit (symptomatic + asymptomatic),

whereby, blossom blight locations maintained a fixed position throughout the simulations. For analysis of spatial associations within the pre-harvest fruit rot epidemic, both the newly affected fruit and the previously affected fruit were randomly simulated across the measured coordinates of all fruit (symptomatic + asymptomatic) in the respective tree. In both cases, the cumulative frequency distributions of the observed and simulated nearest-neighbor distances were compared by Kolmogorov-Smirnov test, and d_w, the maximum vertical departure of the two distributions, was used as an index of association. A significant positive value of d_w indicates positive spatial association (i.e., newly affected and previously affected fruit are located closer to each other than by random chance), whereas a significant negative value signifies negative spatial association.

Results and discussion

Pre-harvest fruit rot epidemics were monitored and mapped in a total of 13 tree canopies across the 3 years, five in 2009, seven in 2010, and one in 2011 (Table 4.1). Disease development was limited in 2011 due to dry weather during the spring and summer, hence only one tree was included from that year; this tree, O'Henry 26, was monitored in all 3 years of the study. Across the 13 trees, the total number of fruit per tree ranged from 126 to 861 (a function of tree size and fruit set in a given year) and final disease incidence at the tree-ripe stage of fruit development from 11.1 to 58.2%.

Median nearest-neighbor distances among all fruit (symptomatic + asymptomatic) varied from 4.5 to 16.9 cm (average: 6.9 cm) across the 13 canopies (Fig. 4.1a) and, as expected based on the laws of geometry, correlated negatively with fruit number per tree ($r = -0.595$, $P = 0.0320$). For symptomatic fruit at the end of the assessment period, median nearest-neighbor distances were in the range of 10.7 to 20.6 cm with an average of 15.2 cm (Fig. 4.1b). Disease

incidence correlated negatively with the number of fruit per tree (Fig. 4.2; $r = -0.613$, $P = 0.0260$), indicating that canopies with more fruit had a higher disease incidence. This could have been due to a more favorable microclimate and/or more conducive conditions for disease spread via splashing or direct fruit-to-fruit contact in canopies with closely spaced fruit (Luo and Michailides 2003; Michailides and Morgan 1997).

The spatial pattern of pre-harvest fruit rot within individual canopies was assessed at successive intervals (early, mid-period, and late) during the epidemic. Correlation analysis using data from all trees and all intervals revealed a negative relationship between the index of aggregation and disease incidence (Fig. 4.3; $r = -0.653$, $P < 0.0001$). Thus, trees with higher brown rot incidence had lower aggregation of affected fruit within their canopies. Decreasing spatial structure with increasing disease incidence is also commonly observed in studies reporting two-dimensional spatial analyses, e.g., among plants within a field (Pethybridge et al. 2010; Vereijssen et al. 2006). In the present study, there was no correlation between the index of disease aggregation and the total number of fruit per tree ($P = 0.3214$).

Nine of the 13 trees showed significant within-canopy aggregation of disease for at least one phase of the epidemic, with the remaining four exhibiting random patterns during all phases (Table 4.1). Three of the four trees with consistently random pattern were of the late-season cultivar Flameprince. In these trees, the lack of spatial structure among brown rot-infected fruit could have been due to a dominance of external sources of inoculum in the orchard late in the season owing to the presence of high levels of brown rot in the surrounding early- and mid-season cultivars. For example, the earlier-maturing Contender and Redglobe harbored numerous diseased fruit with abundant *M. fructicola* sporulation in the tree and/or on the ground while Flameprince was nearing commercial harvest maturity. The fourth tree with a consistently

random pattern of pre-harvest brown rot in the canopy was Redglobe 7, a mid-season cultivar that differed from the other trees in that it suffered above-average (>25%) bird damage to the fruit owing to its location near the edge of the orchard and being the first to ripen among trees of the same cultivar. Since wounds can serve as important points of entry for *M. fructicola* (Kable 1969), the spatial pattern of wounding and disease may have been confounded in this tree.

All of the early- and mid-season cultivars (with the exception of the aforementioned Redglobe 7) showed an aggregated within-canopy pattern of fruit rot at the early phase of the epidemic. This is consistent with the notion of a greater importance of localized, within-tree sources of inoculum at the beginning of the epidemic in the orchard. Indeed, the earliest-maturing tree, Sureprince 79, exhibited disease aggregation throughout its entire epidemic. In contrast, late-season cultivars showed a lower prevalence of trees with aggregation in the early phase of the epidemic (four of nine trees). Furthermore, regardless of cultivar maturity class, aggregation was less common in the late phase of the epidemic (only five of 13 trees showed significant aggregation), whereby trees with aggregation in the late phase of the epidemic also had aggregation of disease in the early or mid-phase of the epidemic.

Thus, both cultivar maturity season and within-tree epidemic phase (early, mid-period, and late) affected the aggregation pattern of brown rot within canopies, with aggregation being most pronounced for early-season cultivars and/or early in the epidemic for a given tree. In contrast, aggregation was least pronounced in late-season cultivars and/or late into the within-tree epidemic, most likely due to increased inoculum loads in the orchard and in individual trees leading to a more random pattern of disease. A conceptual model linking time, cultivar maturity season, epidemic phase, disease incidence, and disease aggregation based on the relationships observed in this study is depicted in Fig. 4.4.

There were five out of 13 trees that had ten or more blighted blossoms, which allowed examination of spatial association of pre-harvest fruit rot to blossom blight earlier in the season (Table 4.2). Results showed that, with the exception of the smallest tree (O'Henry 127), all trees showed a significant positive association of pre-harvest fruit rot to blossom blight symptoms within the same canopy. This result is consistent with previous work showing that removing blighted blossoms reduced fruit rot incidence within an orchard (Dunegan and Goldsworthy 1948) and that blossom blight incidence within individual trees was related to latent fruit infections (Emery et al. 2000). Whether blossom blight provided a continuous source of inoculum through the fruit ripening phase to result in positive spatial association, or whether blossom blight led to latent infections that then served as the source of inoculum during the pre-harvest epidemic can not be determined from this data.

Each tree was also analyzed for spatial association within the pre-harvest epidemic. Results revealed that most new fruit rot symptoms were either not significantly or were significantly negatively associated with previous fruit rot symptoms in the same tree canopy (Table 4.3). Only two trees showed a significantly positive association between groups of fruit that became symptomatic within successive phases of the epidemic. There were no significant correlations or nonlinear relationships between the index of association and other variables such as number of fruit per tree or level of aggregation of diseased fruit in the previous phase (data not shown).

The lack of a positive spatial association among fruit that became symptomatic in a later phase of the epidemic with those that were symptomatic in the preceding phase in the same tree was unexpected in that it seemed reasonable to hypothesize that newly infected fruit would, on average, be closer to previously infected fruit than by random chance. Instead, eight of the 20 (=

40.0%) tree-epidemic phase comparison combinations showed significant negative associations, meaning that newly diseased fruit were on average farther away from previously diseased fruit than expected. One explanation could be the timescale over which associations were examined. For example, it is possible that an association between diseased fruit in the pre-harvest epidemic would be strongest during the time when conditions are conducive for disease (i.e., within each phase rather than between phases).

Another possible explanation for the negative association between phases of the epidemic may be a reflection of the relatively greater importance of external sources of inoculum vs. within-tree sources. This idea is supported by the fact that significant negative associations were more common (six out of 13 combinations = 46.2%) in late-season cultivars (where overall orchard-wide inoculum load would have been higher) than in early- and mid-season cultivars (two out of seven combinations = 28.6%). In addition to external inoculum load, another potential explanation for the lack of positive spatial associations among fruit becoming symptomatic within different epidemic phases may be that the pattern of fruit ripening may affect the timing of symptom development, such that uneven fruit ripening in different sectors of the canopy (Lewallen and Marini 2003) could lead to negative associations among newly developing brown rot symptoms.

Conclusions

We are aware of no previous studies that characterized the spatio-temporal within-canopy development of disease season-long across multiple years. High-resolution three-dimensional maps conveniently generated with an electromagnetic digitizer enabled characterization of disease aggregation and association patterns within each of the 13 intensively monitored trees. In

general, this approach to canopy mapping and spatial analysis should be applicable to a wide range of studies in plant pathology, pest management, and canopy ecology in trees with complex structure. For pre-harvest brown rot of peach, our analyses supported some commonly held epidemiological concepts, e.g., that aggregation among symptomatic individuals decreases as disease incidence increases, and that fruit rot symptoms are positively associated with the locations of blossom blight earlier in the season. However, the analyses also revealed complex interactions between time, cultivar maturity season, within-tree epidemic phase, disease incidence, and disease aggregation that could not have been predicted *a priori*. Finally, the analyses also produced some unexpected results, particularly the lack of a positive spatial association among fruit that became symptomatic in a later phase of the epidemic with those that were symptomatic in the preceding phase in the same tree, leading to the formulation of testable hypotheses about the impact of uneven fruit ripening patterns within the tree on disease spread. Ultimately, the high complexity of tree canopies is evidenced by this outcome, whereby factors such as microclimatic variation, host physiology, and biotic influences (bird or insect damage) may play an important role in shaping disease aggregation and association patterns. Further interpretation of the spatial patterns observed in this study will be possible through population genetics analyses of pathogen isolates obtained from each symptomatic fruit in select trees in this study (Chapter 5).

Acknowledgements

We thank Amy Savelle, Sara Thomas, and Lucky Mehra for their assistance in digitizing tree canopies. Funded in part by grant no. 2009-34103-19818 from the USDA Southern Region IPM Program. Additional financial support provided by the American Phytopathological Society's

Tarleton Fellowship, a Sigma Xi Grant-in-Aid of Research, and a University of Georgia Dissertation Completion Award to S.E.E.

References

Batzer, J. C., Gleason, M. L. Taylor, S. E., Koehler, K. J. & Monteiro, J. E. B. A. (2008) Spatial heterogeneity of leaf wetness duration in apple trees and its influence on performance of a warning system for sooty blotch and flyspeck. *Plant Disease, 92*, 164-170.

Coomes, D., Rees, M. & Turnbull, L. (1999) Identifying aggregation and association in fully mapped spatial data. *Ecology, 80*, 554-565.

Dunegan, J. C. & Goldsworthy, M. C. (1948) The control of blossom blight and its relation to brown rot of Red Bird peaches at harvest. *Plant Disease Reporter 32*, 136-137.

Emery, K. M., Michailides, T. J. & Scherm, H. (2000). Incidence of latent infection of immature peach fruit by *Monilinia fructicola* and relationship to brown rot in Georgia. *Plant Disease, 84*, 853-857.

Everhart, S. E., Askew, A., Seymour, L., Glenn, T. C. & Scherm, H. (2012) Spatial patterns of brown rot epidemics and development of microsatellite markers for analyzing fine-scale genetic structure of *Monilinia fructicola* populations within peach tree canopies. *Plant Health Progress*, in press.

Everhart, S. E., Askew, A., Seymour, L., Holb, I. J. & Scherm, H. (2011) Characterization of three-dimensional spatial aggregation and association patterns of brown rot symptoms within intensively mapped sour cherry trees. *Annals of Botany, 108*, 1195-1202.

Holb, I. J. & Scherm, H. (2007) Temporal dynamics of brown rot in different apple management systems and importance of dropped fruit for disease development. *Phytopathology, 97*, 1104-1111.

Horton, D., Brannen, P., Bellinger, B., Lockwood, D. & Ritchie, D. 2011. Southeastern peach, nectarine, and plum pest management and culture guide. Athens, GA: University of Georgia Cooperative Extension Service.

Jeger, M. J. (1999) Improved understanding of dispersal in crop pest and disease management: current status and future directions. *Agricultural and Forest Meteorology, 97*, 331-349.

Lewallen, K. S. & and Marini, R. P. (2003) Relationship between flesh firmness and ground color in peach as influenced by light and canopy position. *J. Amer. Soc. Hort. Sci., 128*, 163-170.

Kable, P. (1969) Brown rot of stone fruits on the Murrumbidgee Irrigation Areas. I. Aetiology of the disease in canning peaches. *Australian Journal of Agricultural Research*, 20, 301-316.

Luo, Y. & Michailides, T. J. (2003) Threshold conditions that lead latent infection to prune fruit rot caused by *Monilinia fructicola*. *Phytopathology, 93*, 102-111.

Michailides, T. J. & Morgan, D. P. (1997) Influence of fruit-to-fruit contact on the susceptibility of French prune to infection by *Monilinia fructicola*. *Plant Disease, 81*, 1416-1424.

Moslonka-Lefebvre, M., Finley, A., Dorigatti, I., Dehnen-Schmutz, K., Harwood, T., Jeger, M. J., Xu, X., Holdenrieder, O. & Pautasso, M. (2010) Networks in plant epidemiology: from genes to landscapes, countries, and continents. *Phytopathology, 101*, 392-403.

Pethybridge, S. J., Hay, F. S. & Gent, D. H. (2010) Characterization of the spatiotemporal attributes of sclerotinia flower blight epidemics in a perennial pyrethrum pathosystem. *Plant Disease, 94*, 1305-1313.

Plantegenest, M., Le May, C. & Fabre, F. (2007) Landscape epidemiology of plant diseases. *Journal of the Royal Society Interface, 4*, 963-972.

Sinoquet, H., Rivet, P. & Godin, C. (1997) Assessment of the three-dimensional architecture of walnut trees using digitising. *Silva Fennica, 31*, 265–273.

Smith, F. D. & MacHardy, W. E. (1984) The retention and redistribution of captan on apple foliage. *Phytopathology, 74*, 894-899.

Spósito, M. B., Amorim, L., Bassanezi, R. B., Filho, A. B. & Hau, B. (2008) Spatial pattern of black spot incidence within citrus trees related to disease severity and pathogen dispersal. *Plant Pathology, 57*, 103-108.

Vereijssen, J., Schneider, J., Stein, A. & Jeger, M. (2006) Spatial pattern of Cercospora leaf spot of sugar beet in fields in long- and recently-established areas. *European Journal of Plant Pathology, 116*, 187-198.

Vereijssen, J., Schneider, J. H. M. & Jeger, M. J. (2007) Epidemiology of Cercospora leaf spot on sugar beet: modeling disease dynamics within and between individual plants. *Phytopathology, 97*, 1550-1557.

Waggoner, P. E. & Aylor, D. E. (2000) Epidemiology: a science of patterns. *Annual Review of Phytopathology, 38*, 71-94.

Tables

Table 4.1. Spatial aggregation patterns of pre-harvest brown rot, caused by *Monilinia fructicola*, in 13 intensively mapped peach tree canopies.

Cultivar and tree number [a]	Year	Total fruit	Assessment period [b]	Symptomatic fruit	Disease incid. (%)	d_w [c]	*P*	Pattern
Early-season cultivar								
Sureprince 79	2010	250	Early	26	10.4	0.375	0.004	Aggregated
			Mid	48	19.2	0.291	0.004	Aggregated
			Late	83	33.2	0.177	0.015	Aggregated
Mid-season cultivars								
Redglobe 7	2009	248	Early	26	10.5	0.135	0.812	Random
			Mid	63	25.4	0.116	0.454	Random
			Late	87	35.1	0.099	0.405	Random
Contender 74	2010	433	Early	41	9.5	0.240	0.042	Aggregated
			Late	123	28.4	0.123	0.075	Random
Contender 75	2010	392	Early	12	3.1	0.616	0.000	Aggregated
			Mid	48	12.2	0.254	0.018	Aggregated
			Late	59	15.1	0.179	0.103	Random
Late-season cultivars								
O'Henry 26	2009	244	Early	35	14.3	0.360	0.003	Aggregated
			Mid	128	52.5	0.079	0.342	Random
			Late	142	58.2	0.047	0.806	Random
O'Henry 26	2010	486	Early	18	3.7	0.440	0.010	Aggregated
			Mid	67	13.8	0.330	0.000	Aggregated
			Late	88	18.1	0.290	0.000	Aggregated

O'Henry 26	2011	861	Early	21	2.4	0.226	0.310	Random
			Mid	56	6.5	<u>0.290</u>	0.031	Aggregated
			Late	96	11.1	0.104	0.363	Random
O'Henry 127	2009	126	Early	25	19.8	<u>0.359</u>	0.024	Aggregated
			Late	38	30.2	<u>0.264</u>	0.026	Aggregated
Flameprince 45	2009	385	Early	122	31.7	-0.116	0.097	Random
			Late	169	43.9	-0.064	0.450	Random
Flameprince 45	2010	739	Pre-	10	1.4	<u>0.408</u>	0.049	Aggregated
			Early	74	10.0	<u>0.193</u>	0.034	Aggregated
			Mid	133	18.0	<u>0.203</u>	0.000	Aggregated
			Late	155	21.0	<u>0.216</u>	0.000	Aggregated
Flameprince 87	2010	601	Early	31	5.2	0.263	0.079	Random
			Mid	61	10.1	<u>0.218</u>	0.023	Aggregated
			Late	74	12.3	<u>0.186</u>	0.036	Aggregated
Flameprince 88	2010	369	Early	30	7.6	0.223	0.213	Random
			Mid	46	11.6	0.201	0.107	Random
			Late	62	15.7	0.146	0.237	Random
Flameprince 120	2009	396	Early	76	19.2	0.128	0.256	Random
			Late	128	32.3	0.054	0.821	Random

[a] Arranged in order of earliest to latest-maturing cultivar.

[b] Trees were monitored for disease at 1- to 4-day intervals during the pre-harvest period, and data are summarized for two, three, or four assessment periods for each tree to facilitate data presentation and analysis. In Flameprince 45 (2010), "Pre-" represents fruit affected by green fruit rot that directly preceded the pre-harvest epidemic.

[c] d_w represents the index of disease aggregation and is calculated based on the cumulative frequency distribution of nearest-neighbor distances among brown rot-affected fruit. Significant positive values indicate aggregation, whereas significant negative values correspond to a more regular distribution compared with the random simulation. Significant d_w values ($P \leq 0.05$) are underlined.

Table 4.2. Spatial association patterns of pre-harvest brown rot, caused by *Monilinia fructicola*, with blossom blight earlier in the season in 5 of 13 intensively mapped peach tree canopies.

Season and cultivar[a]	Year	Pre-harvest fruit rot	Blighted blossoms	d_w [b]	*P*	Pattern of association
Redglobe 7	2009	87	30	<u>0.213</u>	0.000	Positive
O'Henry 26	2009	142	43	<u>0.101</u>	0.002	Positive
O'Henry 26	2010	88	10	<u>0.153</u>	0.010	Positive
O'Henry 26	2011	96	28	<u>0.174</u>	0.002	Positive
O'Henry 127	2009	38	22	0.125	0.297	n.s.

[a] Arranged in order of earliest to latest-maturing cultivar.
[b] d_w represents the index of spatial disease association and is calculated based on the cumulative frequency distribution of nearest-neighbor distances among brown rot-affected fruit and blighted blossoms present in the same canopy earlier in the season. Significant positive values ($P \leq 0.05$, underlined) indicate positive spatial aggregation.

Table 4.3. Spatial association patterns of pre-harvest brown rot, caused by *Monilinia fructicola*, in 13 intensively mapped peach tree canopies.

Cultivar and tree number [a]	Year	Comparison	New fruit rot	Existing fruit rot	d_w [c]	*P*	Pattern of association
Early-season cultivar							
Sureprince 79	2010	Mid vs. early	22	26	-0.334	0.004	Negative
		Late vs. mid	35	48	-0.186	0.116	n.s.
Mid-season cultivars							
Redglobe 7	2009	Mid vs. early	37	26	0.149	0.337	n.s.
		Late vs. mid	24	63	0.211	0.143	n.s.
Contender 74	2010	Late vs. early	82	41	-0.370	0.000	Negative
Contender 75	2010	Mid vs. early	36	12	-0.116	0.628	n.s.
		Late vs. mid	11	48	0.122	0.979	n.s.
Late-season cultivar							
O'Henry 26	2009	Mid vs. early	93	35	-0.204	0.000	Negative
		Late vs. mid	14	128	-0.344	0.030	Negative
O'Henry 26	2010	Mid vs. early	49	24	0.097	0.625	n.s.
		Late vs. mid	21	73	-0.366	0.003	Negative
O'Henry 26	2011	Mid vs. early	35	21	-0.331	0.000	Negative
		Late vs. mid	40	56	-0.295	0.002	Negative
O'Henry 127	2009	Late vs. early	13	25	-0.340	0.051	n.s.
Flameprince 45	2009	Late vs. early	47	122	-0.106	0.440	n.s.
Flameprince 45	2010	Early vs. pre-	64	10	0.265	0.001	Positive
		Mid vs. early	59	74	0.191	0.025	Positive
		Late vs. mid	22	133	0.443	0.000	Positive
Flameprince 87	2010	Mid vs. early	30	31	0.177	0.213	n.s.

		Late vs. mid	13	61	-0.290	0.136	n.s.
Flameprince 88	2010	Mid vs. early	16	30	<u>0.389</u>	0.005	Positive
		Late vs. mid	16	46	-0.221	0.281	n.s.
Flameprince 120	2009	Late vs. early	52	76	<u>-0.181</u>	0.032	Negative

[a] Arranged in order of earliest to latest-maturing cultivar.

[b] Trees were monitored for disease at 1- to 4-day intervals during the pre-harvest period, and data were summarized for two, three, or four assessment periods for each tree. Spatial associations were calculated among the fruit that had become newly symptomatic during one period and those that were symptomatic in the previous period. In Flameprince 45 (2010), "Pre-" represents fruit affected by green fruit rot that directly preceded the pre-harvest epidemic.

[c] d_w represents the index of spatial disease association between the successive epidemic phases and is calculated based on the cumulative frequency distribution of nearest-neighbor distances among brown rot-affected fruit in one period and those that were symptomatic in the previous period. Significant positive values indicate positive spatial association, whereas significant negative values signify negative spatial association compared with the random simulation. Significant d_w values ($P \leq 0.05$) are underlined.

Figures

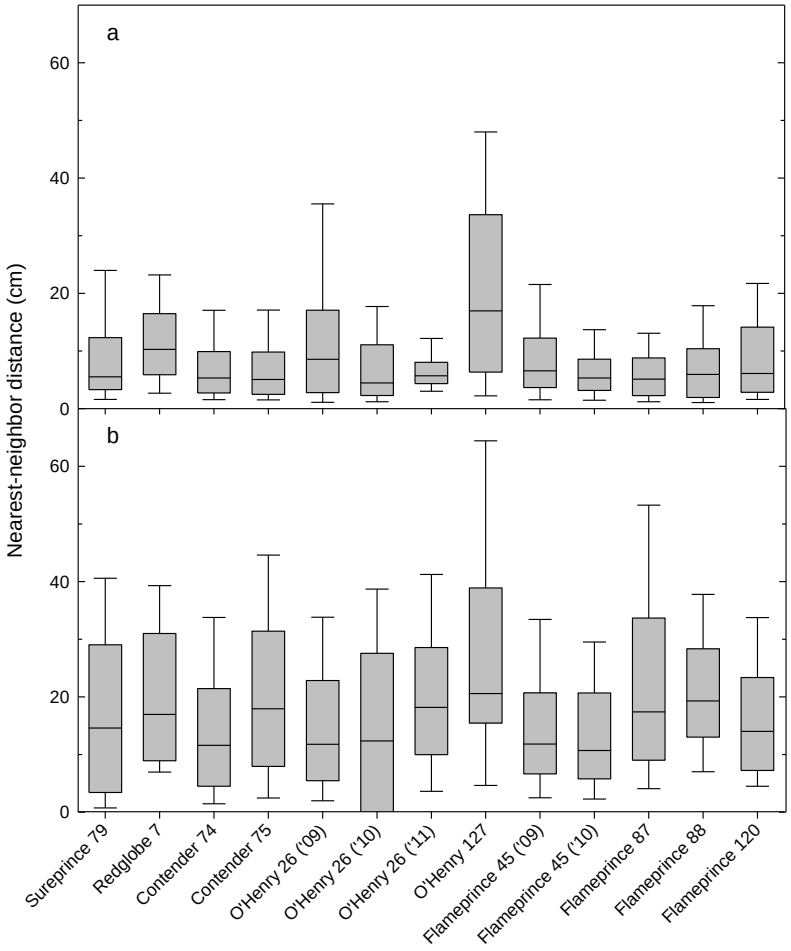

Fig. 4.1 Distribution of nearest-neighbor distances among all fruit (a) and among brown rot-affected fruit at the end of the epidemic (b) in 13 intensively mapped peach tree canopies. Horizontal axis labels correspond to cultivar names (arranged in the order of earliest to latest maturity), tree number, and year (in cases where the same tree was monitored in multiple years).

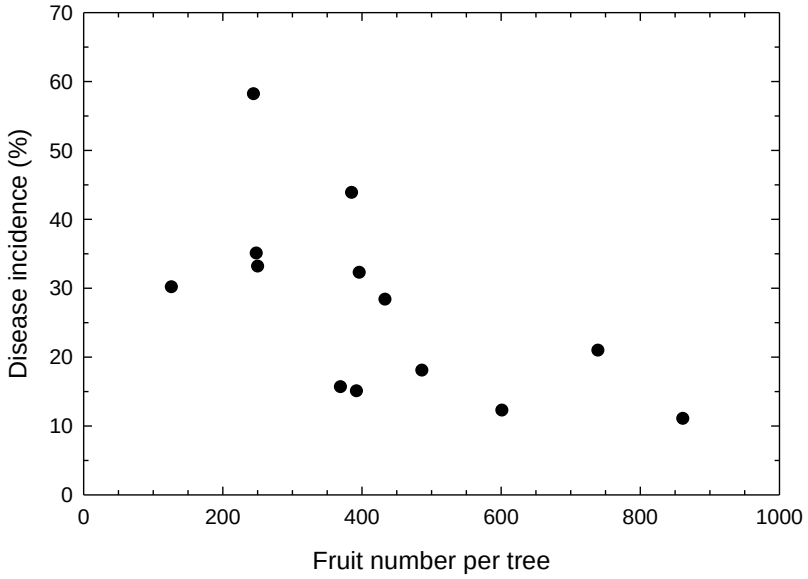

Fig. 4.2 Relationship between brown rot incidence at the end of the epidemic and total fruit number in 13 intensively mapped peach tree canopies. The two variables correlated significantly ($r = -0.613$, $P = 0.0260$).

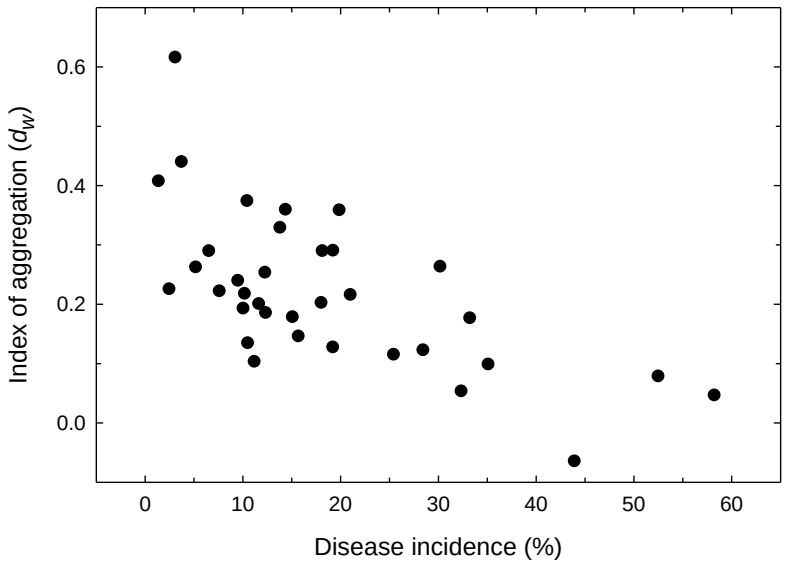

Fig. 4.3 Relationship between spatial aggregation of brown rot-affected fruit and brown rot incidence in 13 intensively mapped peach tree canopies. The two variables correlated significantly ($r = -0.653$, $P < 0.0001$) The index of aggregation d_w is calculated based on the cumulative frequency distribution of nearest-neighbor distances among brown rot-affected fruit. Positive values indicate aggregation, whereas negative values correspond to a more regular distribution compared with the random simulation. Data are from early, mid, and late assessment periods during the epidemic as shown in Table 4.1.

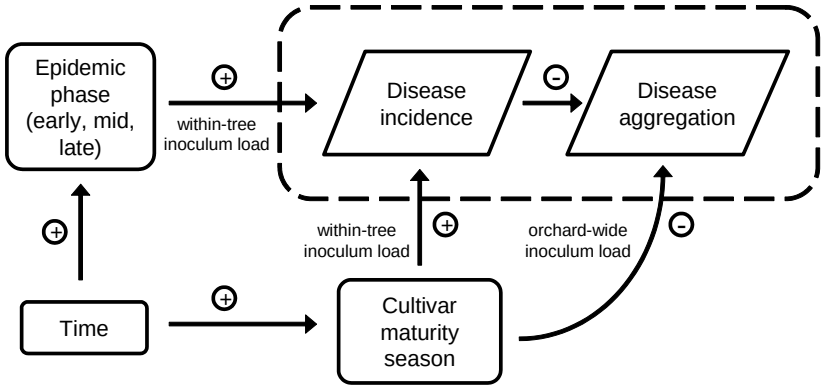

Fig. 4.4 Conceptual model linking time, cultivar maturity season, within-tree epidemic phase, brown rot incidence, and spatial aggregation of brown rot-affected fruit in peach tree canopies. Disease aggregation and disease incidence are correlated negatively (Fig. 4.3). The influence of time is reflected both orchard-wide (varying cultivar maturity classes) and within each tree (successive epidemic phases from early to late). Time increases disease incidence through increasing inoculum loads both within each tree and as disease develops on successively later maturity classes across the orchard. This reduces the level of disease aggregation both via increasing disease incidence per tree and through an increase in the orchard-wide inoculum load providing more external sources of inoculum.

CHAPTER 5

FINE-SCALE GENETIC STRUCTURE OF *MONILINIA FRUCTICOLA* DURING DISEASE EPIDEMICS WITHIN INDIVIDUAL PEACH TREE CANOPIES[1]

[1]Everhart, S.E., and H. Scherm. To be submitted to *Phytopathology*.

Abstract

The purpose of this study was to determine the fine-scale genetic structure of populations of the brown rot pathogen, *Monilinia fructicola*, within individual peach tree canopies to better understand within-tree plant pathogen diversity and to complement previous work on spatio-temporal development of brown rot disease at the canopy level. Across 3 years in a total of six trees, we monitored and collected isolates from every *M. fructicola* symptom within each tree during the course of the season and created high-resolution three-dimensional maps of all symptom and isolate locations within individual canopies using an electromagnetic digitizer. Each canopy population (65 to 173 isolates per tree) was characterized using a set of 16 polymorphic microsatellite markers and analyzed for evidence of spatial autocorrelation among fruit rot isolates during the epidemic phase of the disease. Results showed high genetic diversity (average $uh = 0.629$) and high genotypic diversity (average $D = 0.927$) within canopies. The percentage of unique multilocus haplotypes within trees was greater for blossom blight isolates (average 96.9%) than for fruit rot isolates (average 62.7%), indicating a greater contribution of clonal reproduction during the pre-harvest fruit rot phase. Spatial genetic structure was observed among fruit rot isolates, with all six populations showing positive and significant autocorrelation within the first and/or second distance class, up to 0.37 and/or 0.73 m. Despite high levels of within-tree pathogen diversity, the relative contribution of locally available inoculum combined with short-distance dispersal is likely the main factor in generating the observed fine-scale spatial patterns within trees.

Introduction

Knowledge of pathogen dynamics and genetic structure can provide powerful insights into patterns and processes in plant pathogen populations, which are important for understanding the occurrence and spread of plant disease (21; 22). For brown rot of stone and pome fruits caused by fungi in the genus *Monilinia*, the disease cycle and epidemiology have been well-characterized (3). However, little is known about pathogen genetic variation or processes at the population level. Most studies on *Monilinia* spp. using molecular markers have focused on species delineations and/or quantifying broad-level population diversity (11; 14; 16; 19; 20; 26). In contrast, studies with indirect genetic markers have provided some indication of population variation in orchards and within individual tree canopies. For example, the frequency within trees of *M. fructicola* isolates resistant to dicarboximide fungicide was used as an indirect marker to evaluate the spatial pattern and spread of strains in an orchard (6). Results showed variation in the frequency of resistant strains within individual tree canopies, suggesting establishment and spread at the tree level, but there was limited evidence for spread of resistant strains among canopies within a season and no evidence for spatial dependence in year-to-year frequency of resistant strains within the same canopy. When vegetative compatibility groups (VCGs) were used as an indirect marker to differentiate *M. fructicola* isolates from diseased fruit within individual peach tree canopies (24), fruit rot isolates were found to be relatively diverse, yielding 23 different VCGs out of 100 isolates (23.0% incompatibility) in one orchard and 37 VCGs out of 88 isolates (42.0% incompatibility) in another. Most VCGs were represented by a single isolate, although one VCG representing a large percentage of isolates was obtained from a group of neighboring trees, suggesting short-distance spread among nearby trees from a common source of inoculum. In a similar study on nectarine, three tree canopies from which *M. fructicola*

isolates were obtained from fruit lesions harbored 36.8, 62.5, and 94.7% unique VCGs, and only one VCG was common in the sample of 54 fruit rot isolates from the three canopies (27). These studies thus suggested considerable genetic variation at the canopy level, but also provided some evidence for genetic relatedness within and among trees. These results need to be confirmed with direct genetic markers and more explicit statistical approaches for determining fine-scale genetic structure and genetic autocorrelation within canopies

In a multi-year study on peach (*Prunus persica*), we monitored the within-canopy development of brown rot (caused by *M. fructicola*) during the course of the season and created three-dimensional maps of all symptoms within individual canopies using an electromagnetic digitizer (8). Explicit spatial analysis of the pattern of diseased fruit within canopies indicated the presence of significant disease aggregation early in the fruit rot epidemic, especially on early- and mid-season peach varieties. We hypothesized that these patterns of disease aggregation were due to disease spread from within-tree sources of inoculum (such as previously infected blossoms or twig cankers) at a time in the season when orchard-wide inoculum was still limiting. Since fungal isolates were obtained from each of the symptomatic fruit mapped in this study, a more complete insight into disease progression may be obtained by analyzing genotypic data about the isolates associated with each symptom. Thus, the objective of the present study was to genotype the georeferenced isolates obtained previously from individual peach tree canopies using high-resolution microsatellite markers (9), generate genetic similarity matrixes among all isolates within each tree, and conduct spatial autocorrelation analysis to quantify fine-scale genetic structure of *M. fructicola* isolates within canopies. The results will provide insight into genetic variation and dissemination of *M. fructicola* during fruit rot epidemics within peach tree canopies.

Materials and Methods

Disease Monitoring and Mapping. The study was conducted in a research peach orchard at the University of Georgia Horticulture Farm (Watkinsville, GA) from late March to September in 2009, 2010, and 2011. The orchard had been planted in 2000 and consisted of six cultivars of varying maturity dates, arranged in replicate four-tree plots having within and across-row spacing of 4.8 and 6.1 m, respectively. Across the 3 years, a total of 13 trees of the cultivars Sureprince (early-maturing), Redglobe (mid-season), and O'Henry and Flameprince (both late-maturing) were included in disease monitoring and mapping (7). During the study, no fungicide applications to control brown rot were made in the orchard, but foliar sprays of wettable sulfur were applied during the cover spray period to suppress peach scab (caused by *Fusicladium carpophilum*). All other horticultural and pest management followed standard commercial practice (15). Trees were thinned relatively lightly to ensure a sufficient number of fruit per tree for within-tree mapping and spatial analysis.

Trees were monitored for symptoms and signs associated with *M. fructicola* infections (blossom blight, twig blight, twig cankers, green fruit rot, and brown rot of mature fruit) at 3- to 5-day intervals through final fruit swell and then every 1 to 4 days until fruit were tree-ripe. When a new symptom was detected, it was swabbed with a sterile cotton-tipped applicator to sample conidia, which was then stored at 4^{o}C until pathogen isolation. A plastic tag was tied to the branch proximal to the point where the symptomatic element originated, and each label was marked with the date of symptom appearance and a unique identifying number. Thus, the spatial location and approximate date of appearance of each symptom, and the associated fungal isolates, were known.

High-resolution three-dimensional maps of the positions of symptom tags and of all fruit (symptomatic and asymptomatic) were created for each tree using an electromagnetic digitizer (FASTRAK 3Space, Polhemus, Colchester, VT) (25). This device creates a low-level electromagnetic field from an emitter positioned at the base of the tree and allows the user to position a sensor at the location of each point and record the corresponding *x*, *y*, and *z*-coordinates (8). Trees were digitized once (when fruit were tree-ripe) in 2009 and twice (at the beginning of the pre-harvest interval for all fruit and again at the end of the epidemic for all tagged symptoms) in 2010 and 2011. The resultant data set consisted of georeferenced coordinates for every fungal isolate within each tree and the date when it was obtained.

Pathogen Culturing and Genotyping. Single-spore isolations were performed for each sample. Conidia were dislodged from the cotton tipped applicator by tapping it lightly along the edge of a Petri dish containing water agar. After 24 h, germinating conidia were transferred individually onto potato dextrose agar. After 6 to 8 days of growth, aerial mycelium was harvested for DNA extraction using a DNeasy Plant Mini Kit (Qiagen, Valencia, CA).

Six of the 13 trees were selected for pathogen population analysis based on having 65 or more *M. fructicola* isolates that represented samples taken from every symptom that arose from blossom blight to fruit drop. This resulted in a total of 694 *M. fructicola* isolates, 114 from blossoms and 580 from fruit (Table 5.1). Purified DNA from each isolate was screened with 21 microsatellite markers, 16 from Everhart et al. (9) and 5 from Jänsch et al. (16). To enable indirect fluorescent labeling, primer pairs were synthesized with the addition of a CAG label (CAGTCGGGCGTCATCA added to the 5'-end of the shorter primer), and each PCR reaction included a HEX-labeled primer complementary to the CAG-label (2; 10). PCR reactions were

mixed using hot-start Taq (JumpStart Taq; Sigma-Aldrich, St. Louis, MO) following the manufacturer's reaction specifications, scaled to 12.5 μL, and modified to contain a 1:10 ratio of CAG-labeled-primer to CAG label. PCR conditions utilized a touchdown treatment where 20 cycles from 60 to 50.5°C enabled a range of primer melting temperatures to be met, followed by 15 cycles to increase the number of amplicons (4). Specifically, thermocycle conditions consisted of an initial treatment at 95°C for 2.5 min; 20 cycles of 95°C for 20 sec, 60°C for 20 sec (decreased by 0.5°C for every cycle), and 72°C for 30 sec; followed by 15 cycles of 95°C for 20 sec, 50°C for 20 sec, and 72°C for 30 sec. A 1:10 dilution of amplicons was denatured and analyzed using capillary electrophoresis (3730xl Analyzer; Applied Biosystems, Carlsbad, CA).

All 21 microsatellite markers showed amplification, but four markers were eliminated since they had >10% null alleles that were not resolved after re-screening. Another marker priming a dinucleotide repeat showed single-nucleotide polymorphisms, which did not allow accurate scoring of alleles, hence it was also eliminated. Thus, among the 21 markers applied in this study, 16 were suitable for final analysis [SEA, SEC, SED, SEE, SEF, SEG, SEI, SEK, SEL, SEN, SEP, SEQ, and SER published in Everhart et al. (7); and CHMFc4, CHMFc5, and CHMFc12 from Jänsch et al. (16)]. These markers were consistent and yielded fragment sizes as expected based on known repeat lengths, with ≤1.7% null alleles at each locus (average of 0.43%).

Genetic Analysis. Two types of datasets were generated for population genetic analyses: one that contained all genotypes from each canopy population and the other that was a clone-corrected subset where every multilocus genotype was represented only once. Genetic diversity and population differentiation statistics were based on allele frequencies estimated from clone-

corrected data, whereas genotypic diversity was estimated from complete data. Genetic diversity at each locus was estimated using Nei's genetic diversity, *h* (Nei 1973). This parameter was subsequently weighted based on sample size to estimate unbiased haploid genetic diversity (*uh*). Genetic (*uh*) and genotypic (*D*) diversity were calculated using GenAlEx 6.4 (23) and Multilocus 1.3b (1), respectively.

The Index of Association (I_A), Analysis of Molecular Variance (AMOVA), and spatial autocorrelation analyses were based on genetic distance. Genetic distance between two isolates within a canopy was derived from a pairwise comparison between individuals, where the difference in basepairs is calculated at each locus. These distances were summed over loci to give a total genetic distance in a pairwise matrix between individuals. The variance among genetic distances within a canopy population was used to calculate I_A, where variance of pairwise distances is compared to variance expected in the absence of linkage disequilibrium, estimated from 1000 randomizations. Similarly, AMOVA provides a comparison of genetic variance within and among two populations, where a significant negative value suggests a greater amount of genetic variation is present among populations. These analyses were conducted in Multilocus 1.3b.

Spatial autocorrelation analyses of genetic distances were performed on populations within each tree canopy. Because we are interested in the effect of clonal dispersal within the canopy, data were not clone-corrected for this analysis. Both pairwise geometric and pairwise squared genetic distance matrices are required inputs for this analysis (23). Genetic distance matrices were calculated as described previously, and linear distance based on *x*, *y,* and *z*-coordinates for each isolate were calculated using Matlab R2011b (Mathworks, Natick, MA). The resulting matrices were used to asses each canopy population for spatial genetic

autocorrelation using GenAlEx 6.4 software. A distance class of 0.37 m was chosen, showing a good compromise between spatial resolution and sample size within each class.

Results

Genetic Variation and Distribution of Genotypes. Thirteen trees were surveyed and mapped for symptoms and signs of disease caused by *M. fructicola* from bloom to fruit drop in 2009, 2010, and 2011. A total of 694 fungal isolates (114 from blighted blossoms and 580 from infected fruit) were obtained from symptomatic elements in six of these trees and subsequently genotyped with 16 polymorphic microsatellite markers (Table 5.1). For each population, all loci were polymorphic, with an average of 5.5 alleles per locus and 2.6 effective alleles per locus. These values did not vary much from population to population or within the pooled versus the mean data, indicating that the partitioning of allelic variation was approximately the same at all scales and within each population; thus, comparisons among populations using frequency-based statistics would be meaningful. The number of private alleles for each population (alleles unique to that population) varied, where the tree with the fewest isolates (Sureprince 79-2010; $n = 65$) had the fewest private alleles (2) and that with the most isolates (O'Henry 26-2009, $n = 173$) was one of two trees with the most private alleles (8). Unbiased haploid genetic diversity (*uh*) in each tree ranged from 0.588 to 0.674, with *uh* in the pooled population equal to 0.649.

Within each tree there were between 29 and 72 multilocus haplotypes representedfor a total of 291 haplotypes across the six trees, with an average of 67.8% being unique, i.e., represented only once (Table 5.2). The non-unique haplotypes from the fruit rot sub-populations fell into 11 to 22 clonal groups per tree (total of 92 clonal groups across all trees), with the largest clonal groups in each tree having between 9 and 34 members (Fig. 5.1). There were 5.2

isolates per clonal haplotype on average. Among all 291 haplotyopes, there were only 11 that were found in two trees. As a function of both the number and frequency of genotypes, genotypic diversity (*D*) ranged from 0.885 (Sureprince 79-2010) to 0.969 (Flameprince 45-2010), with an average of 0.927 across trees.

Sub-populations of isolates obtained in the spring from blighted blossoms and those later in the season from affected fruit were also characterized (Table 5.2). The number of isolates obtained from blighted blossoms was always smaller than that from fruit affected by pre-harvest brown rot, and in some cases there were too few blossom blight isolates to calculate separate sub-population parameters (trees Sureprince 79-2010, O'Henry 26-2010, and Flameprince 45-2010). Not surprisingly, fewer haplotypes were present within the blossom blight sub-populations (average 17) than from fruit rot sub-population (average 37). A higher percentage of the haplotypes was unique among the blossom blight sub-population (average across trees 96.9%; pooled 86.8%) than from the fruit rot sub-population (average across trees of 62.7%; pooled 61.8%). Across the six trees there were 16 isolates obtained from blighted blossoms that were from the same clonal haplotype group as a fruit rot isolate (*data not shown*).

Based on the magnitude and significance level of I_A, significant linkage among loci was detected within each tree population, blossom blight and fruit rot sub-population, and within pooled data, rejecting the null hypothesis of random mating. I_A was consistently higher for fruit rot sub-populations than for blighted blossom sub-populations (Table 5.2).

Comparison of Populations and Spatial Genetic Autocorrelation. Differentiation between populations within each tree canopy was tested using AMOVA. Overall, results of this analysis determined that 1.6% of molecular variance was present among trees, whereas 98.4% was within

trees (Phi_{PT} = 0.016, P = 0.004). In pairwise comparisons of variance in genetic distance, more than half (8 of 15) of the comparisons showed no significant population differentiation (Table 5.3). Specifically, in all cases where trees monitored within the same year were compared (four cases in Table 5.3), no significant differences were observed. When the same tree, O'Henry 26, was monitored in 2009, 2010, and 2011, two of the three pairwise comparisons were not significant; the one significant comparison in this case was between 2009 and 2011. In the remaining eight comparisons which involved pairwise comparisons across both cultivars and years, only two comparisons were not significant (Table 5.3). When the same comparison among populations was carried out for non-clone-corrected data, it showed that all populations were significantly different (Table 5.4).

In one tree (O'Henry 26), the *M. fructicola* population was monitored in 2009, 2010, and 2011. The clone-corrected sub-population of isolates from blossom blight symptoms and from fruit rot symptoms were compared sequentially by AMOVA, as they would occur over time (Fig. 5.2). This showed no significant differences in the sub-populations from one phase to the next (i.e., blossom blight in one year to fruit rot in the same year, or fruit rot in one year to blossom blight in the next). Only comparisons skipping successive phases were significant, specifically fruit rot sub-populations in 2009 or 2010 compared with those in 2011 (Fig. 5.2). The greatest difference was observed for fruit rot sub-populations that occurred across the greatest time span (2009 to 2011; Phi_{PT} = 0.043, P = 0.004). This analysis was also performed using non-clone-corrected data in order to determine the level of relatedness that may be attributable to clonal haplotypes (Fig. 5.3). Overall, this did not change many of the pairwise comparison outcomes, with the exception of the two comparisons made across a single year (2009 to 2010 fruit rot isolates showed significant difference without clone correction, whereas 2010 to 2011 no longer

showed significant difference) and the within-season comparison in 2009 (blossom blight to fruit rot showed significant difference).

Fine-scale spatial genetic structure was assessed with three-dimensional spatial autocorrelation analysis for each tree canopy (Table 5.5, Fig. 5.4). All populations showed positive and significant autocorrelation within the first and/or second distance class, up to 0.37 and/or 0.73 m. Two populations, O'Henry 26 in 2009 and 2010, showed significance up to the third distance class tested, 1.1 m. There were no other consistent patterns of significant spatial genetic autocorrelation that were present in more than one trees.

Discussion

This is the first study to quantify the fine-scale population structure of a plant pathogen within its host canopy in a spatial context. Genotyping all isolates from six peach trees showed that the genetic diversity of *M. fructicola* was typical of other ascomycete plant pathogens characterized using microsatellite markers (5; 13; 28). The intermediate to high level of genotypic diversity and presence of 92 clonal haplotypes among the total of 291 haplotypes is consistent with fungal pathogens that follow an "epidemic" model of population structure (21). A combination of many genotypes and some clones is typical of fungi with a mixed mode of reproduction, producing sexual ascospores in the spring, followed by successive waves of clonal reproduction during the season. The distribution in number of clones within each haplotype showed that some trees had 1 to 3 large clonal groups (>10 clones per haplotype) that dominated, while others had a more even distribution of clones per haplotype. The fact large clonal groups did not dominate in the current study may be explained by the fact that pre-harvest brown rot epidemics are oligocyclic,

allowing only a limited number of epidemic cycles to occur during the 3- to 4-week fruit ripening phase within each tree.

Comparing the six tree populations showed that there were many haplotypes within each canopy (average of 51), and these differed among trees to the extent that 98.4% of molecular variance was within trees and only 11 clonal haplotypes were represented in more than one tree. Pairwise comparison (including clones) showed that all trees had differentiated populations, which may indicate that the majority of the population structure was due to individuals already established locally and serving as the predominant source of inoculum within the tree canopy. The importance of within-tree inoculum sources was also evidenced by significant spatial autocorrelation among genotypes found within each tree. Not surprisingly, the populations with the strongest spatial genetic structure were those with the largest number of isolates belonging to a clonal haplotype. For example O'Henry 26-2009 had 137 isolates that belonged to one of 21 clonal haplotypes; among these, most (79.2%) were members of one of the three most represented clonal haplotypes (34, 32, and 19 isolates in each).These three haplotype groups likely contributed to the majority of the spatial genetic structure observed within the sub-population up to 1.1 m. In contrast, all other trees had only one clonal haplotype represented by 19 or more isolates. For example, the next highest autocorrelation coefficient was observed for population O'Henry 26-2010 at 0.37 m, which had five clonal haplotypes represented by 6 to 9 isolates in each group. Overall, the fact that all six populations showed positive and significant autocorrelation within the first and/or second distance class (up to 0.37 and/or 0.73 m) suggests a relatively consistent dispersal distance from disease foci during the within-tree pre-harvest brown rot epidemic.

These results can be interpreted in light of what is and is not known about the disease cycle of *M. fructicola*. The high uniqueness (low clonality) of isolates from blighted blossoms suggests independent sources of primary inoculum infecting each flower. Subsequently, some of these haplotypes became a source of secondary inoculum because the same haplotype was recovered from isolates in the fruit rot phase. However, relatively few of the fruit rot haplotypes were haplotypes represented within the blossom blight sub-population, indicating that most were from a source other than within-canopy blossom blight (or that genetic recombination occurred between the blossom blight and fruit rot stages). Thus, internal and external sources of secondary inoculum are contributing to pre-harvest disease development. It is important to note, however, that the *M. fructicola* populations genotyped within these six trees represent only a sub-sample of the total trees with brown rot disease in the orchard. Connectivity between populations within individual trees in the same orchard was not fully explored. It is likely that more shared haplotypes would have been found between different populations if all trees were located within the same row or next to each other. Indeed, the two trees sharing the greatest number of clonal haplotypes, O'Henry 26 in 2010 and Flameprince 45 in 2010, are cultivars whose fruit mature within an overlapping period of ~3 weeks. None of the other trees were as close together in space and time, and fewer clonal haplotypes were found within all other pairs of trees.

Further insight into the orchard-level population connectivity was achieved by comparing the six populations after clone-correction, which showed that more than half of the pairwise comparisons were no longer significantly different. This suggests that there is lack of differentiation of the gene pool within isolates contributing to the epidemics within those trees. In addition, this was more common in late-season cultivars than in early- or mid-season cultivars, suggesting late-season cultivars (O'Henry and Flameprince) harbor populations that contribute a

greater proportion of surviving pathogen propagules for the following season. For example, when examining the sub-populations across years for O'Henry 26 in 2009, 2010, and 2011, there was evidence of within-tree spatio-temporal population continuity. When examining the relationships for clone-corrected data, there were no significant population differences from the blossom blight sub-population to the fruit rot sub-population within the same year and from the fruit rot sub-population to blossom blight sub-population in the following year. The majority of comparisons did not change when the analysis was done including all clones, suggesting that the predominant clonal haplotypes within the trees are from the existing within-tree genetic pool, but not identical as no haplotypes were recovered in more than 1 year. Thus, examining the population structure within an individual tree over time showed connectivity within the population, despite lack of shared clonal haplotypes across years.

Overall, the high genotypic diversity obtained using microsatellite markers is consistent with the number of VCGs obtained for *M. fructicola* in peach and nectarine trees in previous studies (24; 27). Both these latter studies showed that multiple VCGs were obtained from isolates within individual trees. From other studies it is known that a single VCG may represent multiple microsatellite genotypes (17). In addition, both studies found 31.1 to 77.0% of fruit rot isolates were vegetatively compatible, suggesting clonal dispersal within individual trees may also occur. The results of these previous studies show that the high level of genotypic diversity obtained in the present study is an accurate representation of phenotypic variability.

The primary mode of overwintering of *M. fructicola* in peach orchards in the southeastern United States is not well known. In general, apothecial production within managed orchards in the region is considered rare, but is thought to occur more readily underneath wild plums (18). Another form of overwintering thought to play a more important role in areas lacking survival

via sexual apothecial production from fruit mummies on the ground is asexual survival in twig cankers, peduncles, and fruit mummies in the tree (3). The lack of population differentiation among all pairwise comparisons of populations within trees for clone-corrected data suggests that these trees share the same genetic pool, although reshuffling of genotypes may be occurring. Such reshuffling could occur through sexual reproduction or via the parasexual cycle. Although it is not possible to determine from the data which mode of recombination is contributing to the high level of genetic diversity observed, detection of significant linkage disequilibrium could ensue if the fungus is homothallic and outcrosses, which is thought to occur in California (12).

Acknowledgments

We thank Amy Savelle, Sara Thomas, and Lucky Mehra for their assistance in digitizing tree canopies, and Drs. Dorset Trapnell and Marin Brewer for useful discussions. Funded in part by grant no. 2009-34103-19818 from the USDA Southern Region IPM Program. Additional financial support provided by the American Phytopathological Society's Tarleton Fellowship, a Sigma Xi Grant-in-Aid of Research Award, and a University of Georgia Dissertation Completion Award to S.E.E.

Literature Cited

1. Agapow, P. M., and Burt, A. 2001. Indices of multilocus linkage disequilibrium. Molecular Ecology Notes 1(1-2):101-102.

2. Boutin-Ganache, I., Raposo, M., Raymond, M., and Deschepper, C.F. 2001. M13-tailed primers improve the readability and usability of microsatellite analyses performed with two different allele-sizing methods. BioTechniques 31(1):24-6, 28.

3. Byrde, R. J. W., and Willetts, H. J. 1977. The Brown Rot Fungi of Fruit. Their Biology and Control. Pergamon, Oxford.

4. Don, R. H., Cox, P. T., Wainwright, B. J., Baker, K., and Mattick, J. S. 1991. 'Touchdown'PCR to circumvent spurious priming during gene amplification. Nucleic Acids Res 19(14):4008.

5. Douhan, G. W., Peever, T. L., and Murray, T. D. 2002. Multilocus population structure of *Tapesia yallundae* in Washington State. Molecular Ecology 11(11):2229-2239 doi:10.1046/j.1365-294X.2002.01607.x.

6. Elmer, P. A. G., Gaunt, R. E., and Frampton, C. M. 1998. Spatial and temporal characteristics of dicarboximide-resistant strains of *Monilinia fructicola* and brown rot incidence in stone fruit. Plant Pathology 47(4):530-536.

7. Everhart, S. E., Askew, A., Seymour, L., and Scherm, H. 2012. Spatio-temporal patterns of pre-harvest brown rot epidemics within individual peach tree canopies. European Journal of Plant Pathology *in review*.

8. Everhart, S. E., Askew, A., Seymour, L., Holb, I. J., and Scherm, H. 2011. Characterization of three-dimensional spatial aggregation and association patterns of brown rot symptoms within intensively mapped sour cherry trees. Annals of Botany 108(6):1195-1202.

9. Everhart, S. E., Askew, A., Seymour, L., Glenn, T. C., and Scherm, H. 2012. Spatial patterns of brown rot epidemics and development of microsatellite markers for analyzing fine-scale genetic structure of *Monilinia fructicola* populations within peach tree canopies. Plant Health Progress *in press.*

10. Faircloth, B. C., Terhune, T. M., Schable, N. A., Glenn, T. C., Palmer, W. E., and Carroll, J. P. 2008. Ten microsatellite loci from Northern Bobwhite (*Colinus virginianus*). Conservation Genetics 10(3):535-538.

11. Fan, J.-Y., Guo, L.-Y., Xu, J.-P., Luo, Y., and Michailides, T. J. 2010. Genetic diversity of populations of *Monilinia fructicola* (Fungi, Ascomycota, Helotiales) from China. J Eukaryot Microbiol 57(2):206-212.

12. Free, S. J., Holtz, B. A., and Michailides, T. J. 1996. Mating behavior in field populations of *Monilinia fructicola.* Mycologia 88(2):208-211.

13. Frenkel, O., Portillo, I., Brewer, M. T., Péros, J. P., Cadle-Davidson, L., and Milgroom, M. G. 2012. Development of microsatellite markers from the transcriptome of *Erysiphe necator* for analysing population structure in North America and Europe. Plant Pathology 61(1):106-119.

14. Gell, I., Larena, I., and Melgarejo, P. 2007. Genetic diversity in *Monilinia laxa* populations in peach orchards in Spain. Journal of Phytopathology 155(9):549-556.

15. Horton, D., Brannen, P., Bellinger, B., Lockwood, D., and Ritchie, D. 2011. Southeastern Peach, Nectarine, and Plum Pest Management and Culture Guide. University of Georgia Cooperative Extension Service, Athens, GA.

16. Jänsch, M., Frey, J. E., Hilber-Bodmer, M., Broggini, G. A. L., Weger, J., Schnabel, G., and Patocchi, A. 2012. SSR marker analysis of *Monilinia fructicola* from Swiss apricots suggests introduction of the pathogen from neighbouring countries and the United States. Plant Pathology 61(2):247-254.

17. Kohn, L. M., Schaffer, M. R., Anderson, J. B., and Grünwald, N. J. 2008. Marker stability throughout 400 days of in vitro hyphal growth in the filamentous ascomycete, *Sclerotinia sclerotiorum*. Fungal Genetics and Biology 45(5):613-617.

18. Landgraf, F. A., and Zehr, E. I. 1982. Inoculum sources for *Monilinia fructicola* in South Carolina peach orchards. Phytopathology 72:185-190.

19. Luo, C. X., and Schnabel, G. 2008. The cytochrome P450 lanosterol 14α-demethylase gene is a demethylation inhibitor fungicide resistance determinant in *Monilinia fructicola* field isolates from Georgia. Appl. Environ. Microbiol. 74(2):359-366.

20. Ma, Z., Yoshimura, M. A., and Michailides, T.J. 2003. Identification and Characterization of Benzimidazole Resistance in *Monilinia fructicola* from Stone Fruit Orchards in California. Appl. Environ. Microbiol. 69(12):7145-7152.

21. McDonald, B. A. 1997. The population genetics of fungi: tools and techniques. Phytopathology 87(4):448-453.

22. McDonald, B. A., and McDermott, J. M. 1993. Population genetics of plant pathogenic fungi. BioScience 43(5):311-319.

23. Peakall, R., and Smouse, P. E. 2006. GENALEX 6: genetic analysis in Excel. Population genetic software for teaching and research. Molecular Ecology Notes 6(1):288-295.

24. Scherm, H., and Emery, K. M. 2002. Vegetative compatibility in populations of *Monilinia fructicola* from Georgia peach orchards. Acta Horticulturae 592:725–727.

25. Sinoquet, H., Rivet, P., and Godin, C. 1997. Assessment of the three-dimensional architecture of walnut trees using digitising. Silva Fennica 31:265-273.

26. Snyder, C. L., and Jones, A. 1999. Genetic variation between strains of *Monilinia fructicola* and *Monilinia laxa* isolated from cherries in Michigan. Canadian Journal of Plant Pathology 21(1):70-77.

27. Sonoda, R. M., Ogawa, J. M., and Manji, B. T. 1991. Population structure of *Monilinia fructicola* in *Prunus persica* var. *nucipersica* tree canopies. Mycological Research 95(7):893-895.

28. Stukenbrock, E. H., Banke, S., and McDonald, B. A. 2006. Global migration patterns in the fungal wheat pathogen *Phaeosphaeria nodorum*. Molecular Ecology 15(10):2895-2904.

Tables

Table 5.1. Microsatellite variation at 16 polymorphic loci in six populations of *Monilinia fructicola* from individual peach tree canopies, where each population represents every fungal isolate obtained during an entire season (blossom blight to fruit drop).

Tree population	Sample size	Alleles per locus	Effective alleles per locus[a]	Private alleles[b]	Polymorphic loci (%)	Gene diversity (*uh*)[c]
SP79-10	65	4.19	2.10	2	100	0.617
RG7-09	96	5.00	2.38	5	100	0.601
OH26-09	173	5.69	2.05	8	100	0.588
OH26-10	90	5.56	3.13	4	100	0.674
OH26-11	127	6.25	2.87	8	100	0.644
FP45-10	143	6.19	3.26	6	100	0.647
Population level mean	116	5.48	2.63	5.50	100	0.629
Pooled	694	8.69	3.17	–	100	0.649

[a]Estimate of the number of equally frequent alleles in a population with the equivalent level of gene diversity.
[b]Equivalent to the number of alleles unique to the individual population.
[c]Unbiased haploid gene diversity (*uh*) estimated according to Nei (1978).

Table 5.2. Distribution of genotypes in six populations of *Monilinia fructicola* from individual peach tree canopies, where each population represents every fungal isolate obtained during an entire season (blossom blight to fruit drop).

	Tree population							
	SP79-10	RG7-09	OH26-09	OH26-10	OH26-11	FP45-10	Mean	Pooled
Number of isolates	65	96	173	90	127	143	116	694
from blighted blossoms	1	24	41	5	30	13	19	114
from affected fruit	64	72	132	85	97	130	97	580
Haplotypes	29	41	57	36	72	68	51	291
from blighted blossoms	1	23	28	5	30	13	17	99
from affected fruit	28	22	40	33	45	56	37	212
Unique haplotypes (%)	65.5	73.2	63.2	55.6	81.9	67.6	67.8	68.4
from blighted blossoms	100	95.7	85.7	100	100	100	96.9	86.8
from affected fruit	64.3	59.1	60	54.5	77.8	60.7	62.7	61.8
Genotypic diversity[a]	0.885	0.892	0.910	0.959	0.945	0.969	0.927	0.987
from blighted blossoms	-	0.989	0.959	-	1.000	-	0.983	0.994
from affected fruit	0.881	0.813	0.891	0.956	0.906	0.997	0.907	0.983
Index of Association (I_A)[b]	5.653*	4.181*	2.377*	1.834*	1.942*	1.889*	2.979	0.361*
from blighted blossoms	-	1.447*	0.446*	-	0.186*	-	0.876	0.410*
from affected fruit	2.972*	1.746*	1.254	0.759*	0.815*	0.835*	1.397	0.442*

[a]Genotypic diversity is defined as the probability that two individuals taken at random have different genotypes.
[b]The Index of Association (I_A) tests for linkage disequilibrium, where an asterisk indicates statistical significance compared with 1000 randomizations.

Table 5.3. Pairwise comparison of clone-corrected molecular variance in six populations of *Monilinia fructicola* from individual peach tree canopies, where each population represents every fungal isolate obtained during an entire season (blossom blight to fruit drop)[a].

	Tree population					
Population	SP79-10	RG7-09	OH26-09	OH26-10	OH26-11	FP45-10
SP79-10	–					
RG7-09	0.069*	–				
OH26-09	0.029*	0.007	–			
OH26-10	0.000	0.036*	0.001	–		
OH26-11	0.034*	0.019*	0.023*	0.019	–	
FP45-10	0.005	0.029*	0.014	0.000	0.000	–

[a]Asterisks denote significant Phi_{PT} values compared with 1000 randomizations.

Table 5.4. Pairwise comparison of molecular variance in six populations of *Monilinia fructicola* from individual peach tree canopies, where each population represents every fungal isolate obtained during an entire season (blossom blight to fruit drop)[a].

	Tree population					
Population	SP79-10	RG7-09	OH26-09	OH26-10	OH26-11	FP45-10
SP79-10	–					
RG7-09	0.192*	–				
OH26-09	0.159*	0.049*	–			
OH26-10	0.049*	0.190*	0.166*	–		
OH26-11	0.068*	0.123*	0.136*	0.067*	–	
FP45-10	0.046*	0.150*	0.152*	0.025*	0.062*	–

[a]Asterisks denote significant Phi_{PT} values compared with 1000 randomizations.

Table 5.5. Three-dimensional spatial autocorrelation coefficients (*r*) of genetic distances in six populations of *Monilinia fructicola* from individual peach tree canopies, where each population represents every fungal isolate obtained during the pre-harvest fruit rot phase[a].

	Tree population											
Interval (m)[b]	SP79-10		RG7-09		OH26-09		OH26-10		OH26-11		FP45-10	
0.37	0.052*	(157)	0.122*	(69)	0.219*	(110)	0.165*	(38)	0.060	(74)	0.049*	(443)
0.73	0.039	(140)	0.053	(203)	0.148*	(388)	0.047	(136)	0.075*	(263)	0.001	(941)
1.10	0.020	(215)	0.015	(316)	0.064*	(708)	0.064*	(216)	0.000	(404)	0.015	(840)
1.46	0.021	(295)	0.036	(432)	0.024	(630)	-0.018	(280)	0.011	(389)	0.003	(920)
1.83	-0.013	(307)	0.001	(447)	-0.016	(678)	0.006	(283)	0.039*	(368)	-0.002	(985)
2.20	-0.038	(278)	0.014	(348)	0.001	(733)	-0.043	(391)	0.002	(380)	-0.015	(879)
2.56	-0.015	(243)	-0.101*	(257)	-0.009	(907)	-0.009	(430)	-0.010	(423)	-0.024	(934)
2.93	0.021	(170)	-0.161*	(170)	-0.018	(796)	-0.001	(419)	-0.039	(480)	-0.019	(865)
3.29	-0.030	(107)	0.012	(125)	-0.020	(723)	0.002	(417)	-0.002	(515)	0.013	(704)
3.66	-0.078	(41)	0.039	(54)	-0.050	(529)	-0.014	(418)	-0.012	(462)	0.006	(305)

[a]Asterisks denote significant *r* values compared with 1000 randomizations.
[b]The number of comparisons for each spatial distance class is shown in parenthesis, and the maximum distance is truncated at 3.7 m.

Figures

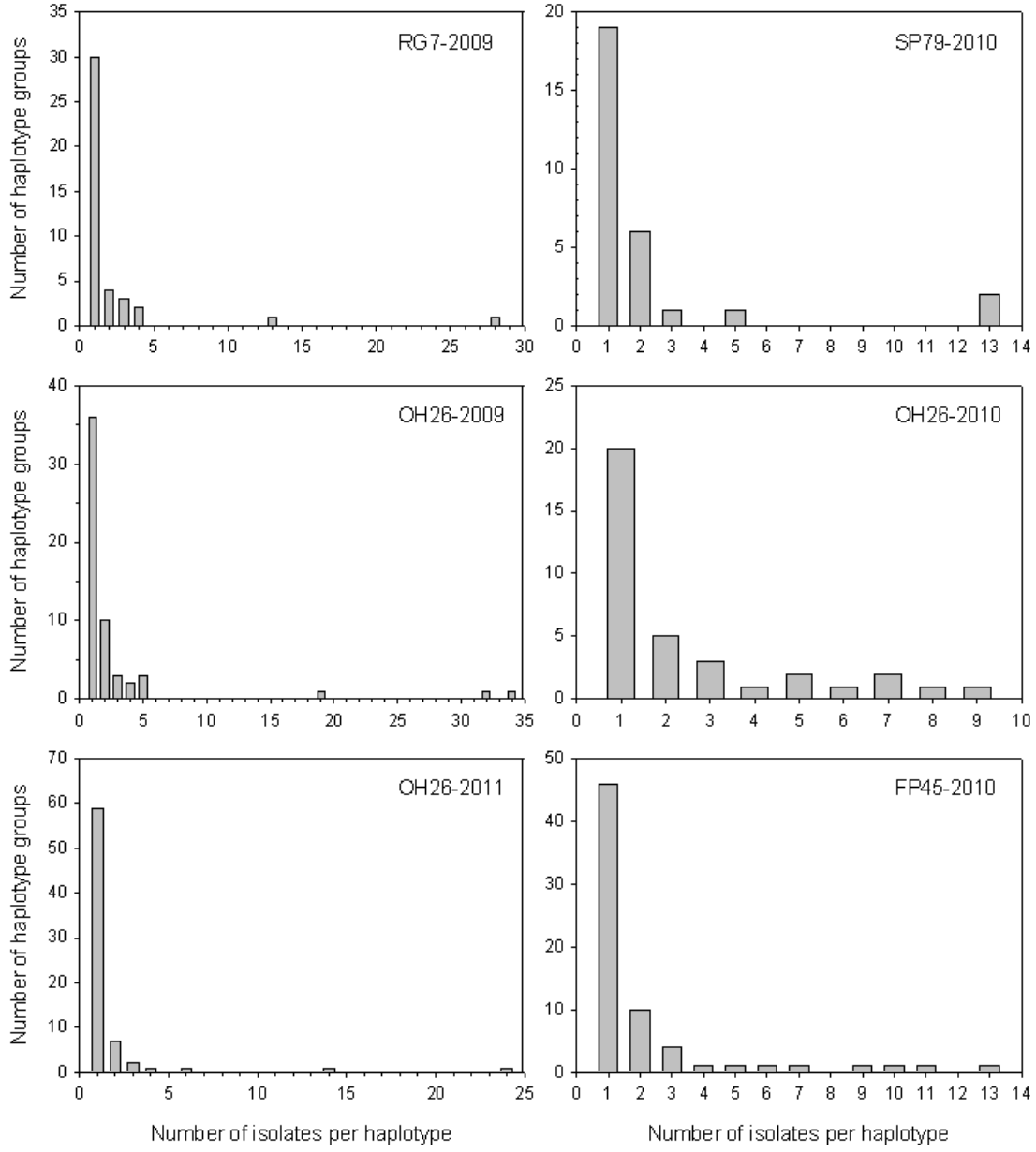

Fig. 5.1. Frequency distribution of the number of *Monilinia fructicola* isolates belonging to each haplotype group in each tree, where unique haplotypes are those represented by only one isolate.

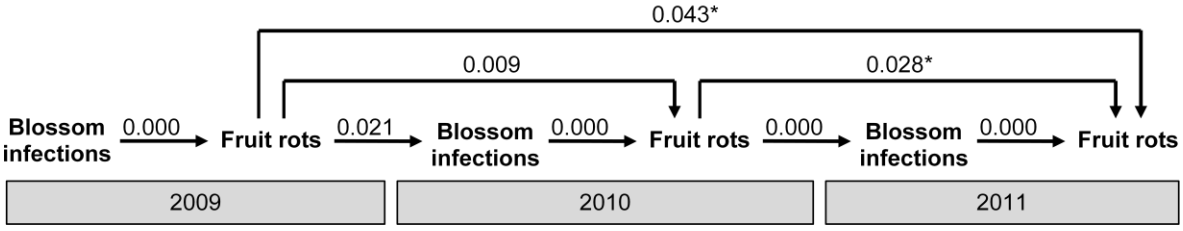

Fig. 5.2. Pairwise analysis of molecular variance in clone-corrected populations of *Monilinia fructicola* from the same peach tree canopy (OH26) across 3 successive growing seasons. Asterisks denote significant Phi_{PT} values compared with 1000 randomizations.

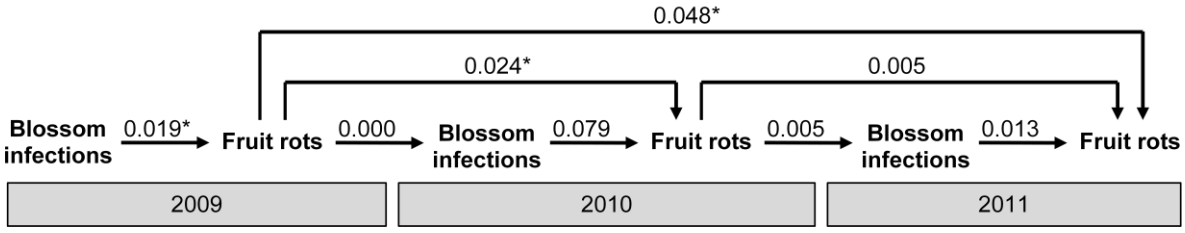

Fig. 5.3. Pairwise analysis of molecular variance in populations of *Monilinia fructicola* from the same peach tree canopy (OH26) across 3 successive growing seasons. Asterisks denote significant Phi_{PT} values compared with 1000 randomizations.

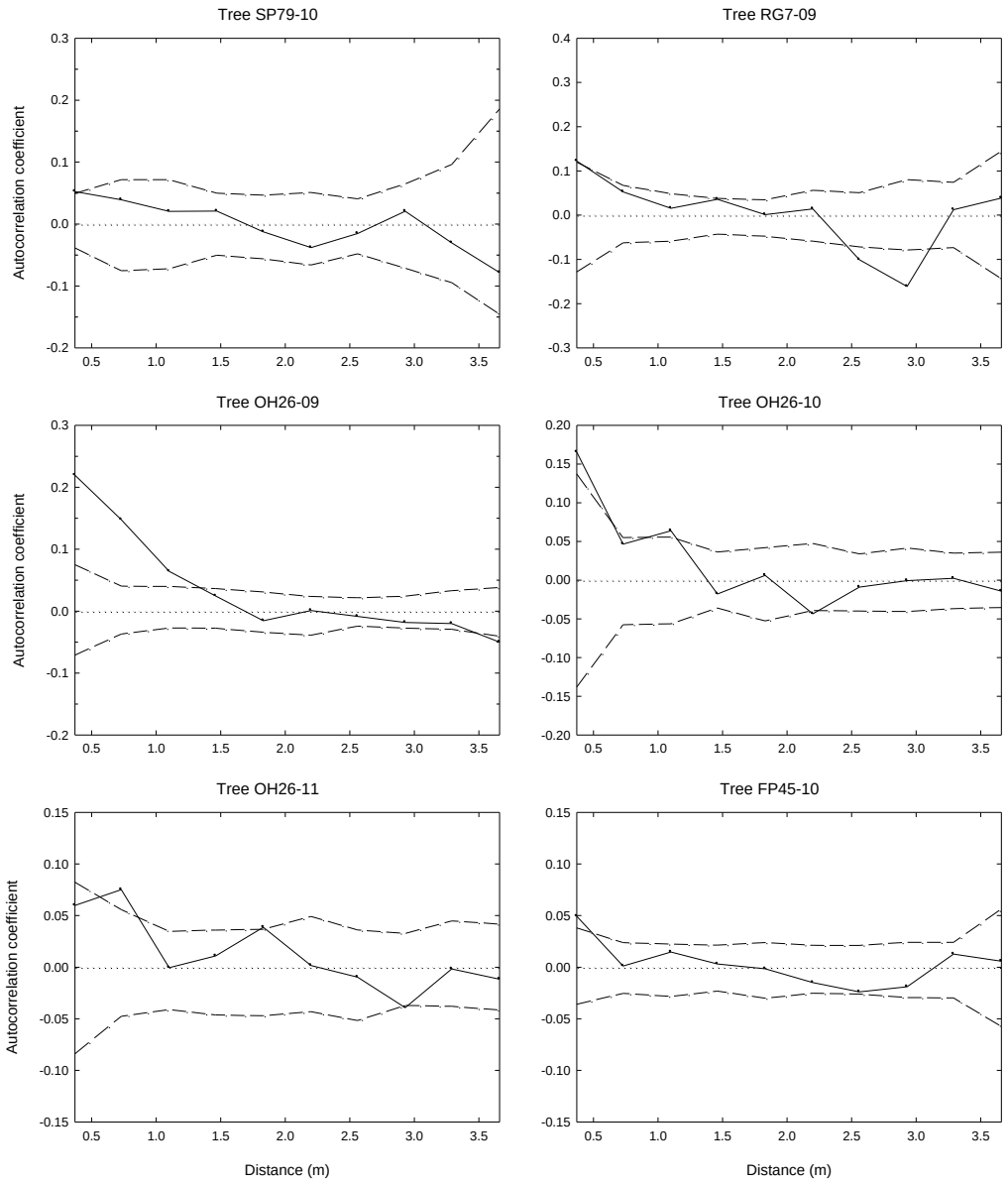

Fig. 5.4. Three-dimensional spatial autocorrelation coefficients of genetic distances in six populations of *Monilinia fructicola* from individual peach tree canopies, where each population represents every fungal isolate obtained during the pre-harvest fruit rot phase. The dashed lines represent a 95% confidence interval about the null hypothesis of no genetic autocorrelation.

CHAPTER 6

CONCLUSIONS

It is hoped that the chapters in this dissertation have served to increase the understanding of the epidemiological processes related to brown rot disease development and spread within individual tree canopies. Although the brown rot disease cycle and temporal development of different aspects of the disease have been well-studied at the orchard level, there is limited information on spatial patterns of disease during within-tree epidemics or the resulting fine-scale pathogen population structure in individual canopies. Knowledge of such patterns can shed light on the relative importance of different inoculum sources within and outside of peach trees.

Spatial Pattern of Disease Within Canopies. In Chapter 2, the sour cherry-brown rot pathosystem was selected as a model for development of the canopy mapping and analysis approach. One of the rationales for choosing this system was that, unlike with *Monilinia fructicola, M. laxa* in this organically managed cherry orchard produced large numbers of blossom and twig blight symptoms that remained in the tree perennially (Byrde and Willets 1977), thereby allowing the spatial association between current and previous year's symptoms to be determined. An electromagnetic digitizer was used to create high-resolution, three-dimensional maps of different brown rot symptom types (blossom blight, shoot blight, and twig cankers) present at the time of digitization. One major hurdle in this project was developing a statistical analysis procedure that would not be influenced by the finite canopy volume and also account for natural aggregation patterns of asymptomatic tree elements (given that structures

such as flowers or fruit are not distributed randomly within the canopy volume). Although previous ecological studies examined three-dimensional spatial aggregation patterns, these typically were in infinite systems (such as the ocean) and/or used complete spatial randomness within the cubic volume as the null model for comparison. Ultimately, the best approach was determined through this study to use all symptomatic and asymptomatic digitized tree elements as an empty set of coordinates for performing randomizations, simultaneously accounting for the natural distribution of unaffected plant parts and any edge effects.

The results of the analysis showed that symptoms were clustered significantly within the tree canopy and that there was a significant association of the current year's symptoms with positions of the previous year's symptoms. Epidemiologically, these spatial patterns suggested that the previous year's twig cankers likely produced the inoculum that infected the current year's blossoms in the spring. However, since disease assessment and mapping in this pilot study were done at a single point in time, prior to the period of fruit maturation, it was not possible to analyze spatio-temporal disease development or to quantify spatial patterns of pre-harvest fruit rot, the economically most important symptom type, within the canopy. Based on these considerations, we designed a 3-year follow-up study on peach to monitor the spatio-temporal development of brown rot (caused by *M. fructicola*) during the course of the season and quantify spatial aggregation and association patterns within each tree canopy.

Using the methods developed in the sour cherry pathosystem, fine-scale canopy mapping and three-dimensional spatial pattern analysis were applied for analysis of spatio-temporal development of pre-harvest brown rot in 13 peach trees of different maturity classes (Chapters 3 and 4). We observed a negative correlation between the index of disease aggregation and disease incidence in the same tree, showing that trees with higher brown rot incidence had lower

aggregation of affected fruit. Significant aggregation among symptomatic fruit was most pronounced for early-maturing cultivars and/or early in the epidemic. This is consistent with the notion of a greater importance of localized, within-tree sources of inoculum at the beginning of the epidemic.

Spatial association analyses revealed that pre-harvest fruit rot was positively associated with the position of blossom blight symptoms within the same tree canopy earlier in the season. However, the same was not true when the data were examined for spatial association between fruit rot symptoms during successive phases (early, middle, and late) of the pre-harvest fruit rot epidemic. In all cases either no association or a negative spatial association was observed between fruit rot symptoms across epidemic phases. This was likely an artefact of having clusters of affected fruit appear successively in different parts of the canopy, perhaps as a result of differences in microclimate or the rate of fruit ripening. Thus, when calculating associations among two clusters of symptomatic fruit in different parts of the canopy, an overall negative association may ensue. Taken as a whole, these results indicated that blossom blight is an important source of inoculum within canopies and that aggregation of pre-harvest fruit rot is more often observed with lower disease incidence and for trees maturing earlier in the season. Since the study on aggregation and association patterns of disease could not exclude a role of within-tree environmental factor in shaping these patterns, an attempt was made to gain further insight into the mechanism behind generating spatial patterns of symptoms (environmental vs. dispersal-related) by examining the pathogen's population structure within tree canopies.

Fine-Scale Pathogen Population Structure Within Canopies. Gaining deeper insight into the importance of within-tree inoculum sources during the pre-harvest epidemic was the main goal

behind analyzing genotypic data from fungal isolates associated with each symptom in individual peach canopies. This project required development of genetic markers for *M. fructicola* that have high resolution and are co-dominant to potentially resolve heterokaryiotic isolates. A set of microsatellite markers was developed and assayed on a preliminary set of isolates from several locations within the southeastern United States, ultimately yielding 16 polymorphic markers deemed suitable for fine-scale genetic analysis (Chapter 3).

All isolates collected from six trees monitored for brown rot symptom development from blossom blight to fruit drop were used to characterize the fine-scale pathogen population genetic structure (Chapter 5). Within each tree canopy, results showed high genetic diversity and high genotypic diversity of the *M. fructicola* populations, with all showing evidence of linkage disequilibrium. The percentage of unique haplotypes among blossom blight isolates was higher than for fruit rot isolates. Thus, a larger proportion of the isolates obtained from fruit rot were clones as compared with blossom blight. Spatial genetic structure was also observed among fruit rot isolates at the canopy scale, with all six populations showing positive and significant autocorrelation among genotypes. This is the strongest evidence for pathogen dispersal generating the aggregated disease patterns reported in Chapter 4.

These results can be interpreted in light of what is and is not known about the disease cycle of *M. fructicola*. The high uniqueness (low clonality) of isolates from blighted blossoms suggests independent sources of primary inoculum infecting each flower. Subsequently, some of these haplotypes became a source of secondary inoculum because the same haplotype was recovered from isolates in the fruit rot phase. However, relatively few of the fruit rot haplotypes were haplotypes represented within the blossom blight sub-population, indicating that most were from a source other than within-canopy blossom blight (or that genetic recombination occurred

between the blossom blight and fruit rot stages). Thus, it is likely that internal and external sources of secondary inoculum are contributing to pre-harvest disease development.

Among all 291 clonal haplotypes across the six trees, only 11 were represented in more than one tree. It is important to note, however, that the *M. fructicola* populations genotyped from these six trees represent only a sub-sample of the total trees with brown rot disease in the orchard. Connectivity between populations within trees in the same orchard was not fully explored. It is likely that more shared haplotypes would have been found among different tree populations if all trees were located within the same row or next to each other. Indeed, it is not surprising that the two trees sharing the greatest number of clonal haplotypes, O'Henry 26 in 2010 and Flameprince 45 in 2010, are cultivars whose fruit mature within an overlapping period of ~3 weeks. None of the other trees were as close together in space and time, and fewer clonal haplotypes were found within all other pairs of trees.

The primary mode of overwintering of *M. fructicola* in peach orchards in the southeastern United States is not well known. In general, apothecial production within managed orchards in the region is considered rare, but is thought to occur more readily underneath wild plums (Landgraf and Zehr 1982). Another form of overwintering thought to play a more important role in areas lacking survival via sexual apothecial production from fruit mummies on the ground is asexual survival in twig cankers, peduncles, and fruit mummies in the tree (Byrde and Willets 1977). The lack of population differentiation among all pairwise comparisons of populations within trees for clone-corrected data suggests that these trees share the same genetic pool, although reshuffling of genotypes may be occurring. Such reshuffling could occur through sexual reproduction or via the parasexual cycle. Although it is not possible to determine from the data which mode of recombination is contributing to the high level of genetic diversity observed,

detection of significant linkage disequilibrium could ensue from sexual recombination if the fungus is homothallic and outcrosses, which is thought to occur in California (Free et al. 1996).

Future Directions. Collectively, this dissertation deepens our understanding of the spatial patterns of symptoms and the relative importance of inoculum sources within individual tree canopies. Moreover, this research has created new tools applicable for future research. The approach and analysis methodology developed in Chapter 2 are applicable in many areas of canopy research. In addition, the polymorphic microsatellite markers generated for *M. fructicola* in Chapter 3 can be used to help further our understanding of the population biology of this important pathogen. For example, one suggested future direction would be to perform a regional survey of *M. frucicola* populations within major growing areas in the southeastern United States, using a hierarchical approach that will enable inferences on population structure and dynamics at several spatial scales. Other key questions that remain unanswered have to do with the source of genetic variation within *M. fructicola* populations.

Monilinia fructicola is reportedly homothallic in early literature (Harada et al. 1977), although this work was not specific as to whether crosses were made between single ascospore isolations. Later work has shown that *M. fructicola* is out-crossing as evidenced by segregation of fungicide resistance of ascospores progeny (Free et al. 1996). In our study, it was not possible to determine whether the level of genetic variability with the presence of linkage disequilibrium is the result of homothallic or heterothallic out-crossing or parasexual recombination. Direct evidence of apothecia produced within an orchard would be the easiest way to determine if sexual recombination is occurring. A comprehensive surveying method as used previously in South Carolina might yield this evidence. If found, isolations of ascospores could be made and

used to make self-pairs to determine whether homothallic sexual fruiting body production can occur. Alternatively, a potential molecular-based approach to examine the mating behavior of *M. fructicola* would be to identify the regulatory genes within the mating-type locus, *MAT* (Rydholm et al. 2007). The *MAT* locus sequence is known for other ascomycetes, enabling a degenerate primer-based approach to amplify, sequence, and identify whether single or dual *MAT* ideomorphs are present within the *M. fructicola* populations genotyped in this study. Thus, the presence of a single idiomorph would suggest that the fungus is homothallic, whereas presence of two idiomorphs would be characteristic of a heterothallic species.

Parasexual recombination may also be a potential source of the high genetic variation observed in this study. One potential approach that may resolve this question would be the pairing of isolates with known genotypes and vegetative compatibility in a way that may lead to the production of recombined progeny if parasexual recombination occurs. This is important because pathogen populations with high diversity and some clonal structure are capable of faster genomic adaptation to selection pressures (e.g., fungicide applications or host plant resistance; Milgroom 1996). Although sexual or parasexual recombination may be rare in *M. fructicola*, only periodic recombination is necessary to yield a moderately high level of genotypic and genetic variation (Milgroom 1996). Thus, deeper insight into the mode of recombination would be important for developing targeted control methods that could limit generation of *M. fructicola* population diversity. This, in turn, may ultimately serve as an important management technique to help delay the development of fungicide-resistant strains and improve control of the disease in commercial production.

Literature Cited

Byrde, R.J.W., and Willetts, H.J. 1977. The Brown Rot Fungi of Fruit. Pergamon, Oxford.

Free, S. J., Holtz, B.A., and Michailides, T. J. 1996. Mating behavior in field populations of *Monilinia fructicola*. Mycologia 88(2):208-211.

Harada, Y. 1977. Studies on the Japanese species of *Monilinia* (*Sclerotinaceae*). Bulletin of the Faculty of Agriculture, Hirosaki University 27:30-109.

Landgraf, F. A., and Zehr, E. I. 1982. Inoculum sources for *Monilinia fructicola* in South Carolina peach orchards. Phytopathology 72:185-190.

Milgroom, M. G. 1996. Multilocus structure of fungal populations. Annual Review of Phytopathology 34:457-477.

Rydholm, C., Dyer, P. S., and Lutzoni, F. 2007. DNA Sequence characterization and molecular evolution of *MAT1* and *MAT2* mating-type loci of the self-compatible ascomycete mold *Neosartorya fischeri.* Eukaryotic Cell 6:868-874.